Periodic Monopoles

RAFAEL MALDONADO

Periodic Monopoles

Rafael Maldonado

A thesis presented for the degree of
Doctor of Philosophy

Centre for Particle Theory
Department of Mathematical Sciences
University of Durham

July 2014

Dedicated to

my grandfather

Ricardo Maldonado Gómez

Periodic Monopoles

Rafael Maldonado

Submitted for the degree of Doctor of Philosophy
July 2014

Abstract

This thesis discusses periodic one dimensional arrays of BPS monopoles. An approximation based on the spectral curve is shown to provide an increasingly accurate description of the monopole fields in the limit of large monopole size to period ratio. Away from this limit the periodic monopole is studied by means of the Nahm transform, which leads to a dual system of Hitchin equations on a cylinder. A combination of analytical and numerical techniques is used to study the spatial symmetries of the periodic 2-monopole and its moduli space. In particular, the asymptotic moduli space metric is determined from the Nahm data, and symmetric one parameter families of monopole scattering processes are identified through the core of the moduli space. These ideas are readily applicable to higher charge periodic monopoles.

Declaration

The work presented in this thesis is based on research carried out in the Centre for Particle Theory, Department of Mathematical Sciences, in the University of Durham, UK. No part of this thesis has been submitted elsewhere for any other degree or qualification and it is all my own work unless referenced to the contrary in the text.

Chapters 1 and 2 are summaries of the work of others and are given here in order to place subsequent material into context. Chapter 3 is my own work, and was published in JHEP. Chapter 4 is based on an article published in Phys. Rev. **D** in collaboration with my supervisor, Prof. R. S. Ward, whose contributions are acknowledged where appropriate. Chapters 5 and 6 are based on my own work, and are pending publication.

Figure 4.6 and section 5.1.2 are unpublished work of Prof. Ward and of Dr D. G. Harland, respectively, for which no suitable references were available. Some of the numerical procedures used were adapted from my supervisor's, and are again acknowledged where appropriate.

Acknowledgements

First and foremost, I would like to express my gratitude to my supervisor, Richard Ward, for being a constant source of ideas, and for always being approachable whenever I needed to discuss my work - sometimes at very short notice! It was a pleasure and an honour to collaborate with Richard on our joint publications. I also thank Derek Harland and Paul Sutcliffe for their patience in answering many a monopole-related question over the course of my studies. I am fortunate to have had the opportunity to discuss my work with Sergey Cherkis and Kimyeong Lee, whose work motivated much of the research presented in this thesis.

I thank my officemates James Allen, Tim Goddard and Craig Robertson, who were always available to hear my most outlandish ideas and for our weekly crossword sessions.

Thanks also to Catherine Banner, Pierre-Philippe Dechant, Kate Norman, Douglas Smith and Richard Ward for proofreading various parts of this thesis.

Most importantly, special thanks are due to my parents, Arturo and Kate, without whose constant support I would never have got this far.

I am grateful to the UK Science and Technology Facilities Council (STFC) for a studentship, and to my examiners Derek Harland and Wojtek Zakrzewski for their careful reading of this thesis.

Contents

List of Figures

1

Introduction

1.1 Overview of the Thesis

This chapter sets the scene by reviewing what is known of monopoles in $\mathbb{R}^3$, highlighting in particular the results and techniques used in their study, while referring to the original papers for full details. Following on from these classical results, chapter 2 discusses a modification of the mathematical tools to infinite singly periodic chains of monopoles and discusses previous work in this area.

The first main strand of this thesis, chapter 3, describes an approximation to the monopole fields in the limit in which the size of each monopole in the chain is much larger than the spacing between monopoles. The content of this chapter was published as *Periodic monopoles from spectral curves* (reference [Mal13]), and evidence for the validity of the 'spectral approximation' is provided throughout the remaining chapters.

The second topic involves using the Nahm transform to study spatial symmetries of the monopole solutions and to describe the low energy interaction of such monopole chains via the moduli space approximation. This is done in chapter 4, which contains work published in [Mal13] and in collaboration with my supervisor in *Geometry of periodic monopoles*, [MW13].

These chapters are followed by three shorter chapters: chapter 5 describes the limits of the scaling of the monopole size to period ratio, while chapter 6 generalises the discussion of the preceding chapters to higher charge chains. These chapters are based on the preprints [Mal*b*] and [Mal*a*], respectively. Chapter 7 summarises the thesis and outlines ideas for future work.

Throughout the thesis, mention will be made of the applicability of our ideas to the doubly periodic monopole on a square lattice, drawing from [MW14].

1.2 BPS Monopoles

The Bogomolny-Prasad-Sommerfield (BPS) monopole in $\mathbb{R}^3$ is described by classical solutions to the Bogomolny equations,

$$F = -*D\Phi \qquad \text{with} \qquad F = dA + A \wedge A \tag{1.1}$$

where F is a 2-form field strength, A is a 1-form gauge potential valued in the Lie algebra of some group G (we will consider $G = \mathrm{SU}(N)$, and in particular $G = \mathrm{SU}(2)$ for the remainder of this discussion) and Φ is a Lie-algebra-valued scalar, the 'Higgs field' which is constrained to satisfy $\mathrm{tr}(\Phi^2) =$ constant at large distances. The covariant derivative D acts on p-forms ω via

$$D\omega = d\omega + A \wedge \omega - (-1)^p \omega \wedge A \qquad \Rightarrow \qquad D^2\omega = F \wedge \omega - \omega \wedge F.$$

The Hodge $*$ acts on 1-forms by $*\omega_i dx^i = \frac{1}{2}\epsilon_{ijk}\omega_i dx^j \wedge dx^k$ (the summation convention applies, and we are working with the Euclidean metric throughout). In components, we then have $F = \frac{1}{2}F_{ij}dx^i \wedge dx^j$ and the Bogomolny equations become

$$\begin{aligned} F_{ij} = [D_i, D_j] &= \partial_i A_j - \partial_j A_i + [A_i, A_j] \\ &= -\epsilon_{ijk} D_k \Phi = -\epsilon_{ijk} \left(\partial_k \Phi + [A_k, \Phi]\right). \end{aligned}$$

As we are dealing with gauge theories, the monopole fields are defined up to gauge transformations. For $\mathfrak{su}(2)$-valued fields, the Bogomolny equations are invariant under the action of $g \in \mathrm{SU}(2)$,

$$A \to g^{-1}Ag + g^{-1}dg \qquad\qquad \Phi \to g^{-1}\Phi g.$$

We will motivate the Bogomolny equations (1.1) in two ways. Firstly, we perform a dimensional reduction on the anti-self-duality equations on $\mathbb{R}^4$,

$$F_{ij} = -\frac{1}{2}\epsilon_{ijkl}F_{kl}, \tag{1.2}$$

whose solutions describe Yang-Mills instantons. Requiring that all the fields are independent of one of the coordinate directions, x^4, say, and setting $A_4 = \Phi$ returns the Bogomolny equations. Similar dimensional reductions will be considered in sections 2.2 and 3.5.

The Bogomolny equations are also obtained from the three-dimensional Yang-Mills-Higgs action,

$$S \;=\; -\frac{1}{4}\int_{\mathbb{R}^3} \mathrm{tr}\left(F\wedge *F + D\Phi\wedge *D\Phi + \lambda(1-\|\Phi\|^2)\omega\right), \qquad (1.3)$$

where ω is the volume form on $\mathbb{R}^3$, the length-squared of Φ for $G = \mathrm{SU}(2)$ is $\|\Phi\|^2 = -\frac{1}{2}\mathrm{tr}(\Phi^2)$ and the trace is taken in the Lie algebra. From this perspective, the Higgs field is introduced in order to circumvent Derrick's theorem and allow solutions which are stable under an isotropic rescaling of the spatial coordinates. Exact solutions to the resulting equations of motion are only known for $\lambda = 0$, as long as, in this limit, the boundary condition $\|\Phi\|^2 \to 1$ is retained (this is known as the 'BPS limit'). A lower energy bound can be computed by looking for stationary points of the action (1.3), an argument due to Bogomolny:

$$S \;=\; -\frac{1}{4}\int_{\mathbb{R}^3} \mathrm{tr}\left((F + *D\Phi)\wedge *\left(F + *D\Phi\right) - 2F\wedge D\Phi\right).$$

The first term is positive, such that minimum energy solutions obey (1.1) and have an energy

$$E \;=\; -\frac{1}{2}\int_{\mathbb{R}^3} \mathrm{tr}\left(*D\Phi\wedge D\Phi\right) \;=\; -\frac{1}{2}\int_{\mathbb{R}^3} d\,\mathrm{tr}\left(\Phi * D\Phi\right), \qquad (1.4)$$

where use has been made of the Jacobi identity, which together with (1.1) implies the Bianchi identity,

$$\epsilon_{ijk}[D_i,[D_j,D_k]] \;=\; 0 \qquad \stackrel{(1.1)}{\Longrightarrow} \qquad D*D\Phi \;=\; 0. \qquad (1.5)$$

The total energy can be computed using the divergence theorem,

$$E \;=\; -\frac{1}{2}\int_{\partial\mathbb{R}^3 = S^2_\infty} \mathrm{tr}\left(\Phi * D\Phi\right), \qquad (1.6)$$

and straightforward manipulations [War81] show that the energy density is given by

$$\mathcal{E} \;=\; -\frac{1}{4}\, d*d\,\mathrm{tr}\left(\Phi^2\right) \;=\; -\frac{1}{4}\,\nabla^2\,\mathrm{tr}\left(\Phi^2\right) \;=\; \frac{1}{2}\,\nabla^2\|\Phi\|^2. \tag{1.7}$$

Equations 1.6 and 1.7 will be used later in this thesis.

Solutions to (1.1) in $\mathbb{R}^3$ describe non-Abelian core regions, which allows them to be smooth and free of singularities (although smooth solutions in the presence of point-like Dirac monopoles have also been studied [ChD08]). Away from the core region, the fields can be seen to approach those of an Abelian magnetic monopole exponentially fast.

Monopole solutions are characterised by their topological charge. In the SU(2) case this is computed via

$$k \;=\; -\int_{S^2_\infty} \frac{\mathrm{tr}(F\Phi)}{4\pi\|\Phi\|} \;\in\; \mathbb{Z}, \tag{1.8}$$

and turns out to be identical to the number of zeros of Φ counted with multiplicity, [Sut96*a*].[1] Then, the asymptotic length of the Higgs field is

$$\|\Phi\|_\infty \;=\; 1 - \frac{k}{2r} + \mathcal{O}(r^{-2}). \tag{1.9}$$

Topologically, the charge arises due to the Higgs field breaking the gauge symmetry G to a residual symmetry group H. Then Φ_∞ lies in the gauge orbit of the coset group G/H, allowing a classification of monopoles by the homotopy group $\pi_2(G/H)$ of maps from the 2-sphere at spatial infinity to G/H. The number of topological invariants generated in this way depends on the pattern of symmetry breaking (which is said to be 'maximal' if all the eigenvalues of Φ_∞ are distinct, or 'minimal' if all but one of them are the same). For $G = \mathrm{SU}(2)$ we have $H = \mathrm{U}(1)$ and one magnetic charge. In the SU(3) case there are two possibilities, and we discuss how these apply to the periodic monopole in chapter 3.

The interpretation of monopoles as possessing magnetic charge equal to their topological charge arises from consideration of the fields far from the non-Abelian core. In this region the Abelian field strength and magnetic field

[1] Although this observation also holds for the periodic monopole, there is evidence that it is not the case for the doubly periodic monopole, [MW14].

are defined through

$$f_{ij} \;=\; -\frac{\mathrm{tr}(F_{ij}\Phi)}{2\|\Phi\|}, \qquad\qquad b_i \;=\; \frac{1}{2}\,\epsilon_{ijk} f_{jk},$$

such that the magnetic and topological charges are related by

$$g \;=\; \int b_i \, dS_i \;=\; 2\pi k.$$

As such, far from the non-Abelian core these solutions behave much like the Abelian magnetic monopoles studied by Dirac [Dir31], who first realised their topological nature. The development of non-Abelian gauge theory by Yang and Mills [YM54] paved the way towards singularity-free solutions with magnetic charge.

Solutions to the Bogomolny equations (1.1) have been studied using a range of methods. The observation that non-Abelian gauge theories support regular monopole solutions with the action (1.3) was made by 't Hooft and Polyakov ['tHo74, Pol74]. The exact solution of charge 1 with $\lambda = 0$ was given by Prasad & Sommerfield [PS75], and is spherically symmetric. It has, however, been shown [WG76] that no spherically symmetric monopoles exist for $k > 1$, although axially symmetric toroidal configurations are always a possibility in this case. Charge 2 monopoles were studied soon thereafter by a variety of methods, although formulæ for the Higgs field are only known explicitly on the coordinate axes. The techniques used include Ward's adaptation of the twistor construction of instantons [War81] and the approach of Forgács *et al.* in terms of integrable systems and Bäcklund transformations [FHP81], while many of the analytical details were studied by Jaffe & Taubes [JT80]. We will focus primarily on Nahm's adaptation of the Atiyah-Drinfeld-Hitchin-Manin (ADHM) construction of instantons [Nah80, AHDM75], which is the method most easily applicable to $k > 2$, and a working description of this technique is given in the following section. Our discussion will draw both from the original papers and from the exposition of Manton & Sutcliffe [MS04].

Charge k monopoles are characterised by $4k$ parameters, known as 'moduli'. Roughly speaking, for well separated monopoles, they describe the positions and phases of the monopoles (although this interpretation fails when two monopoles are in close proximity to one another). The moduli describe solutions to the Bogomolny equations of equal energy, an observation which provides a method of determining the low energy dynamics of multimonopoles via the

'moduli space approximation'. This procedure will be discussed in section 1.4. The dimension of the moduli space was computed rigorously by Weinberg [Wei80].

Within mathematical physics, non-Abelian monopoles appear in a variety of settings. In cosmology, they occur as topological defects created by phase transitions in the early universe and diluted during inflation [VS94]. They played an important part in the development of electromagnetic and strong/weak coupling duality [MO77] and their existence has been predicted by string theory [HW97] (see also section 2.4 of this thesis). M-theory has led to the Basu-Harvey generalisation of the Nahm equations [BH05], and there has been some headway into understanding monopoles in the 'bulk' spacetime of the anti-de Sitter/conformal field theory correspondence [Sut10]. Although direct experimental evidence of monopoles is lacking, effective monopoles have been detected in condensed matter contexts, most notably in spin ices [MT+09]. A brief overview of these topics is given in [Raj12].

1.3 Nahm Transform and Spectral Curves

In this section we discuss two tools which prove useful in the study of monopoles: the Nahm transform and spectral curves. The key characteristics of these methods will be described, paving the way for their subsequent application to monopoles on $\mathbb{R}^2 \times S^1$ later in this thesis.

The Nahm transform provides a bijection between solutions to the Bogomolny equations and solutions of the Nahm equations on a line segment [Nak93]. The transformed set of equations is usually easier to address, both analytically and numerically, than the Bogomolny equations. However, carrying out the inverse transform to obtain the monopole fields must generally be performed numerically. The other strength of the Nahm transform is the way spatial symmetries are encoded, which allows the construction of monopoles of high symmetry such as those of the Platonic solids, [HS96].

Spectral curves describe monopoles by means of their scattering data, and are related to the Nahm description by the Lax formalism. Knowledge of the allowed polynomial form of the spectral curve gives information about both the monopole and Nahm transformed fields, as well as indicating the spatial locations of the monopoles.

1.3.1 Nahm Transform

The Nahm transform extends the ADHM construction of instantons by replacing the linear ADHM operator by a differential operator built from the monopole fields and twisted by a parameter $z \in \mathbb{R}$ which is interpreted as a coordinate on the reciprocal space. For the SU(2) monopole of charge k the procedure was well described by Corrigan & Goddard [CG84], which we now summarise.

Given $\mathfrak{su}(2)$-valued monopole fields $\Phi(\boldsymbol{x})$, $A_i(\boldsymbol{x})$ we construct the differential operator

$$\tilde{\Delta} \;=\; \sigma_i \otimes (\mathbf{1}_2 \partial_i + A_i) - \mathbf{1}_2 \otimes (\mathrm{i}\Phi + z)$$

where we make use of the Pauli matrices with conventions

$$\sigma_1 \;=\; \begin{pmatrix} 0 & 1 \\ 1 & 0 \end{pmatrix} \qquad \sigma_2 \;=\; \begin{pmatrix} 0 & -\mathrm{i} \\ \mathrm{i} & 0 \end{pmatrix} \qquad \sigma_3 \;=\; \begin{pmatrix} 1 & 0 \\ 0 & -1 \end{pmatrix}.$$

The idea is to look for k independent spinors v_α satisying $\tilde{\Delta} v_\alpha = 0$. These are arranged into the columns of a $2 \times k$ matrix V normalised to $\int V^\dagger V \, d^3\boldsymbol{x} = \mathbf{1}_k$. From V we construct three anti-Hermitian $k \times k$ matrices $T_i(z)$ defined in the domain $z \in (-\frac{1}{2}, \frac{1}{2})$,

$$T_i(z) \;=\; -\mathrm{i} \int_{\mathbb{R}^3} x_i \, V^\dagger V \, d^3\boldsymbol{x}.$$

These are known as 'Nahm matrices' and satisfy the Nahm equations

$$\frac{dT_i}{dz} \;=\; -\epsilon_{ijk} T_j T_k \tag{1.10}$$

together with the boundary condition that the $\{T_i\}$ have simple poles at $z = \pm\frac{1}{2}$ whose residues define a k-dimensional representation of $\mathfrak{su}(2)$. Solving the Nahm equations can be a lot simpler than tackling the Bogomolny equations directly. For example, the charge 1 monopole has $T_i = x^i$ (where the $\{x^i\}$ denote the Cartesian coordinates of the location of the monopole), while the charge 2 case can be solved in terms of elliptic functions (see [BPP82] for details). In general, the trace of the Nahm matrices gives the monopole centre of mass, allowing us to consider only their trace free part. For convenience, we introduce the terminology '*forward Nahm transform*' to refer to the above procedure of mapping from monopole fields to Nahm equations.

Given a solution to the Nahm equations, we will use the '*inverse Nahm transform*' to construct the monopole fields from the Nahm data. This requires

us to find the two dimensional kernel Ψ of the operator

$$\begin{aligned}\Delta &= \mathbf{1}_{2k} \otimes \partial_z - \left(\sigma_i \otimes \mathbf{1}_2\, x^i\right)^\dagger - \mathrm{i}\,(\sigma_i \otimes T_i)^\dagger \\ &= \begin{pmatrix} \mathbf{1}_k(\partial_z - x^3) + \mathrm{i}T_3 & -\mathbf{1}_k(x^1 - \mathrm{i}x^2) + \mathrm{i}(T_i - \mathrm{i}T_2) \\ -\mathbf{1}_k(x^1 + \mathrm{i}x^2) + \mathrm{i}(T_1 + \mathrm{i}T_2) & \mathbf{1}_k(\partial_z + x^3) - \mathrm{i}T_3 \end{pmatrix} \end{aligned} \tag{1.11}$$

with Ψ normalised to

$$\int_{-1/2}^{1/2} \Psi^\dagger \Psi \, dz \;=\; \mathbf{1}_2.$$

Then the monopole fields satisfying the Bogomolny equations (1.1) are given by

$$\Phi(\boldsymbol{x}) \;=\; \mathrm{i}\int_{-1/2}^{1/2} z\, \Psi^\dagger \Psi \, dz \qquad\qquad A_i(\boldsymbol{x}) \;=\; \int_{-1/2}^{1/2} \Psi^\dagger \partial_i \Psi \, dz.$$

In chapter 2 we will make use of the result of Braam & van Baal [BvB89] that a generalised Nahm transform maps between solutions of self-duality equations on reciprocal 4-tori. By rescaling the radii of these tori, and suitably amending the boundary conditions, this picture has led to a variety of Nahm transforms on different manifolds, as has been summarised by Jardim [Jar04]. In later chapters, we will see how the $\mathbb{R}^3$ monopole Nahm data arises as a limit of the Nahm data of a periodic monopole.

The Nahm transform also allows the construction of monopoles of higher gauge group, in which case the Nahm matrices are defined over a sequence of line segments with certain matching conditions. For an example of this use, see [HS97].

1.3.2 Spectral Curves

Hitchin [Hit82] defines the monopole spectral curve as the set of lines γ in $\mathbb{R}^3$ on which the operator

$$(D_\gamma + \mathrm{i}\Phi)v \;=\; 0 \tag{1.12}$$

has a normalisable solution. This set of lines describes a complex curve on $T\mathbb{CP}^1$, the tangent space to the Riemann sphere. In complex coordinates (ξ, η), where ξ is a coordinate on the Riemann sphere and η is a suitably normalised coordinate on the tangent plane at ξ, the spectral curve of a monopole centered at $\boldsymbol{x} = (x^1, x^2, x^3)$ is

$$\eta - (x^2 - \mathrm{i}x^1) + 2x^3\xi + (x^2 + \mathrm{i}x^1)\xi^2 \;=\; 0,$$

which is known as the 'star' at (x^1, x^2, x^3). The spectral curve for well separated higher charge monopoles is closely approximated by the product of stars at each monopole location.

From the Nahm transform perspective, the same spectral curve is obtained by expressing the Nahm equations (1.10) in Lax form with ξ as a spectral parameter,

$$\frac{dT}{dr} = [T, T^+] \qquad \text{where} \qquad \begin{cases} T &= (T_1 + \mathrm{i}T_2) - 2\mathrm{i}T_3\xi + (T_1 - \mathrm{i}T_2)\xi^2 \\ T^+ &= -\mathrm{i}T_3 + (T_1 - \mathrm{i}T_2)\xi \end{cases}$$

then the characteristic equation $\det(\mathbf{1}_k\eta + T(\xi)) = 0$ is the k-monopole spectral curve. Conversely, given a spectral curve we can deduce the eigenvalues of the Nahm matrices.

The fact that the spectral curve is a polynomial in both η and ξ, together with other data that can be derived relating the coefficients of the various terms, restricts our attention to a specific form of spectral curve. One can then impose certain symmetries on the spectral curve to obtain the curve corresponding to a monopole with these symmetries, such as the axially symmetric case [Hit82] or to families of solutions with Platonic symmetry [HS96]. Many of the features of the spectral curve of monopoles in $\mathbb{R}^3$, including the approximate factorisation of the spectral curve and the way symmetries are encoded, extend to the periodic case, as will be seen in chapters 3 and 6.

It should be noted in this section that the scattering data (1.12) is only holomorphic if the operator $(D_\gamma + \mathrm{i}\Phi)$ is compatible with the Bogomolny equations [Hit82]. For instance, holomorphicity of scattering in the z direction,

$$[D_x + \mathrm{i}D_y, D_z + \mathrm{i}\Phi] = 0, \tag{1.13}$$

is implied by the Bogomolny equations.

1.4 Moduli Space

The force between two 't Hooft-Polyakov monopoles was computed by Manton [Man77], who found that for monopoles of equal charge the scalar attraction exactly cancels the electromagnetic repulsion. This allows the existence of the static multimonopole solutions described in section 1.2. Introducing a Lorentzian time direction, one can begin to consider the behaviour of multimonopoles with initial velocities. At large separations, the lack of

inter-monopole forces implies that the monopoles move with constant velocity. Studying the detailed behaviour at small separations in principle requires a solution to the full second-order field equations obtained from the action (1.3) in Minkowski space. However, a major result in soliton theory is the 'moduli space approximation' due to Manton [Man82] who showed that the dynamics of slowly-moving monopoles can be approximated by an effective Lagrangian on the $4k$-dimensional moduli space.

The moduli space $\mathcal{M}_k$ is defined as the space of admissible solutions to the Bogomolny equations within the topological sector of charge k modulo gauge transformations which preserve the boundary data. The zero binding energy means that all configurations on the moduli space have the same potential energy, so that no values of the moduli are energetically favoured. Thus, if the initial motion is at small kinetic energy and tangent to the moduli space then subsequent motion will remain in the moduli space (so it can be assumed that the static Bogomolny equations are always satisfied). Rigorous results describing the régime of validity of the approximation and the effect of radiative corrections were provided by Stuart [Stu94]. In particular, it is found that the smaller the initial velocity the longer the moduli space approximation can be trusted.

Motion on the moduli space is governed by the kinetic energy, resulting in a Lagrangian which is quadratic in the time derivatives of the moduli. This provides a metric on the moduli space, which is constructed explicitly by taking the L^2 norm of tangent vectors, given by the perturbations (which arise due to a small change in one of the moduli)

$$A_i \;\rightarrow\; A_i + \delta A_i \qquad\qquad \Phi \;\rightarrow\; \Phi + \delta\Phi$$

satisfying the Bogomolny equations (linearised in the perturbations)

$$D_i(\delta A_j) - D_j(\delta A_i) \;=\; -\epsilon_{ijk}\left(D_k(\delta\Phi) - [\Phi, \delta A_k]\right). \tag{1.14}$$

The effect of the gauge freedom on the moduli space is removed by projecting the perturbations to the component orthogonal to the gauge orbits. Equivalently, we impose that the perturbations satisfy the gauge orthogonality condition

$$D_i(\delta A_i) + [\Phi, \delta\Phi] \;=\; 0 \tag{1.15}$$

which arises from consideration of the effect of infinitesimal gauge transformations $g = (\mathbf{1}_2 + \epsilon)$, which map

$$A_i \;\to\; A_i + D_i\epsilon \qquad\qquad \Phi \;\to\; \Phi + [\Phi, \epsilon], \tag{1.16}$$

which, considered as perturbations, also satisfy the linearised Bogomolny equations (1.14). We ensure that perturbations are orthogonal to gauge orbits by imposing that the kinetic energy

$$\frac{1}{2}\int_{\mathbb{R}^3} \mathrm{tr}\left((\delta A_i)^2 + (\delta\Phi)^2\right) d^3\boldsymbol{x}$$

is invariant under the gauge transformation (1.16), leading to the condition

$$\int_{\mathbb{R}^3} \mathrm{tr}\left(\delta A_i D_i\epsilon + \delta\Phi[\Phi,\epsilon]\right) d^3\boldsymbol{x} \;=\; 0.$$

Using the cyclic property of the trace to rearrange the commutators and integrating the first term by parts leads to the gauge condition (1.15), together with the requirement that δA falls sufficiently fast at large radial distance. A similar exercise for instantons gives the gauge condition $D_\mu(\delta A_\mu) = 0$, of which (1.15) is simply a dimensional reduction. Tangent vectors satisfying these requirements are known in the literature as 'zero modes'. The metric on the moduli space is then given by

$$g_{ab} \;=\; \frac{1}{2}\int_{\mathbb{R}^3} \mathrm{tr}\left(\delta_a A_i \delta_b A_i + \delta_a\Phi\delta_b\Phi\right) d^3\boldsymbol{x},$$

where $a, b = 1, \ldots, 4k$ label perturbations arising from a change in each of the moduli.

Parameters whose variation leads to non L^2 normalisable deformations of the fields should be kept fixed, as such perturbations require an infinite energy.

1.4.1 The Atiyah-Hitchin Metric

In general, it is hard to compute the metric on the moduli space explicitly. One of the major successes in the field was Atiyah & Hitchin's computation of the metric of the 2-monopole system, [AH85, AH88]. This made use of the facts that $\mathcal{M}_2$ is of dimension 8, has a hyper-Kähler metric and an SO(3) symmetry

group. Furthermore, the centre of mass can be factored out,

$$\mathcal{M}_2 \simeq \mathbb{R}^3 \times S^1 \times \mathcal{M}_2^0 \,/\, \mathbb{Z}_2,$$

where the quotient by $\mathbb{Z}_2$ is due to centering the total phase (for a description in terms of Donaldson rational maps see [MS04]) and $\mathcal{M}_2^0$ has dimension 4. As we shall see, for the periodic monopole we have no choice but to factor out the centre of mass.

The Atiyah-Hitchin metric has two important geodesic submanifolds, which are known as the Atiyah-Hitchin cone and Atiyah-Hitchin trumpet. The first of these describes planar scattering, including the celebrated 90° scattering angle for head-on collisions (in which case there is an intermediate step comprising the axially symmetric 2-monopole discussed in section 1.2). The Atiyah-Hitchin trumpet allows for full three dimensional motion of the monopoles, and assigns to them an electric charge due to variation in the phase parameter (such 'dyon' solutions were considered by Julia & Zee [JZ75]). Details of these geodesics are discussed in the book [AH88], and it will be seen in chapter 4 that qualitatively similar geodesic submanifolds can be identified for the periodic monopole.

The asymptotic form of the Atiyah-Hitchin metric simplifies considerably, and was first computed by Manton [Man85]. The metric is of Taub-NUT type with negative mass parameter, and can be written in Gibbons-Hawking form [GH78], an observation which can equally be made for periodic monopoles. For a radial coordinate r, spherical angular coordinates θ and ϕ and a phase angle ψ, the asymptotic (large r) metric is

$$ds^2 = \left(1 - \frac{1}{r}\right)\left(\dot{r}^2 + r^2\dot{\theta}^2 + r^2\sin^2(\theta)\dot{\phi}^2\right) + \left(1 - \frac{1}{r}\right)^{-1}\left(\dot{\psi} + \cos(\theta)\dot{\phi}\right)^2 \tag{1.17}$$

and the corrections to this are exponentially small. Manton's calculation is based on using the forces between well separated monopoles to write down an effective Lagrangian in terms of the relative positions of the monopoles. This procedure can be employed more generally, and is of use when the complete details of the fields are unknown: the periodic monopole is a prime example [ChK02].

For other cases in which the metric is unknown, one can obtain geodesic submanifolds as the fixed point of some spatial symmetry group acting on the

monopole space. This has allowed, for example, the identification of one parameter families of a charge 3 monopole scattering process [HS96] with tetrahedral symmetry. Similar arguments will be made to describe geodesic submanifolds of the monopole chain in section 4.3.6.

Another example for which the full metric is known is the Lee-Weinberg-Yi metric [LWY96] for certain SU(3) monopoles. In this case, head-on scattering leads to a 180° scattering angle. Again, similar results have been found for the periodic monopole (sections 3.4.3 and 4.3.2).

Finally, we remark that the bijection between the monopole and Nahm spaces leads to an isometry in their moduli spaces. This allowed Houghton *et al.* [HIM99] to explicitly regain the Atiyah-Hitchin metric from the Nahm data. These findings inspire the approach taken in chapters 3 and 4 to deduce the moduli space metric of the periodic monopole from the Nahm transformed fields. The results can then be favourably compared with the asymptotic metric deduced from the monopole side of the transform [ChK02].

1.5 Periodic Instantons

Before commencing our discussion of periodic monopoles, it will be useful to review the better studied periodic instanton, or 'caloron', with which the periodic monopole shares qualitative features.

This system was motivated by Harrington & Shepard [HS77] by its contribution to the vacuum state of a thermal field theory (with the instanton corresponding to the zero temperature limit), who also constructed the first examples, [HS78]. The construction makes use of the JNR family of instantons, [JNR77], in which a charge n instanton gauge potential is given by the derivative of a sum over $(n+1)$ weighted double poles in $\mathbb{R}^4$. This allows a construction of calorons by equally spacing the poles along a line (as it stands, this construction does not work for the doubly periodic instanton as the double sum required for this case is divergent). The effect of altering the relative size and period of the instantons in the chain was studied by Gross *et al.* [GPY81], where it was shown that taking the small period (infinite temperature) limit of the caloron recovers the Prasad-Sommerfield monopole [PS75].

Garland & Murray [GM88] noticed that calorons can be understood as monopoles whose gauge group is a loop group (an affine extension of a semi-simple Lie group). In sections 2.4 and 3.5 we will describe the string theoretical interpretation of this result, as applied to the compactified case (i.e. doubly

periodic instantons as periodic monopoles whose gauge group is a loop group). This leads to the interpretation of a caloron as being made up of constituent monopoles. In fact, an SU(N) caloron may be composed of up to N monopole constituents, [KvB98*a*]. In order for a caloron to display the maximal number of constituent monopoles, the boundary conditions must be sufficiently general. In particular, the asymptotic holonomy of the gauge potential in the periodic direction must be non-trivial. A consequence of this is that the Harrington-Shepard caloron does not split into constituents. Solutions with constituents were constructed by Kraan & van Baal [KvB98*b*] using the Nahm transform (which for the caloron leads to Nahm data on a circle), and by Lee & Lu [LL98], who suitably glued together the Nahm data of the two constituent monopoles.

Other systems of periodic solitons have also been studied, such as periodic Skyrmions, periodic sigma models and doubly periodic instantons. Some examples can be found in the references [FP04, Har08]. In all of these cases there is a splitting into constituents, and as we shall see, the periodic monopole is no different.

2

Monopole Chains

The Bogomolny equations on $\mathbb{R}^2 \times \hat{S}^1$ were first studied by Cherkis & Kapustin [ChK01, ChK02, ChK03].[2] We refer to solutions of these equations interchangeably as *periodic monopoles*, or *monopole chains* when visualised as an embedding into $\mathbb{R}^3$ (there is the interesting question of non-periodic perturbations to such a chain, although this lies outside the scope of this thesis). Approximate analytical and numerical solutions of topological charge 1 and 2 were constructed by Ward and Harland [War05, HW09] using the Nahm transform, while numerical studies were also carried out by Dunne & Khemani [DK05]. The remainder of this chapter describes the setup and introduces the spectral curve and Nahm transform for monopole chains.

2.1 Monopole Data

As discussed in chapter 1, BPS monopoles are described by a dimensional reduction of the anti-self-dual Yang-Mills equations to three Euclidean dimensions. Then the component of the gauge potential in the suppressed direction becomes a scalar Higgs field $\hat{\Phi}$ valued in the Lie algebra $\mathfrak{su}(N)$ and satisfying the Bogomolny equations (1.1)

$$\hat{F} = - * \hat{D}\hat{\Phi}. \tag{2.1}$$

In this thesis, we will be concerned with solutions periodic in one of the remaining spatial directions, and will use coordinates $x + \mathrm{i}y = \rho \mathrm{e}^{\mathrm{i}\theta} = \zeta \in$

[2] From this point on we use the notation $\hat{}$ to distinguish the monopole fields and physical space from their Nahm transformed counterparts.

$\mathbb{C} \cong \mathbb{R}^2$ and $z \in \mathbb{R}/\beta\mathbb{Z}$. The fields at large ρ are chosen to match those of an Abelian chain, such that $\hat{\Phi}_\infty$ behaves as $\log(\rho)$, and the Bianchi identity (1.5) requires $\hat{\Phi}_\infty$ to be a harmonic function on $\mathbb{R}^2 \times \hat{S}^1$. Imposing strict periodicity in θ and z then requires θ dependence to enter $\hat{\Phi}_\infty$ at $\mathcal{O}(\rho^{-1})$ and z dependence to contribute at $\mathcal{O}(\rho^{-1/2}\mathrm{e}^{-\rho})$, well within the core non-Abelian region.

Monopoles for gauge group SU(N) have been discussed by various authors, [Wei80, War82, LWY96, MS04, Har08, Shn]. In the case of SU(N) periodic monopoles the boundary data is defined by an N-component vector of integers, $\boldsymbol{\ell}$. Recalling that the monopole fields are valued in $\mathfrak{su}(N)$ (so are $N \times N$ traceless anti-Hermitian matrices) and noting that we are free to permute the entries in $\hat{\Phi}$ by a choice of gauge, the elements of $\boldsymbol{\ell}$ satisfy

$$\sum_{i=1}^{N} \ell_i \,=\, 0 \qquad \text{and} \qquad \ell_i \,\geq\, \ell_{i+1}. \tag{2.2}$$

We also have real vectors $\boldsymbol{v}$ and $\boldsymbol{b}$ and a complex vector $\boldsymbol{\mu}$, whose components again sum to zero, and obey $v_i \geq v_{i+1}$ if $\ell_i = \ell_{i+1}$. These coefficients (as well as other subleading terms) are the parameters and moduli of a solution. From now on we make the distinction between *parameters*, which must be kept fixed (such as the boundary conditions and the centre of mass) and *moduli*, which are allowed to vary. The physical significance of the parameters and moduli of the periodic monopole will be identified in section 3.1.

At large radial distance ρ the fields must resemble a chain of Dirac monopoles, and are hence Abelian and diagonal, such that (up to a choice of gauge) the N diagonal entries are

$$\begin{aligned} -\mathrm{i}\beta\hat{\Phi}_\infty &= \boldsymbol{\ell}\log(\rho) + \boldsymbol{v} + \mathrm{Re}(\boldsymbol{\mu}\zeta^{-1}) + \mathcal{O}(\rho^{-2}) \\ \mathrm{i}\beta\hat{A}_\infty &= \big(\boldsymbol{\ell}\theta + \boldsymbol{b} + \mathrm{Im}(\boldsymbol{\mu}\zeta^{-1})\big)\,\mathrm{d}z + \mathcal{O}(\rho^{-2}), \end{aligned} \tag{2.3}$$

and are combined, defining $\mathfrak{v} = \boldsymbol{v} + \mathrm{i}\boldsymbol{b}$, into

$$\beta\hat{\phi}_\infty \;=\; -\mathrm{i}\beta(\hat{\Phi} - \mathrm{i}\hat{A}_z)_\infty \;=\; \boldsymbol{\ell}\log(\zeta) + \mathfrak{v} + \boldsymbol{\mu}\zeta^{-1} + \mathcal{O}(\rho^{-2}). \tag{2.4}$$

Such a monopole can be constructed by a minimal embedding of fundamental SU(2) monopoles in the $(N-1)$-dimensional co-root space with integer magnetic weights k_i arranged into a vector $\boldsymbol{k}$,

$$\boldsymbol{\ell} \,=\, \sum_{i=1}^{N} \ell_i \boldsymbol{e}_i \,=\, \sum_{i=1}^{N-1} k_i \boldsymbol{\beta}_i^*$$

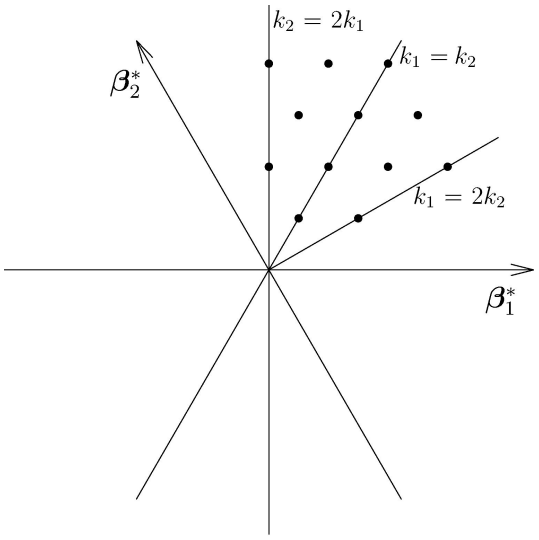

Figure 2.1: Root diagram for SU(3) showing magnetic weights (k_1, k_2) allowed by (2.2).

where for convenience the co-root vectors are represented in terms of N-dimensional vectors $\boldsymbol{\beta}_i^* = \boldsymbol{e}_i - \boldsymbol{e}_{i+1}$ and the $\{\boldsymbol{e}_i\}$ are basis vectors for $\boldsymbol{\ell}$. The SU(3) case is illustrated in figure 2.1. It is possible to convert between the elements of $\boldsymbol{\ell}$ and those of $\boldsymbol{k}$ using

$$k_j \;=\; \sum_{i=1}^{j} \ell_i \qquad \text{and} \qquad \ell_i \;=\; k_i - k_{i-1}, \tag{2.5}$$

where it should be understood that $k_0 = k_N = 0$ and we define $K = \max\{k_i\}$. Throughout this thesis, a specific class of SU(N) periodic monopole will often be referred to simply by its $(N-1)$-dimensional charge vector $\boldsymbol{k}$.

As is done for monopoles in $\mathbb{R}^3$ [War82, MS04, Har08], fundamental monopole masses are defined by the pattern of symmetry breaking of the leading terms in $\hat{\Phi}$. In particular, the i^{th} mass is

$$m_i \;=\; \ell_i - \ell_{i+1}$$

where an interpretation as a physical mass requires the specification of a radial cut-off, due to the logarithmic growth of the Higgs field at large ρ. If all the masses are non-zero (in other words, if the leading diagonal entries in $\hat{\Phi}$ are distinct), the SU(N) gauge symmetry is maximally broken by the asymptotic Higgs field to $\mathrm{U}(1)^{N-1}$. Otherwise, there may be unbroken subgroups according to whether the corresponding $\mathfrak{v}_i$ are the same or different. This can occur for

configurations lying on the lines $k_1 = 2k_2$ and $k_2 = 2k_1$, and we will see examples of this in section 3.4.2. On the other hand, if $k_1 = k_2$ we are open to the possibility of an SU(2) monopole 'trivially embedded' into SU(3) via a negative root. This will be discussed further in section 3.4.1.

Motivated by (1.8), we define the total monopole charge

$$q = -\lim_{R\to\infty}\int_{\rho=R}\frac{\mathrm{tr}(\hat{F}\hat{\Phi})}{4\pi\|\hat{\Phi}\|} \tag{2.6}$$

where integration is over the 2-torus at radial infinity, the length of the Higgs field is defined by $\|\hat{\Phi}\|^2 = -\frac{1}{2}\mathrm{tr}(\hat{\Phi}^2)$ and $\mathrm{tr}(\cdot)$ denotes the trace in the Lie algebra. Applying (2.6) to the $\mathfrak{su}(N)$-valued fields (2.3), the total charge, q, is given by the product of fundamental charges and masses,

$$q^2 \propto \sum_{i=1}^{N}\ell_i^2 = \sum_{i=1}^{N-1}k_i m_i. \tag{2.7}$$

A similar result holds for SU(N) monopoles in $\mathbb{R}^3$ [Wei80], although it is noteworthy that in contrast to the $\mathbb{R}^3$ case (1.9) both the charges and masses are now determined from the leading asymptotic term in $\hat{\Phi}$ (which explains why q^2, not q, appears in (2.7)). Consequently, as described in the preceding paragraph, certain patterns of symmetry breaking can only be achieved by a particular choice of fundamental charges.

As pointed out in [ChK01], the total energy is logarithmically divergent, such that the Bogomolny bound (1.4) is

$$\begin{aligned} E = -\frac{1}{2}\int_{\mathbb{R}^2\times\hat{S}^1}\mathrm{tr}(*\hat{D}\hat{\Phi}\wedge\hat{D}\hat{\Phi}) &= -\frac{1}{2}\int_{\rho=R}\mathrm{tr}(\hat{\Phi}*\hat{D}\hat{\Phi}) \\ &= \frac{\pi}{\beta}\sum_{i=1}^{N}\ell_i\left(\ell_i\log(R)+v_i\right) \end{aligned} \tag{2.8}$$

and we understand the Bogomolny equations to give a solution which minimises the energy in a region with R large but finite. The appearance of q^2 in the leading term of (2.8) supports our identification of the $\{m_i\}$ as the masses of the constituent monopoles.

As is done for the periodic instanton (section 1.5), it is useful to consider the holonomy in the periodic direction. Explicitly, we are to solve the matrix equation

$$\partial_z V(\zeta,z) = \hat{\phi}\,V(\zeta,z) \tag{2.9}$$

with boundary condition $V(\zeta,0) = \mathbf{1}_N$, for $V(\zeta,\beta)$; in particular this fixes $\det(V) = 1$. Under a gauge transformation with $\hat{g} = \hat{g}(\zeta,z) \in \mathrm{SU}(N)$, the fields and holonomy transform as

$$\begin{aligned}\hat{\Phi} &\mapsto \hat{g}^{-1}\hat{\Phi}\hat{g}\\ \hat{A} &\mapsto \hat{g}^{-1}\hat{A}\hat{g} + \hat{g}^{-1}\mathrm{d}\hat{g}\\ V(\zeta,z) &\mapsto \hat{g}^{-1}(\zeta,z)V(\zeta,z)\hat{g}(\zeta,0),\end{aligned}$$

where $\hat{g}(\zeta,0)$ is introduced to ensure the boundary condition on $V(\zeta,z)$ is satisfied. As long as $\hat{g}$ is strictly periodic, i.e. $\hat{g}(\zeta,\beta) = \hat{g}(\zeta,0)$, then the characteristic polynomial of $V(\zeta,\beta)$ is gauge invariant. Asymptotically, using (2.4), the holonomy takes the form

$$V(\zeta,\beta) \;=\; \mathrm{diag}\left(\zeta^{\ell_1}\mathrm{e}^{\mathfrak{v}_1}(1+\mu_1\zeta^{-1}+\mathcal{O}(\rho^{-2})),\ldots\right). \tag{2.10}$$

The analysis of the Bogomolny equations carried out by Cherkis & Kapustin [ChK01] establishes that the characteristic equation of the holonomy is in fact holomorphic, and is thus a polynomial in ζ.

2.2 Nahm Transform

It is shown in [CG84, BvB89] that the Nahm transform provides a bijection between self-dual Yang-Mills fields on the torus $\hat{T}^4$ and the reciprocal torus T^4. It is believed [Jar04] that other self-dual Yang-Mills systems can be obtained by suitable rescalings of the tori. In the present case, it is therefore expected that the Nahm dual to the monopole on $\mathbb{R}^2\times\hat{S}^1$ is a Hitchin system [Hit87] on the 'Hitchin cylinder' $\mathbb{R}\times S^1$ where the S^1 has the dual period $2\pi/\beta$, and this correspondence was established in [ChK01].[3][4] Following the notation of [War05, HW09] the cylinder is parametrised by the coordinates $r\in\mathbb{R}$ and $t\in\mathbb{R}/(2\pi/\beta)\mathbb{Z}$, which are combined into a complex coordinate $s = r+\mathrm{i}t$. The Hitchin fields are a dimensional reduction of the anti-self-duality equations (1.2) with $A_1 = A_s + A_{\bar{s}}$, $A_2 = \mathrm{i}(A_s - A_{\bar{s}})$, $A_3 = \frac{1}{2}(\Phi - \Phi^\dagger)$, $A_4 = -\frac{1}{2}\mathrm{i}(\Phi+\Phi^\dagger)$ valued in $\mathfrak{u}(K)$ (or $\mathfrak{su}(K)$ if the monopole centre of mass is fixed at the origin).

[3] The fact Hitchin equations are conformally invariant allows us to map solutions to other manifolds, including $\mathbb{R}^2$ or S^2. We choose the cylinder to keep explicit the link with the Nahm transform. This gains particular relevance when we make the comparison with doubly periodic instantons in section 3.5.

[4] This argument also suggests that the doubly periodic monopole, or monopole on $\mathbb{R}\times T^2$, is self-reciprocal under the Nahm transform.

This gives

$$F_{s\bar{s}} \;=\; -\frac{1}{4}\,[\Phi, \Phi^\dagger] \qquad\qquad D_{\bar{s}}\Phi \;=\; \partial_{\bar{s}}\Phi + [A_{\bar{s}}, \Phi] \;=\; 0 \tag{2.11}$$

with † denoting the complex conjugate transpose.[5] We shall often refer to this system of Hitchin equations on a cylinder as 'Nahm/Hitchin data', in order to emphasize the fact that the Nahm data is given by Hitchin equations. The monopole fields are recovered, up to a gauge, by finding solutions of the inverse Nahm operator (motivated by the $\mathbb{R}^3$ case, equation 1.11),

$$\Delta\Psi \;=\; \begin{pmatrix} \mathbf{1}_K(2\partial_{\bar{s}} - z) + 2A_{\bar{s}} & \mathbf{1}_K\zeta - \Phi \\ \mathbf{1}_K\bar{\zeta} - \Phi^\dagger & \mathbf{1}_K(2\partial_s + z) + 2A_s \end{pmatrix} \Psi \;=\; 0. \tag{2.12}$$

For SU(N) periodic monopoles, Ψ is a $(2K \times N)$ matrix subject to the normalisation condition

$$\int_{-\infty}^{\infty} dr \int_{-\pi/\beta}^{\pi/\beta} dt\,(\Psi^\dagger\Psi) \;=\; \mathbf{1}_N. \tag{2.13}$$

One can then, in principle, construct the monopole fields using

$$\hat{\Phi} \;=\; \mathrm{i}\int_{-\infty}^{\infty} dr \int_{-\pi/\beta}^{\pi/\beta} dt\,(r\Psi^\dagger\Psi), \qquad \hat{A}_i \;=\; \int_{-\infty}^{\infty} dr \int_{-\pi/\beta}^{\pi/\beta} dt\,(\Psi^\dagger\partial_i\Psi). \tag{2.14}$$

Gauge transformations $\hat{g}$ acting on the monopole fields and g and h on the Nahm fields transform Ψ as

$$\Psi(s;\zeta,z) \;\mapsto\; U(s)^{-1}\Psi(s;\zeta,z)\,\hat{g}(\zeta,z). \tag{2.15}$$

where $U(s) = h \otimes g(s)$, with h a constant 2×2 matrix serving to permute the entries in Δ and also those of Ψ. This freedom to rearrange makes it evident that it is irrelevant whether the derivatives ∂_r and ∂_t are introduced in the same or different entries of Δ, the two configurations differing only by a choice of gauge.

Finally, it should be noted that in the $\beta \to 0$ limit the Nahm transform is expected to be self-reciprocal, mapping between two Hitchin systems of different rank and boundary conditions. Evidence for this is provided in section 5.2.

[5] In this context Φ should more properly be thought of as a 1-form Φds, [Hit87].

2.3 Spectral Data

Following Hitchin [Hit82], we are interested in describing the periodic monopole by means of a holomorphic curve on the twistor space of $\mathbb{R}^2 \times S^1$. The key observation of [ChK01, Che07] is that one can restrict to scattering in the periodic direction and consider the characteristic equation of the z-holonomy, $\det(\mathbf{1}_N w - V(\zeta, \beta)) = 0$, which relates monopole data to Nahm data through the parameter $w = \mathrm{e}^{\beta s}$. This provides a holomorphic curve $\mathbf{S}$ in $\mathbb{C} \times \mathbb{C}^*$ known as the monopole spectral curve, which for an SU(N) periodic monopole of charge $\boldsymbol{k}$ is

$$w^N + P_{1,k_1}(\zeta) w^{N-1} + \ldots + P_{N-1,k_{N-1}}(\zeta) w + (-1)^N \;=\; 0 \tag{2.16}$$

where the $P_{i,k_i}(\zeta)$ denote polynomials in ζ with leading term proportional to ζ^{k_i}. For SU(2) chains this can be written

$$b_k \zeta^k + b_{k-1} \zeta^{k-1} + \cdots + b_1 \zeta + (b_0 + w + w^{-1}) \;=\; 0. \tag{2.17}$$

The relation (2.16) shows that by performing a coordinate redefinition $w \mapsto w^{-1}$ the largest of the k_i (if it is unique) can be chosen to lie in the first half of the entries of $\boldsymbol{k}$. Referring to the SU(3) case (figure 2.1), this amounts to identifying the regions on either side of the line $k_1 = k_2$, and we will choose to work with the configurations below that line.

In addition to the monopole spectral curve (2.16), Cherkis & Kapustin [ChK01, ChK03] introduce a second, equivalent, spectral curve relating the coordinate on $\mathbb{R}^2$ in the monopole space to the characteristic equation of the Hitchin Higgs field Φ,

$$\det(\mathbf{1}_K \zeta - \Phi(s)) \;=\; 0 \qquad \Rightarrow \qquad \zeta^K - \mathrm{tr}(\Phi)\zeta^{K-1} + \ldots + (-1)^K \det(\Phi) \;=\; 0, \tag{2.18}$$

where the intermediate terms are given by symmetric polynomials in the eigenvalues of Φ. By rewriting (2.16) as a polynomial in ζ, a comparison can be made with the coefficients of (2.18) to obtain gauge invariants of Φ. In particular, it should be noted that $\det(\Phi)$ will have singularities at finite $|r|$ if K appears more than once in $\boldsymbol{k}$. Smooth behaviour at large $|r|$ requires the introduction of singularities, both to the monopole and Hitchin fields.

We remark on the similarity of the definition of the spectral curve of the periodic monopole to the scattering data used for monopoles in $\mathbb{R}^3$ (see section

1.3.2), and in particular to scattering data in the periodic (z) direction. In section 3.1 we will see that this spectral data is insensitive to half of the moduli (in particular, z separations and relative phases between the monopoles). The remaining moduli can be introduced to the spectral curve by the use of parabolic line bundles [Har*b*], where additional data is added to the singular points of the spectral curve, at $(w, \zeta) = (0, \infty)$ and (∞, ∞).

One can define complementary spectral data from scattering along a general direction of $\mathbb{R}^2 \times S^1$, [Che07]. The resulting spectral curve has not been studied in detail, but it is reasonable to expect that it would encode the remaining moduli. Note furthermore that although a similar compatibility condition to (1.13) can be given in spherical polar coordinates, it is not possible to do this in cylindrical polars. Consequently the problem cannot be simplified by restricting to scattering data along lines containing $x = y = 0$ and orthogonal to $\boldsymbol{z}$ (as might be tried as a naïve extension of the Jarvis rational map approach [MS04]).

2.4 String Theory Setting

The relation between periodic monopoles and compactified supersymmetric gauge theories is explained in detail in [Kap98, ChK01, ChK03]. It provides a physical context for the root structure presented in section 2.1, as well as a supersymmetric gauge theoretical interpretation of the spectral curve and moduli space. The type IIB setup of interest consists of N parallel D5-branes extended along the x^0-x^5 directions and separated along x^6, with x^3 compactified on a circle. Ending on each of the i^{th} pair of adjacent D5-branes we have $(N-1)$ stacks of k_i D3-branes extended along the x^0-x^2 directions with finite extent in x^6. From the point of view of the D5-brane system, each of the D3-branes is seen as a fundamental SU(2) periodic monopole of type i localised in the x^3-x^5 directions of the D5-brane worldvolume, and translationally invariant along x^0-x^2. Performing a T-duality in the x^3 direction returns a IIA system of D4-branes extended along x^0-x^3, x^6, ending on N other D4-branes extended along x^0-x^2, x^4, x^5. The field equations on the (x^3, x^6)-cylinder are nothing other than the Hitchin equations of section 2.2. The tension between the D4-branes causes them to deform, such that the x^6 direction of the cylinder becomes of infinite extent.

	0	1	2	③	4	5	6	7	8	9
D5	x	x	x	x	x	x				
D3	x	x	x				x			

T_3 ↓

	0	1	2	③	4	5	6	7	8	9
D4	x	x	x		x	x				
D4	x	x	x	x			x			

Introducing n_+ and n_- semi-infinite D3-branes ending on the first and N^{th} D5-branes is equivalent to the introduction of Dirac singularities to the monopole system. Compactifying the x^6 direction, such that the left and right D3-branes coincide, is equivalent to adding an N^{th} root to the Lie algebra $\mathfrak{su}(N)$. The duality described above then leads to Hitchin equations on the 2-torus (x^3, x^6). Such a system of singular monopoles and the relation of the torus to the Nahm data of the doubly periodic instanton will be discussed in section 3.5.

3

The Spectral Approximation

This chapter considers the limit of large monopole size to period ratio and describes an approximation which accurately describes the periodic monopole in this limit. The motivation for this approach is Ward's approximate analytical evaluation of the inverse Nahm transform [War05], together with the study of the spectral curves carried out by Cherkis & Kapustin [ChK01, ChK03]. The recipe for the spectral approximation for the charge 1 case is given in section 3.1. This is then applied to the charge 2 monopole chain (section 3.2), allowing us to consider geodesics on the resulting moduli space (section 3.3). A generalisation to higher gauge groups is considered in section 3.4, and the relation to the doubly periodic instanton is described in section 3.5. A discussion of the application of the spectral approximation to higher monopole charges is postponed to chapter 6. Evidence for the validity of the approximation will be presented throughout the remaining chapters. The work in this chapter was published in JHEP with the title *Periodic monopoles from spectral curves*, [Mal13].

3.1 Introducing the Approximation

Due to the difficulty of finding exact solutions to the inverse Nahm operator (2.12) and motivated by Ward's approximate $\boldsymbol{k} = (1)$ solution [War05],[6] we will consider a construction based on the spectral curves (2.16, 2.18). The following paragraphs describe the procedure to be followed and in the remainder of this section we use the results of [War05] to illustrate the application and régime of validity of the approximation.

[6] Recall that we are using the notation defined on page 17 for the charge vector $\boldsymbol{k}$.

Given an SU(N) monopole with charge vector $\boldsymbol{k}$ it is straightforward to write down the spectral curves (2.16) and (2.18), where the polynomials $P_{i,k_i}(\zeta)$ can be expressed in terms of the data $\mathfrak{v}$, $\boldsymbol{\mu}$. We will be interested in the *spectral points*, those values of ζ at which two or more of the eigenvalues of $V(\zeta,\beta)$ coincide. These points are located by finding the zeros of the discriminant $\mathcal{D}_{\boldsymbol{k}}$ of the polynomial in w (as a function of ζ). Our interest in the spectral points stems from the finding in the $\boldsymbol{k}=(1)$ case, discussed in section 3.1.1, that peaks in energy density are always located at the spectral points (although there can be exceptions when two spectral points coincide). It can be checked by explicit calculation for small N that the highest power of ζ in $\mathcal{D}_{\boldsymbol{k}}$ is $2\sum_{i=1}^{N-1}k_i$, and we expect there to be this many spectral points (this has been checked as far as $N=4$). We will see from various examples that away from the central region of the moduli space, the spectral points occur in pairs, forming $\sum_{i=1}^{N-1}k_i$ fundamental monopoles. This observation is reminiscent of the splitting of periodic instantons into monopole constituents (section 1.5). However, for the periodic monopole, constituents are always present as the holonomy is always non-trivial due to the logarithmic growth of the entries of $\hat{\phi}$. From (2.10), a trivial asymptotic holonomy requires $\ell_i=0$, $\forall i$. Although this condition cannot be achieved for the regular SU(2) monopole, it is possible to set some of the $\ell_i=0$ for higher rank gauge group or upon the addition of Dirac singularities. These cases will be considered in sections 3.4 and 3.5, respectively, and we will see that there is a corresponding pole in the Nahm/Hitchin data.

The spectral curve (2.16) of the SU(N) charge $\boldsymbol{k}$ periodic monopole contains $2\sum_{i=1}^{N-1}(k_i+1)$ real coefficients. We know from [ChK03] that the complex coefficient of ζ^{k_i} in each of the polynomials $P_{i,k_i}(\zeta)$ is a parameter determined by the boundary data $\mathfrak{v}$. The centre of mass of the spectral points is factored out by choosing $\boldsymbol{\mu}$ such that the term of order $\zeta^{2\sum k_i-1}$ in $\mathcal{D}_{\boldsymbol{k}}$ vanishes, and we will say that such a monpole is centered.[7] Overall, this yields $2\sum_{i=1}^{N-1}k_i-2$ real relative moduli, precisely half the number expected were we to consider the full three dimensional picture. This suggests our approach is insensitive to relative z and phase differences between the fundamental monopoles, such that its validity is expected to improve as the ratio of the monopole size to its period becomes large. We will refer to the moduli appearing in the spectral curve as *reduced moduli*, and will see in section 4.1 that in the SU(2) charge

[7] It should be noted [ChK02] that the infinite mass of a periodic monopole precludes variation of the centre of mass coordinates, and that it is thus not physically meaningful to consider an 'uncentered' moduli space.

$\boldsymbol{k} = (2)$ case they parametrise a geodesic submanifold of the full moduli space when certain symmetries are imposed.

3.1.1 SU(2) Charge 1 - Spectral Curve

We illustrate the procedure by reviewing the approximate construction of [War05] for $\boldsymbol{k} = (1)$. In this case the asymptotic monopole field (2.4) and holonomy (2.10) are

$$\hat{\phi} \;=\; \frac{1}{\beta}\left(\log(\zeta) + \mathfrak{v} + \mu\zeta^{-1} + \dots\right)\sigma_3$$

$$V(\zeta,\beta) \;=\; \operatorname{diag}\left(\zeta \mathrm{e}^{\mathfrak{v}} + \mu\mathrm{e}^{\mathfrak{v}} + \dots, \zeta^{-1}\mathrm{e}^{-\mathfrak{v}} + \dots\right)$$

so $\operatorname{tr}(V) = (\zeta+\mu)\mathrm{e}^{\mathfrak{v}}$ holds for all ζ (all subleading terms must cancel if the monopole fields are to be smooth) and the spectral curve is (note that the Nahm/Hitchin fields are of rank 1)

$$w^2 - 2(\zeta+\mu)w/C + 1 \;=\; 0 \qquad\qquad \zeta - \Phi \;=\; 0, \tag{3.1}$$

with spectral points where the roots of the w polynomial coincide, i.e. at $\zeta = -\mu \pm C$ such that C defines the 'size' of the monopole and is given in terms of the boundary data by $C = 2\mathrm{e}^{-\mathfrak{v}}$. Then by rearranging (3.1) and centering the monopole chain by setting $\mu = 0$, the Hitchin Higgs field is

$$\Phi \;=\; C\cosh(\beta s)$$

while the Hitchin gauge potential A_r can be set to zero by a gauge transformation and the Hitchin equations (2.11) are satisfied trivially, for constant A_t. The inverse Nahm transform (2.12) requires a solution of

$$\Delta\Psi \;=\; \begin{pmatrix} 2\partial_{\bar{s}} - z & \zeta - \Phi \\ \bar{\zeta} - \Phi^\dagger & 2\partial_s + z \end{pmatrix} \begin{pmatrix} \psi_{11} & \psi_{12} \\ \psi_{21} & \psi_{22} \end{pmatrix} \;=\; 0 \tag{3.2}$$

(such that A_t is absorbed into z). For $(\zeta, \mathrm{e}^{\beta s_0}) \in \mathbf{S}$, $(\zeta - \Phi)$ will vanish at

$$\beta s \;=\; \pm\beta s_0 \;=\; \pm\cosh^{-1}(\zeta/C)\,, \tag{3.3}$$

such that away from the spectral curve,

$$\zeta - \Phi \;=\; \pm\beta C(s \pm s_0)\sinh(\beta s_0) + \mathcal{O}(s \pm s_o)^2 \;=\; \pm\beta(s \pm s_0)\xi + \mathcal{O}(s \pm s_o)^2$$

where $\xi^2 = \zeta^2 - C^2$. As mentioned by [War05], solutions to (3.2) are supported near the points $s = \pm s_0 = \pm(r_0 + \mathrm{i}t_0)$ on the Hitchin cylinder. The independent solutions take the form of Gaussian peaks localised at each of $\pm s_0$, assembled into

$$\Psi \approx \mathcal{N} \begin{pmatrix} \xi E_- & |\xi| E_+ \\ -|\xi| E_- & \bar{\xi} E_+ \end{pmatrix} \tag{3.4}$$

where

$$\log(E_\pm(s)) = -\tfrac{1}{2}\beta|\xi| \left((r \pm r_0)^2 + (t \pm t_0)^2 \right) - \mathrm{i}zt \tag{3.5}$$

and we have chosen a different gauge to [War05], such that the monopole fields are explicitly independent of z. Such a solution is valid when the peaks on $\mathbb{R} \times S^1$ are well separated, so that there are two independent solutions of (3.2). Furthermore, the peaks must be narrow compared to the cylinder to ensure the correct periodicity in z and t (note that away from this limit it is not possible to extract a phase $\mathrm{e}^{-\mathrm{i}zt}$ from Ψ as is done in equation 3.5, while at the same time preserving the periodicity condition). These conditions are simultaneously ensured if we stay away from the spectral points $\zeta = \pm C$. It follows that a rough estimate for the domain of validity of the spectral approximation is to require the width of the peaks in $E_\pm$ to be much less than the period $2\pi/\beta$, i.e.

$$2\sqrt{\frac{1}{\beta|\xi|}} \ll \frac{2\pi}{\beta} \qquad \Rightarrow \qquad |\zeta^2 - C^2| \gg \frac{\beta^2}{\pi^4}. \tag{3.6}$$

As long as the peaks are narrow, such that the t-integral of $\Psi^\dagger\Psi$ can be evaluated as an infinite Gaussian integral, the normalisation factor $\mathcal{N}$ is determined from (2.13) to be $|\mathcal{N}|^2 = \beta/(2\pi|\xi|)$. After a gauge transformation $\hat{g} = \exp(\frac{1}{4}\log(\bar{\xi}/\xi)\sigma_3)$ the monopole fields are

$$\hat{\Phi} = \mathrm{i}r_0\sigma_3 \qquad \hat{A}_z = -\mathrm{i}t_0\sigma_3 \tag{3.7}$$

$$\hat{A}_\zeta = \frac{\zeta}{4\xi^2}\,\mathrm{e}^{-\beta|\xi||s_0|^2}\sigma_1 \qquad \hat{A}_{\bar{\zeta}} = -\hat{A}_\zeta^\dagger,$$

with r_0 and t_0 defined through (3.3). We choose the branch $t_0 \in (-\pi/\beta, \pi/\beta)$ and $|s_0|$ is to be understood as

$$|s_0|^2 = \inf_{n\in\mathbb{Z}} \left(r_0^2 + (t_0 + \pi n/\beta)^2 \right).$$

It is important to note that the fact the monopole Higgs field can be read off directly from the spectral curve (3.1) via s_0 (3.3) is not simply a restatement of

the boundary conditions, as use has also been made of the fact the coefficients in w of the spectral curve are polynomials in ζ, whose coefficients encode the moduli in a particular way [ChK03]. This result will be used in sections 3.2, 3.4 and 3.5 when we discuss the charge 2, SU(3) and singular periodic monopoles.

It is useful to combine the fields (3.7) into $\mathrm{i}\hat{\phi} = \hat{\Phi} - \mathrm{i}\hat{A}_z$ and $\hat{a} = \hat{A}_\zeta \mathrm{d}\zeta + \hat{A}_{\bar{\zeta}}\mathrm{d}\bar{\zeta}$ (see equation 2.4). We note that $\hat{a}$ approaches zero exponentially fast away from the spectral points $\zeta = \pm C$, and the fields are Abelian and trivially satisfy Hitchin equations in this limit, suggesting that they are truly two dimensional. Noting that $|s_0|$ has dimensions of β^{-1}, we conjecture that in the limit $\beta \to 0$ (where (3.6) holds for all ζ) a solution is provided by

$$\hat{\phi} \;=\; s_0(\zeta)\sigma_3 \qquad\qquad \hat{a} \;=\; 0, \tag{3.8}$$

which satisfies the Bogomolny equations with the correct boundary conditions (2.4). The fact the fields in (3.7) and (3.8) are not smooth (they are continuous, but not differentiable on the line $x \in [-C, C]$, $y = 0$) means the approximation of this section is only expected to be exact as a limiting case. As will be seen in section 3.3, this approximation also leads to the correct asymptotic behaviour of the moduli space metric. Futher evidence for the validity of this approximation is provided by a numerical study of the effect of increasing the size-to-period parameter C (see chapter 5). This procedure is equivalent to reducing β, together with a rescaling of the x and y coordinates by $\sqrt{C}$.

3.1.2 Charge 1 - Energy

We use the energy density formula (1.7)

$$\mathcal{E} \;=\; \frac{1}{4}\nabla^2 \left|\mathrm{tr}(\hat{\Phi}^2)\right|$$

where the Laplacian is $\nabla^2 = 4\partial_\zeta \partial_{\bar{\zeta}}$. The Higgs field (3.7) is

$$\hat{\Phi} \;=\; \frac{\mathrm{i}}{\beta}\,\mathrm{Re}\left(\cosh^{-1}\left(\frac{\zeta}{C}\right)\right)\sigma_3 \;=\; \frac{\mathrm{i}}{\beta}\,\log\left|\frac{\zeta}{C} + \sqrt{\left(\frac{\zeta}{C}\right)^2 - 1}\right|\sigma_3, \tag{3.9}$$

giving an energy density

$$\mathcal{E}_1 \;=\; \frac{1}{\beta^2|\xi|^2} \;=\; \frac{1}{\beta^2}\frac{1}{\sqrt{\rho^4 - 2\rho^2 C^2\cos(2\theta) + C^4}}. \tag{3.10}$$

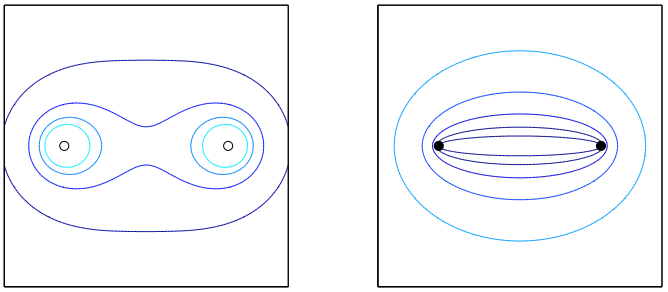

Figure 3.1: An SU(2) periodic monopole. On the left is a contour plot of the energy density (3.10) and on the right of $\log(\mathrm{disc}(\hat{\Phi})+0.001)$. The discriminant vanishes on a line joining the spectral points, whose locations are indicated by black dots on the right hand diagram. Note the loss of axial symmetry and the appearance of constituents, which coincide when the monopole size $|C| = 0$ (when $\arg(C)$ can have no effect).

Contours of $\mathcal{E}_1$ describe Cassini ovals (the locus of points such that the product of distances to two foci is constant) with foci at the spectral points, where the energy is peaked, as shown in figure 3.1. The separation of the spectral points by $2C$ allows us to interpret C as the characteristic size of the monopole. The relation (3.6) gives an estimate as to when it should be possible to resolve the monopole constituents. In particular, the spectral approximation is valid at $\zeta = 0$ if $C \gg \beta/\pi$. In other words, the spectral approximation holds at large C and/or small β. The discriminant of $\hat{\Phi}$, defined as the square of the product of differences between the eigenvalues of $\hat{\Phi}$, is $\mathrm{disc}(\hat{\Phi}) = 4r_0^2$. The profile of $\|\hat{\Phi}\|^2$ is qualitatively in agreement with numerical investigations of n equally spaced monopoles as n is increased, [DK05].

We next use the divergence theorem to compute the total energy enclosed in a region with $\rho = R \gg C$

$$V_1 \;=\; \frac{1}{4}\iiint_{\rho\le R} \nabla^2 |\mathrm{tr}(\hat{\Phi})^2|\,\rho\,d\rho\,d\theta\,dz \;=\; \frac{R\beta}{4}\int_{\rho=R}\Big(\partial_\rho |\mathrm{tr}(\hat{\Phi})^2|\Big)\,d\theta$$

and note that the leading term of the integrand at large ρ is

$$\partial_\rho |\mathrm{tr}(\hat{\Phi})|^2 \;\sim\; \frac{4}{\rho\beta^2}\log\left(\frac{2\rho}{C}\right),$$

resulting in

$$V_1 \;=\; \iiint_{\rho\le R} \mathcal{E}_1\,\rho\,d\rho\,d\theta\,dz \;=\; \frac{2\pi}{\beta}\log\left(\frac{2R}{C}\right) \tag{3.11}$$

in agreement with (2.8). Finally, we note that the Higgs field (3.9) vanishes along a line between the spectral points, figure 3.1. This observation survives for higher charges and gauge groups, where the discriminant of the Higgs field vanishes along lines joining the constituents in pairs. Unlike in the case of the periodic instanton (which develops monopole constituents, section 1.5), this illustrates how the constituents of the periodic monopole are confined. Separating the constituents by increasing C changes the boundary data and leads to non L^2 normalisable deformations of the fields. This fixes C as a parameter rather than a modulus.

As an alternative to using the monopole energy formula (1.7), the energy density (3.10) can also be obtained from a Bogomolny argument for Hitchin equations (the U(1) version of which is given in [Saç84]),

$$\mathcal{E} = -\mathrm{tr}\left(\left(\hat{F}_{\zeta\bar{\zeta}} - \frac{1}{4}\left[\hat{\phi},\hat{\phi}^\dagger\right]^2 \right)^2 + \left(\hat{D}_{\bar{\zeta}}\hat{\phi}\right)\left(\hat{D}_{\zeta}\hat{\phi}^\dagger\right) - \frac{\mathrm{i}}{4}\left(\partial_x(\hat{\phi}\hat{D}_y\hat{\phi}^\dagger) - \partial_y(\hat{\phi}\hat{D}_x\hat{\phi}^\dagger)\right)\right). \tag{3.12}$$

The energy is minimised by setting the first two terms to zero, which are the Hitchin equations and are automatically satisfied by the fields (3.8). Evaluating the third term recovers (3.10). The total energy can be computed using Green's theorem in the plane, giving the energy (3.11) up to a factor of β for the z integral.

3.2 Charge 2

In this section we apply the spectral approximation to the SU(2) monopole of charge $\boldsymbol{k} = (2)$, which has two real reduced moduli. Using symmetries of the spectral curves this can be reduced to two one-parameter families, although we withhold showing that this two dimensional reduced moduli space is itself a geodesic submanifold of the full four dimensional moduli space until section 4.1.2.

In the limit of large monopole size to period ratio in which the spectral approximation becomes exact it is possible to compute a metric on the two dimensional reduced moduli space. Its asymptotic form agrees with the ALG metric of [ChK02], allowing numerical integration of non-trivial geodesics, which will be considered both in the monopole space and on the dual cylinder. Finally,

we will study two solutions of the rank 2 Hitchin system with the same spectral curve [HW09, Har*a*], and briefly compare their scattering properties.

3.2.1 Spectral Approximation

The general form of the monopole spectral curve (2.16) of the charge $\boldsymbol{k} = (2)$ periodic monopole is

$$w^2+P_{1,2}(\zeta)w+1 \,=\, 0 \qquad \text{with} \qquad P_{1,2}(\zeta) \,=\, -\left(2\zeta^2 - 2BC\zeta - K\right)/C \tag{3.13}$$

with $B, K \in \mathbb{C}$. The spectral points are located at the values of ζ where $(P_{1,2}(\zeta))^2 = 4$. Fixing the centre of mass at the origin ($B = 0$), we expect energy peaks at the four points

$$\zeta_i \,=\, \pm\sqrt{K/2 \pm C} \tag{3.14}$$

(where the $\pm$ signs are independent).[8] As in the $\boldsymbol{k} = (1)$ case, C is a parameter fixed by the boundary conditions, while K is a complex modulus. For $|K|/C \gg 2$ the spectral points occur in two pairs which are interpreted as fundamental monopoles of size $|C\sqrt{2/K}|$ separated by a distance $|\sqrt{2K}|$. It is noteworthy that the fundamental monopoles get smaller as they are separated, an effect of the long range Higgs field.

Motivated by (3.7) we assume the monopole Higgs field is given by $\hat{\Phi} = \mathrm{iRe}(s_0)\sigma_3$, where s_0 is obtained by rearranging the spectral curve for $s(\zeta)$,

$$\hat{\Phi} \,=\, \frac{\mathrm{i}}{\beta}\,\mathrm{Re}\left(\cosh^{-1}\left(\frac{2\zeta^2 - K}{2C}\right)\right)\sigma_3 \tag{3.15}$$

and compute the energy in the region $|\zeta| \leq R$, with $R \gg \sqrt{K}$, using (1.7) to find

$$V_2 \,=\, \frac{4\pi}{\beta}\log\left(\frac{2R^2}{C}\right),$$

again in agreement with (2.8). Applying the divergence theorem to $\partial_K\mathcal{E}$ for large ρ,

$$\partial_K\mathcal{E}_{\in} \,\propto\, \partial_K\partial_\rho|\mathrm{tr}(\hat{\Phi}^2)| \,\sim\, \rho^{-3}\log(\rho),$$

confirms that the total energy is independent of the modulus K.

[8] Note that to regain the $\boldsymbol{k} = (1)$ limit we should instead fix $K = 0$, $B \neq 0$ and let $C \to \infty$.

The energy density of a generic SU(2) periodic monopole with spectral curve

$$w^2 + P(\zeta)w + 1 \;=\; 0 \tag{3.16}$$

is obtained from (1.7) via the roots

$$w_\pm(\zeta) \;=\; \frac{1}{2}\left(-P(\zeta) \pm \sqrt{P^2(\zeta) - 4}\right)$$

as

$$\mathcal{E} \;=\; \frac{1}{4}\nabla^2\left((\mathrm{Re}(\log w_+))^2 + (\mathrm{Re}(\log w_-))^2\right). \tag{3.17}$$

Expanding about a point $\zeta = \zeta_0 + \epsilon$, we have $P(\zeta) = P(\zeta_0) + \epsilon P'(\zeta_0) + \mathcal{O}(\epsilon^2)$ and

$$w_\pm \;=\; \frac{1}{2}\left(-P(\zeta_0) - \epsilon P'(\zeta_0) + \cdots \pm \sqrt{(P^2(\zeta_0) - 4) + 2\epsilon P(\zeta_0)P'(\zeta_0) + \ldots}\right).$$

The energy density (3.17) is computed at $\zeta = \zeta_0$ using polar coordinates $\epsilon = \rho \mathrm{e}^{\mathrm{i}\theta}$ centered at ζ_0, and will be finite unless $w_\pm$ contains terms of order ϵ^ℓ with $\ell < 1$. The energy is thus finite everywhere except at those points $\zeta = \zeta_0$ for which $P^2(\zeta_0) = 4$ (in which case the square root introduces a factor of $\epsilon^{1/2}$). In particular, the energy density has a simple pole where the discriminant of (3.16) vanishes. The only exception to this is when $P'(\zeta_0) = 0$, in which case the square root contributes a term of order ϵ and the energy is finite. For the charge 2 monopole, this has the effect of giving a finite energy where two spectral points coincide.

The preceding argument is given for its relevance to monopoles in higher gauge groups: the quadratic spectral curve (3.16) then becomes a cubic or higher order polynomial. A similar argument can be made regarding the positions of energy peaks at spectral points. However, as will be seen in section 3.4, it is not necessarily the case that for gauge groups other than SU(2) the energy density should be finite when two spectral points coincide.

3.2.2 Symmetric Charge k

The spectral curve of the dihedral D_{2k}-symmetric charge $\boldsymbol{k} = (k)$ monopole is

$$C\cosh(\beta s) \;=\; \zeta^k \qquad \Rightarrow \qquad \hat{\Phi} \;=\; \frac{\mathrm{i}}{\beta}\,\mathrm{Re}\left(\cosh^{-1}\left(\frac{\zeta^k}{C}\right)\right)\sigma_3.$$

This time we compute the energy density using the general formula

$$\mathcal{E} \;=\; \frac{1}{\beta^2}\left|\frac{\partial_\zeta P}{\sqrt{P^2-4}}\right|^2 \qquad \text{where} \qquad \hat{\Phi} \;=\; \frac{\mathrm{i}}{\beta}\,\mathrm{Re}\left(\cosh^{-1}\left(\frac{P(\zeta)}{2}\right)\right)\sigma_3,$$

from which we again see that the energy density is peaked at the spectral points unless $\partial_\zeta P(\zeta) = 0$ there. For the case $P(\zeta) = 2\zeta^k/C$, the spectral points are located on a circle of radius $\rho = C^{1/k}$ and the energy density is

$$\mathcal{E}_k \;=\; \frac{k^2}{\beta^2}\frac{\rho^{2k-2}}{\sqrt{\rho^{4k} - 2C^2\rho^{2k}\cos(2k\theta) + C^4}}, \tag{3.18}$$

where we note that the energy density at the origin vanishes for all $k > 1$. The total energy obtained from this formula is again in agreement with (2.8), while the energy per unit charge in the region $0 \le \rho \le aC^{1/k}$ is

$$\begin{aligned}\frac{V_k}{k}\left(0 \le \rho \le aC^{1/k}\right) &= \frac{\pi a^{2k}}{\beta}\,{}_3F_2\left(\tfrac{1}{2},\tfrac{1}{2},\tfrac{1}{2};1,\tfrac{3}{2};a^{4k}\right) \\ &= \begin{cases} \pi a^{2k}\left(1+\mathcal{O}(a^{4k})\right)/\beta & (a<1) \\ 4G/\beta & (a=1) \end{cases}\end{aligned} \tag{3.19}$$

where ${}_3F_2$ is the generalised hypergeometric function, $G \approx 0.916$ is Catalan's constant and we have used the following identities for the elliptic integral $\mathbf{K}(\kappa)$ [GR94*a*]:

$$\mathbf{K}(\kappa) \;=\; \int_0^{\pi/2} \frac{1}{\sqrt{1-2\kappa\cos(2\alpha)+\kappa^2}}\,d\alpha \qquad\qquad (\kappa<1), \tag{3.20}$$

$$4ab\int_0^z \kappa^{2ab-1}\mathbf{K}(\kappa^b)\,d\kappa \;=\; \pi z^{2ab}\,{}_3F_2\left(\tfrac{1}{2},\tfrac{1}{2},a;1,a+1;z^{2b}\right). \tag{3.21}$$

Figure 3.2 shows how the total energy in a period cylinder, (3.19), is increasingly located at its edge as k is increased. An expansion of the fields at small and large ρ yields

$$\begin{cases} -\mathrm{i}\beta\hat{\Phi} \;\sim\; (\rho^k/C)\sin(k\theta)\sigma_3 & (\rho^k \ll C), \\ -\mathrm{i}\beta\hat{\Phi} - \log\left(2\rho^k/C\right)\sigma_3 \;\sim\; (2\rho^k/C)^{-2}\cos(2k\theta)\sigma_3 & (\rho^k \gg C). \end{cases}$$

These results resemble those found for spherical magnetic bags of large charge, as first studied by [Bol06], and it is interesting to see evidence of a 'magnetic cylinder' with similar properties.

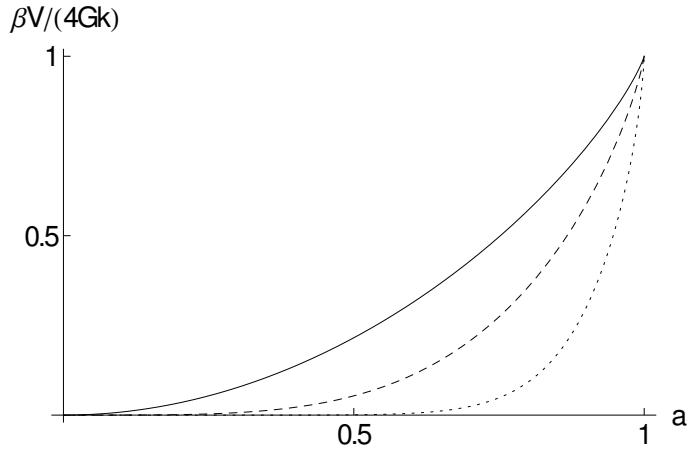

Figure 3.2: Normalised energy per unit charge enclosed in a period cylinder of radius $aC^{1/k}$ for various values of the charge k. Solid line: $k = 1$, dashed: $k = 2$, dotted: $k = 10$. The energy density is increasingly located on a shell of radius $\rho = C^{1/k}$.

3.2.3 Symmetries

Geodesic submanifolds of the two dimensional reduced moduli space are obtained by looking at symmetries of the spectral curve (3.13). Fixing the parameters $B = 0$ and $C \in \mathbb{R}$, we impose invariance of (3.13) under a reflection symmetry in the line $\theta = \alpha/2$, encoded by the map $\zeta \mapsto \mathrm{e}^{\mathrm{i}\alpha}\bar{\zeta}$. This requires that we simultaneously map $w \mapsto \mathrm{e}^{-2\mathrm{i}\alpha}\bar{w}$ ($t \mapsto -t - 2\alpha/\beta$) and $K \mapsto \mathrm{e}^{2\mathrm{i}\alpha}\bar{K}$. The original spectral curve (3.13) is recovered by complex conjugation as long as α is chosen to be 0 or $\pi/4$. These choices of α correspond to the one parameter families $K \in \mathbb{R}$ and $K \in \mathrm{i}\mathbb{R}$, respectively. In section 4.1 it will be shown that the reduced moduli provide a geodesic submanifold of the full four dimensional moduli space, allowing us to consider the above one parameter families as geodesics. The definition of a metric on the reduced moduli space will be considered in the following section.

More information about these geodesics can be obtained by considering the $\pi/2$ rotation symmetry $\zeta \mapsto \mathrm{i}\zeta$, which requires $w \mapsto -w$ ($t \mapsto t + \pi/\beta$) and $K \mapsto -K$. For the one parameter families found above, passing through $K = 0$ leads to the right angled scattering processes shown in figure 3.3 overleaf. Particularly interesting points in the moduli space are $K/C = \pm 2$, where two of the spectral points coincide at the origin (although there is no energy peak associated with them) and $K = 0$, where the D_2 symmetry is enhanced to D_4. This is nothing but the symmetric configuration considered in section 3.2.2. Away from the families $K \in \mathbb{R}$ and $K \in \mathrm{i}\mathbb{R}$, the symmetry group is the cyclic

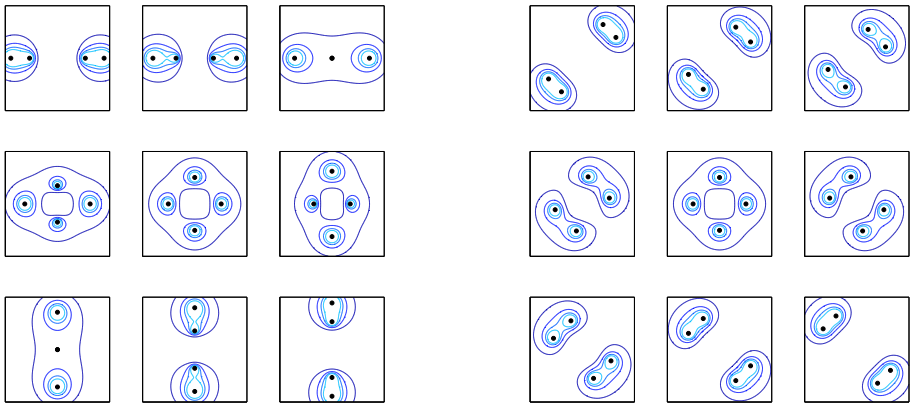

Figure 3.3: Energy density contour plots for charge $k = 2$ within the spectral approximation. Left: geodesic with $K \in \mathbb{R}$ (to be read from left to right and top to bottom). Right: geodesic with $K \in \mathrm{i}\mathbb{R}$. The central symmetric configurations have $K = 0$, while those with just two energy peaks have $K/C = \pm 2$. It is noteworthy that the axial symmetry of the 'doughnut' charge 2 monopole in $\mathbb{R}^3$ [War81] is replaced by a discrete dihedral (D_4) symmetry. Note how the constituents themselves (indicated by black dots) as well as the monopoles as a whole undergo 90° scattering. The spacing between snapshots is taken relative to the metric defined in section 3.3.

group C_2. For $K/C \in [-2, 2]$ the fundamental monopoles lose their individual identities and the discriminant vanishes on a cross shape joining the four peaks.

3.3 Metric

In this section we compute the asymptotic metric of the monopole fields (3.8) for a charge 2 periodic monopole within the spectral approximation. The results are compared to the asymptotic metric obtained by considering the interaction of well separated monopole chains, [ChK02]. Assuming our metric is globally accurate when the spectral approximation is valid, we compute new monopole scattering processes and discuss the dual motion of the zeros of the Hitchin Higgs field Φ on the cylinder.

3.3.1 Definition

We use the general formalism for obtaining the moduli space metric from the variation of the fields (section 1.4). For z-independent fields the metric is given

by

$$g = \frac{1}{2}\dot{K}\dot{\bar{K}}\int_{\mathbb{R}^2}\mathrm{tr}\left(\delta\hat{\phi}\delta\bar{\hat{\phi}}^\dagger + \delta\hat{\phi}^\dagger\delta\bar{\hat{\phi}} - 4\delta\hat{a}_{\bar{\zeta}}\delta\bar{\hat{a}}_\zeta - 4\delta\hat{a}_\zeta\delta\bar{\hat{a}}_{\bar{\zeta}}\right)\rho d\rho d\theta \tag{3.22}$$

where it is understood that the fields satisfy the gauge condition (see section 1.4)

$$4\left(\hat{D}_\zeta\delta(\hat{a}_{\bar{\zeta}}) + \hat{D}_{\bar{\zeta}}\delta(\hat{a}_\zeta)\right) = [\hat{\phi}, \delta(\hat{\phi}^\dagger)] + [\hat{\phi}^\dagger, \delta\hat{\phi}] \tag{3.23}$$

which arises as a dimensional reduction of the equivalent gauge orthogonality condition for instantons, $D_\mu(\delta A_\mu) = 0$. Here δ indicates differentiation with respect to K, and $\dot{}$ is differentiation with respect to an affine time τ.

From (3.8) there is a centered charge 2 solution of the Bogomolny equations with

$$\beta\hat{\phi} = \cosh^{-1}\left(\frac{2\zeta^2 - K}{2C}\right)\sigma_3 \qquad\qquad \hat{a} = 0,$$

valid sufficiently far from the spectral points, for which the orthogonality condition (3.23) holds trivially and only the first term in (3.22) contributes. As discussed in section 3.1.1, it will be assumed that this becomes exact in the limit of z independence. It follows that the metric is given by

$$g = \frac{1}{4\beta^2}\dot{K}\dot{\bar{K}}\int\frac{1}{\sqrt{(\zeta^2 - K/2)^2 - C^2}}\frac{1}{\sqrt{(\bar{\zeta}^2 - \bar{K}/2)^2 - C^2}}\,\rho\,d\rho\,d\theta. \tag{3.24}$$

For given K the integral can be written in terms of products of distances to the four spectral points, which are located at $\zeta_i(K) = \pm\sqrt{K/2 \pm C}$, defining the conformal factor $\Omega(K)$,

$$g = \frac{1}{4\beta^2}\dot{K}\dot{\bar{K}}\int\frac{1}{|\zeta - \zeta_1||\zeta - \zeta_2||\zeta - \zeta_3||\zeta - \zeta_4|}\,\rho\,d\rho d\theta = \Omega\dot{K}\dot{\bar{K}}.$$

3.3.2 Asymptotics

The integral in (3.24) can be computed in the limit in which the monopoles are well separated, $|K|/C \gg 2$. Two of the peaks are placed near the origin, at $\zeta = \pm\epsilon$, and the others are centered at some large distance R along the x-axis (for simplicity we consider $K = k\mathrm{e}^{\mathrm{i}\varphi} \in \mathbb{R}$). Integrating out to some ρ_0 (with $R \gg \rho_0 \gg \epsilon$),

$$\Omega \sim \frac{1}{R^2}\int_0^{\rho_0}\frac{1}{|\zeta + \epsilon||\zeta - \epsilon|}\,\rho\,d\rho\,d\theta.$$

This integrand is identical to that of (3.18), so

$$\Omega \sim \frac{1}{R^2} \log\left(\frac{2\rho_0}{\epsilon}\right).$$

We recall from section 3.2.1 that the separation R and size 2ϵ of the fundamental monopoles in this limit are, respectively, given by

$$R = (2k)^{1/2} \qquad \epsilon = C(2k)^{-1/2} = C/R, \tag{3.25}$$

allowing us to express the metric either in terms of k or of the monopole separation R,

$$g \sim \frac{1}{k}\left(\log(k) + c\right)\dot{k}^2 \sim \left(\log(R) + c'\right)\dot{R}^2.$$

The latter agrees, up to prefactors, with the asymptotic metric computed in [ChK02], which is an ALG metric of limiting Gibbons-Hawking type [GH78]. The constants c and c' depend on the upper limit of integration ρ_0 and are related to the redefinition of $\mathfrak{v}$ performed in [ChK02] when a chain of n monopoles is studied in the limit of $n \to \infty$. The same asymptotic form of the metric will be recovered more carefully in section 4.3.

3.3.3 Integration

There are three specific values of K at which evaluation of the conformal factor $\Omega(K)$ can be performed analytically (see figure 3.3 for the relevant monopole configurations),

$$\begin{aligned} K &= 0 && \Omega = \frac{1}{32\pi\beta^2 C}\left(\Gamma\left(\tfrac{1}{4}\right)\right)^4 \\ K &\to \pm 2C && \Omega \sim -\frac{\pi}{8\beta^2 C}\log\left(|K \mp 2C|\right) \end{aligned} \tag{3.26}$$

where, for $K = 0$, use has been made of (3.21). The integral diverges at $K/C = \pm 2$, when two of the spectral points coincide and there is a double pole in the integrand. We employ these results to ensure a correct numerical implementation of the integral for general K, and the result is shown in figure 3.4. Further evidence for this metric will be provided in section 4.3.2.

Using polar coordinates $K = k\mathrm{e}^{\mathrm{i}\varphi}$, the geodesic equations are

$$\begin{aligned} 2\Omega k^2\ddot{\varphi} + (\partial_\varphi\Omega)(k^2\dot{\varphi}^2 - \dot{k}^2) + 2(\partial_k\Omega)k^2\dot{\varphi}\dot{k} + 4\Omega k\dot{\varphi}\dot{k} &= 0 \\ 2\Omega\ddot{k} + (\partial_k\Omega)(\dot{k}^2 - k^2\dot{\varphi}^2) + 2(\partial_\varphi\Omega)\dot{\varphi}\dot{k} - 2\Omega k\dot{\varphi}^2 &= 0 \end{aligned} \tag{3.27}$$

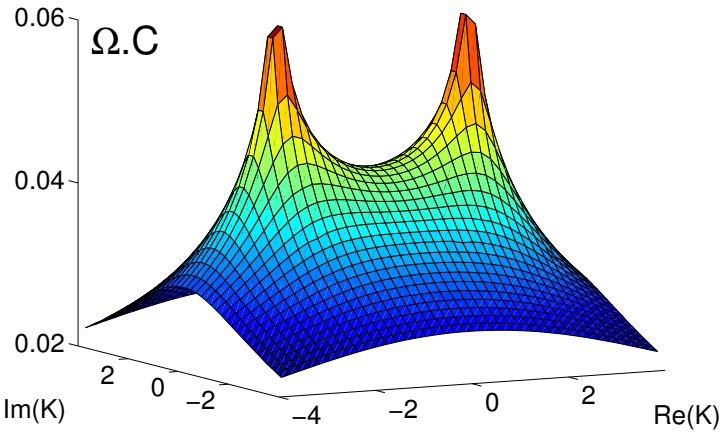

Figure 3.4: Surface plot of the conformal factor, computed from (3.24), for the relative reduced moduli space in the limit of large monopole size to period ratio, with $\beta = 2\pi$. The infinite peaks (3.26) are at $K/C = \pm 2$.

where $\dot{}$ denotes differentiation with respect to the parameter time τ. In particular, there are geodesics with $\dot{\varphi} = 0$, for which the geodesic equations become $\partial_\varphi \Omega = 0$ and

$$2\Omega\ddot{k} + (\partial_k \Omega)\dot{k}^2 \;=\; 0 \qquad \Rightarrow \qquad \int \sqrt{\Omega}\, dk \;=\; b_1\tau + b_2, \tag{3.28}$$

where b_1 and b_2 are constants of integration. As can be seen from figure 3.4 such geodesics are only possible for $\varphi = 0, \pi/2$, which are precisely the geodesic submanifolds $K \in \mathbb{R}$ and $K \in \mathrm{i}\mathbb{R}$ obtained by symmetry arguments in section 3.2.3.

The logarithmic behaviour of Ω in the vicinity of $K/C = \pm 2$ (equation 3.26), combined with the implicit expression for $k(\tau)$ (3.28), is sufficient to show that geodesics can cross the points $K/C = \pm 2$ in finite parameter time. The more complete treatment of the Hitchin system carried out in section 4.1 and [MW13], valid outside of the spectral approximation, shows a branching behaviour at $K/C = \pm 2$, with some geodesics capable of crossing these points, while others appear to turn back on themselves.

3.3.4 New Geodesics

In complex coordinates the geodesic equations (3.27) are

$$\Omega\ddot{K} + (\partial_K \Omega)\dot{K}^2 \;=\; 0$$

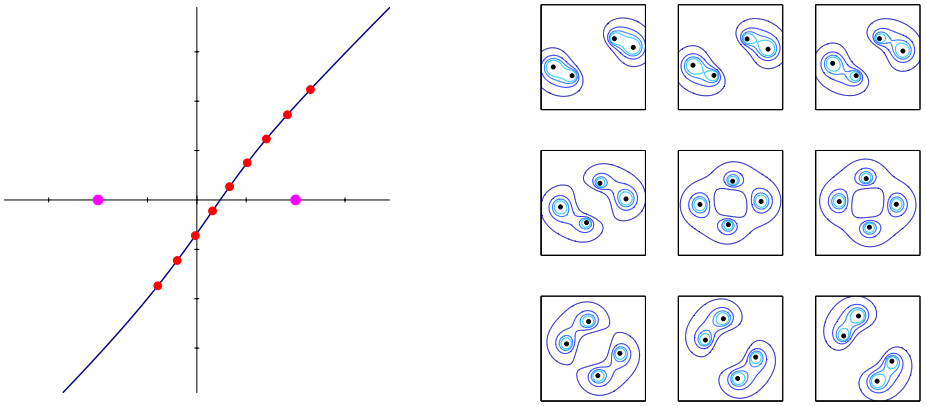

Figure 3.5: Geodesic for initial condition $K/C = 5(1+\mathrm{i})$, $\dot{K}/C = -0.03(1+\mathrm{i})$ with step size 0.03. The left hand plot displays the geodesic on the K-plane (with shaded circles at $K/C = \pm 2$). Tick marks every 722 timesteps indicate the positions of the energy density snapshots displayed to the right.

and its complex conjugate. We write this as a system of coupled partial differential equations,

$$\Omega\dot{v} + (\partial_K\Omega)v^2 \;=\; 0 \qquad\qquad \dot{K} \;=\; v$$

and obtain $\partial_K\Omega$ by differentiating the integrand of Ω before performing the integral (this choice of ordering was found to give greater numerical precision),

$$\partial_K\Omega = \frac{1}{2}\int (\zeta^2 - K/2)\left((\zeta^2 - K/2)^2 - C^2\right)^{-3/2}\left((\bar{\zeta}^2 - \bar{K}/2)^2 - C^2\right)^{-1/2}\rho\, d\rho\, d\theta,$$

which must again be integrated numerically. Then, by specifying initial values of K and $\dot{K}$, geodesics are integrated using a fourth order Runge-Kutta procedure. Two such non-trivial geodesics are displayed in figures 3.5 and 3.6, which are to be compared with those of figure 3.3. It is worth noting that geodesics crossing the line segment $-2 < K/C < 2$ (figure 3.5) scatter by swapping constituents, otherwise there is glancing scattering and each fundamental monopole retains its identity (figure 3.6). As was seen in figure 3.3, a geodesic meeting $K/C = \pm 2$ has two coincident spectral points, whose associated energy density vanishes. Numerical examples suggest that the only geodesic to cross these points is that with $K \in \mathbb{R}$.

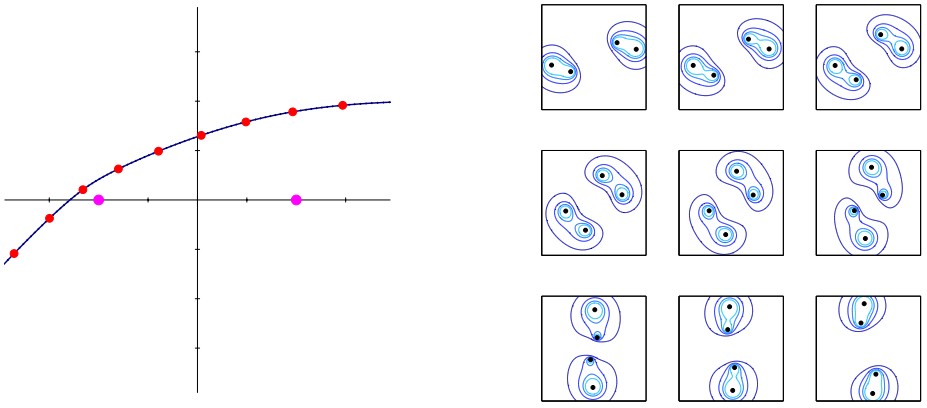

Figure 3.6: Geodesic for initial conditions $K/C = 5 + 2\mathrm{i}$, $\dot{K}/C = -0.042$ with step size 0.03. Tick marks are at every 950 timesteps. In this case the fundamental monopoles retain their separate identities.

3.3.5 Zeros on the Cylinder

Rewriting the spectral curve (3.13) as a polynomial in ζ and comparing with (2.18) we find

$$\zeta^2 - (C\cosh(\beta s) + K/2) = 0 \qquad \Rightarrow \qquad -\det(\Phi) = C\cosh(\beta s) + K/2.$$

Note how setting $B = 0$ means there is no term of order ζ, so Φ is traceless. The determinant of the Hitchin Higgs field has two zeros whose locations on the cylinder depend on K/C. In section 4.1 we will see that these values are of interest as they provide approximate locations for peaks in the gauge field $F_{s\bar{s}}$ on the Hitchin cylinder, defined through equation 2.11. As $\det(\Phi)$ is an even function of s, the zeros are always on opposite sides of the cylinder, at $s = \pm s_0$. They are located on the circle $r = 0$ if $-2 \leq K/C \leq 2$ and coincide at $s_0 = \mathrm{i}\pi/\beta, 0$ if $K/C = 2, -2$. This again illustrates, as discussed in section 3.2.3, that $K = 0$ is a particularly symmetric case, for which the zeros are at $\pm\mathrm{i}\pi/2\beta$. The motion of the zeros corresponding to the geodesics with $K \in \mathbb{R}$ and $K \in \mathrm{i}\mathbb{R}$ are shown in figures 3.7 and 3.8 overleaf. Other geodesics, such as those of figures 3.5 and 3.6, lead either to glancing scattering of the zeros (if K/C passes between -2 and 2, figure 3.5) or to them returning in the same direction they came in from (if K/C does not cross the line segment $[-2, 2]$, figure 3.6).

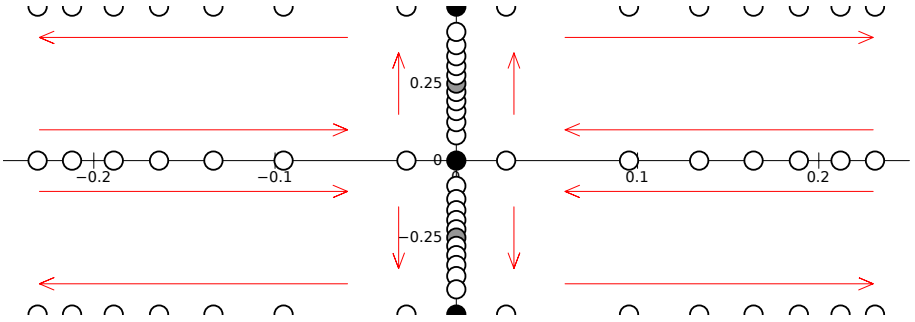

Figure 3.7: Motion of zeros on the Hitchin cylinder for $K \in \mathbb{R}$, where the top and bottom edges of the diagram are identified and the z period is taken to be $\beta = 2\pi$. Arrows indicate the direction of K increasing from $K/C = -4.5$, with spacing determined by the velocity using the metric (3.24). The black dots are at $K/C = \pm 2$ (note that in these cases the zeros coincide), while the grey dots are at $K = 0$. Zeros at the same K are located at opposite points on the cylinder, obtained by reversing the signs of r and t.

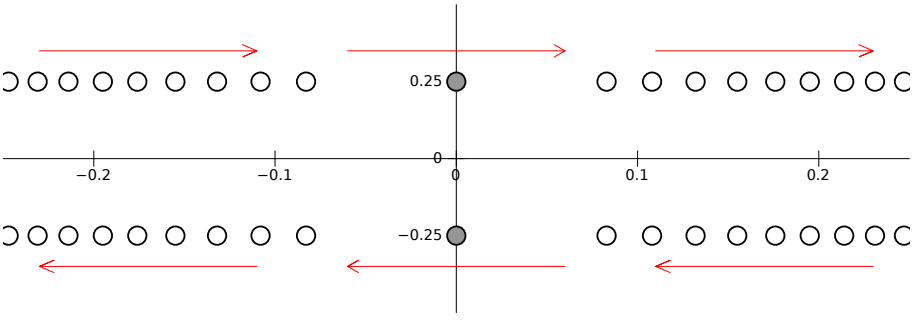

Figure 3.8: The setup is the same as that of figure 3.7, this time with $K \in \mathrm{i}\mathbb{R}$. The arrow indicates the evolution with $\mathrm{Im}(K)$ increasing from $\mathrm{Im}(K) = -4.5$.

3.4 SU(3) Periodic Monopoles

Monopoles in $\mathbb{R}^3$ have been considered for higher rank gauge groups by various authors [Wei80, LWY96, MS04, Shn]. In this section we apply the results of the spectral approximation to the SU(3) periodic monopole and consider the basic properties for $\boldsymbol{k} = (1,1)$ and $\boldsymbol{k} = (2,1)$, which have two and four reduced relative moduli, respectively.

Following the arguments of section 2.1, the SU(3) periodic monopole has spectral curve (2.16)

$$w^3 + P_{1,k_1}(\zeta)w^2 + P_{2,k_2}(\zeta)w - 1 \;=\; 0 \tag{3.29}$$

where

$$P_{i,k_i}(\zeta) \;=\; a_{i,k_i}\zeta^{k_i} + \ldots + a_{i,1}\zeta + a_{i,0}.$$

As discussed in sections 2.1 and 2.3, we take $k_1 \geq k_2$. The root diagram was shown in figure 2.1. Our procedure will be to express the coefficients of $P_{i,k_i}(\zeta)$ in terms of the boundary data (2.4, 2.10) and hence to determine the positions of spectral points from the discriminant $\mathcal{D}_{(k_1,k_2)}$, which we obtain from the rank $(2N-1)$ Sylvester matrix,

$$\mathcal{D}_{(k_1,k_2)} \;=\; \det \begin{pmatrix} 1 & P_{1,k_1} & P_{2,k_2} & -1 & 0 \\ 0 & 1 & P_{1,k_1} & P_{2,k_2} & -1 \\ 3 & 2P_{1,k_1} & P_{2,k_2} & 0 & 0 \\ 0 & 3 & 2P_{1,k_1} & P_{2,k_2} & 0 \\ 0 & 0 & 3 & 2P_{1,k_1} & P_{2,k_2} \end{pmatrix}.$$

In analogy with sections 3.1.1 and 3.2.1, we are interested in the eigenvalues of the holonomy V, i.e. the solutions to the cubic equation (3.29) for $w(\zeta)$. This manipulation is performed numerically to give three eigenvalues $w_i = \exp(\beta(r_i + \mathrm{i}t_i))$ from which $\hat{\Phi} \propto \mathrm{diag}(r_1, r_2, r_3)$ and the quantities of interest are[9]

$$\mathcal{E} \;\propto\; \nabla^2\left(r_1^2 + r_2^2 + r_3^2\right), \qquad\qquad \text{discriminant} \;=\; (r_1 - r_2)^2(r_2 - r_3)^2(r_3 - r_1)^2.$$

[9] Recall that in the SU(2) case (section 3.1 and figure 3.1) a similar calculation gave $\hat{\Phi} = \mathrm{i}r_0\sigma_3$, $\mathcal{E} \propto \nabla^2 r_0^2$ and disc. $= 4r_0^2$.

3.4.1 Trivial Embedding

For $\boldsymbol{k} = (1,1)$, symmetry breaking is maximal (the entries of $\boldsymbol{\ell} = (1,0,-1)$ are all distinct) and we use the standard form of the holonomy (2.10) to identify the spectral curve coefficients with the asymptotic data $\mathfrak{v}$, $\boldsymbol{\mu}$ by

$$\boldsymbol{k} = (1,1) \qquad \begin{cases} a_{1,1} = -\mathrm{e}^{\mathfrak{v}_1} & a_{1,0} = -(\mu_1 \mathrm{e}^{\mathfrak{v}_1} + \mathrm{e}^{\mathfrak{v}_2}) \\ a_{2,1} = \mathrm{e}^{\mathfrak{v}_1+\mathfrak{v}_2} & a_{2,0} = (\mu_1+\mu_2)\mathrm{e}^{\mathfrak{v}_1+\mathfrak{v}_2} + \mathrm{e}^{-\mathfrak{v}_2}. \end{cases} \tag{3.30}$$

The discriminant is

$$\mathcal{D}_{(1,1)} = a_{1,1}^2 a_{2,1}^2 \zeta^4 + 2\left(a_{1,1}a_{2,1}(a_{1,1}a_{2,0} + a_{1,0}a_{2,1}) + 2(a_{1,1}^3 - a_{2,1}^3)\right)\zeta^3 + \ldots, \tag{3.31}$$

such that the spectral points are centered if the coefficient of ζ^3 vanishes,

$$(2\mu_1 + \mu_2)\mathrm{e}^{\mathfrak{v}_1+2\mathfrak{v}_2} = \mathrm{e}^{3\mathfrak{v}_2} + 1.$$

As noted in section 2.3, the fact K is repeated (i.e. $\ell_2 = 0$) means the Nahm data will in general have a singularity at finite $|r|$, namely at $s = \mathfrak{v}_2/\beta$. As we are working with SU(3) the determinant will also have three zeros.

If $\mathfrak{v}_2 = 0$ and $\mu_2 = 0$ (such that the centering condition becomes $\mu_1 \mathrm{e}^{\mathfrak{v}_1} = 1$) then the monopole is an SU(2) monopole embedded along the root $\boldsymbol{\beta}_3^* = -\boldsymbol{\beta}_1^* - \boldsymbol{\beta}_2^*$. This allows the spectral curve to be factorised,

$$(w-1)\left(w^2 - (\mathrm{e}^{\mathfrak{v}_1}\zeta + 1)w + 1\right) = 0.$$

In this limit, three of the spectral points coincide and, as expected, the monopole fields resemble those of an SU(2) monopole with $\boldsymbol{k} = (1)$. In this case the Nahm data is smooth, as the singularity coincides with one of the zeros.

$\underline{\mathfrak{v}_2 \neq 0}$

We deform away from the SU(2) embedding by changing the boundary conditions to allow non-zero $\mathfrak{v}_2$. The spectral curve again factorises, and centering identifies

$$a_{1,0} = -\frac{1}{2}\left(3\mathrm{e}^{\mathfrak{v}_2} + \mathrm{e}^{-2\mathfrak{v}_2}\right) \qquad a_{2,0} = \frac{1}{2}\left(\mathrm{e}^{2\mathfrak{v}_2} + 3\mathrm{e}^{-\mathfrak{v}_2}\right).$$

with $a_{1,1}$ and $a_{2,1}$ as in (3.30). The situation is shown in figure 3.9. In the Nahm picture, the Higgs field has a simple pole at $s = \mathfrak{v}_2/\beta$. For $\mu_2 = 0$ one of

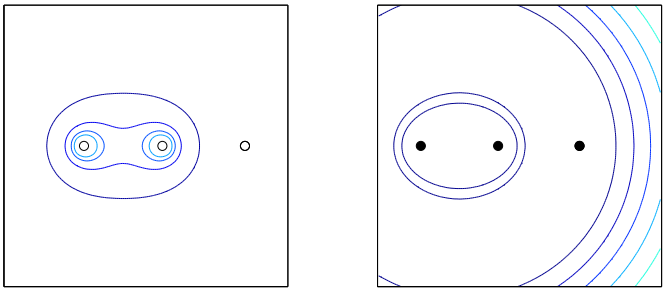

Figure 3.9: Deformations of the $\boldsymbol{k} = (1,1)$ monopole by changing $\mathfrak{v}_2$ away from zero. Here $\mathfrak{v}_2 = 1.2$ and $\mu_2 = 0$. On the left is plotted the energy density and on the right the discriminant of $\hat{\Phi}$. There is no energy density associated with the coincident spectral points on the right. The discriminant vanishes on a line joining the spectral points on the left, and on a circle passing through the double spectral point and surrounding the other two.

the zeros coincides with the pole, giving the two zeros characteristic of SU(2) solutions.

$\mu_2 \neq 0$

In a similar way, we can fix the boundary conditions to $\mathfrak{v}_2 = 0$ and allow the moduli μ_1 and μ_2 to vary in such a way that the spectral points remain centered. The coefficients in (3.30) become

$$\begin{aligned} a_{1,1} &= -\mathrm{e}^{\mathfrak{v}_1} & a_{1,0} &= -(1+\mu_1\mathrm{e}^{\mathfrak{v}_1}) \\ a_{2,1} &= \mathrm{e}^{\mathfrak{v}_1} & a_{2,0} &= 3-\mu_1\mathrm{e}^{\mathfrak{v}_1}. \end{aligned}$$

Varying μ_1 separates the three coincident spectral points and introduces a second fundamental monopole, as shown in figure 3.10 overleaf.

3.4.2 Minimal Symmetry Breaking

The $\boldsymbol{k} = (2,1)$ spectral curve has

$$\boldsymbol{k} = (2,1) \qquad \begin{cases} a_{1,2} = -\mathrm{e}^{\mathfrak{v}_1} & a_{1,1} = -\mu_1\mathrm{e}^{\mathfrak{v}_1} \\ a_{2,1} = \mathrm{e}^{\mathfrak{v}_1+\mathfrak{v}_2} + \mathrm{e}^{-\mathfrak{v}_2} & a_{2,0} = (\mu_1+\mu_2)\mathrm{e}^{\mathfrak{v}_1+\mathfrak{v}_2} - \mu_2\mathrm{e}^{-\mathfrak{v}_2}, \end{cases}$$

and discriminant

$$\mathcal{D}_{(2,1)} = a_{1,2}^2\left(a_{2,1}^2 + 4a_{1,2}\right)\zeta^6 + 2a_{1,2}\left(a_{1,2}a_{2,1}a_{2,0} + a_{1,1}a_{2,1}^2 + 6a_{1,1}a_{1,2}\right)\zeta^5 + \ldots$$

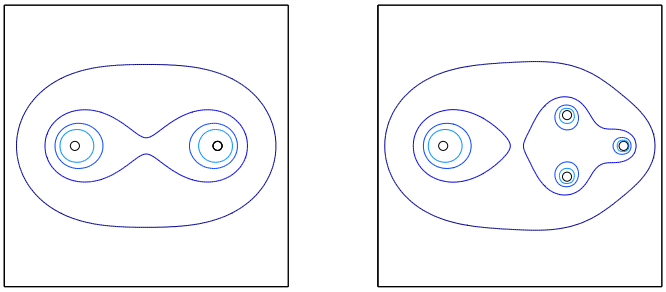

Figure 3.10: Deformations of the $\boldsymbol{k} = (1,1)$ monopole with $\mathfrak{v}_2 = 0$. On the left are contours of energy density for $\mu_1 \mathrm{e}^{\mathfrak{v}_1} = 1$. On the right, for $\mu_1 \mathrm{e}^{\mathfrak{v}_1} = 1.2$. For these examples, the discriminant pairs up the spectral points on the horizontal axis. The line of zero discriminant joining the other two points is found to wrap around the left hand spectral point.

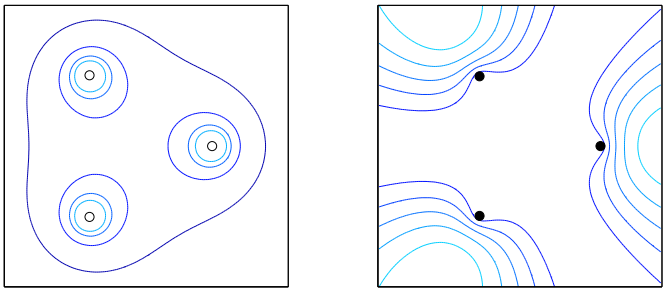

Figure 3.11: D_3-symmetric $\boldsymbol{k} = (2,1)$ periodic monopole with spectral curve $w^3 - \zeta^2 w^2 + 2\zeta w - 1 = 0$. Energy density on the left and the discriminant of $\hat{\Phi}$ on the right.

and the remaining coefficient, $a_{1,0}$, is to be considered a modulus. In this case, two of the ℓ_i are repeated (from (2.5) we have that $\boldsymbol{\ell} = (2,-1,-1)$), allowing minimal symmetry breaking if $\boldsymbol{\mathfrak{v}} = (2\mathfrak{v}, -\mathfrak{v}, -\mathfrak{v})$, for which centering implies that

$$a_{1,2} = -\mathrm{e}^{2\mathfrak{v}} \qquad a_{1,1} = -\mu_1 \mathrm{e}^{2\mathfrak{v}} \qquad a_{2,1} = 2\mathrm{e}^{\mathfrak{v}} \qquad a_{2,0} = \mu_1 \mathrm{e}^{\mathfrak{v}}.$$

In fact, this condition is equivalent to the coefficient of ζ^6 in $\mathcal{D}_{(2,1)}$ vanishing, which was not a possibility for the SU(2) or $\boldsymbol{k} = (1,1)$ cases considered so far. The coefficient of ζ^4 also vanishes if we set $P_{1,2} = -\frac{1}{4}P_{2,1}^2$, such that three of the spectral points are sent to infinity. This leaves μ_1 as a complex modulus, and a symmetric configuration is obtained by taking $\mu_1 = 0$, such that the coefficients of ζ^2 and ζ also vanish, figure 3.11.

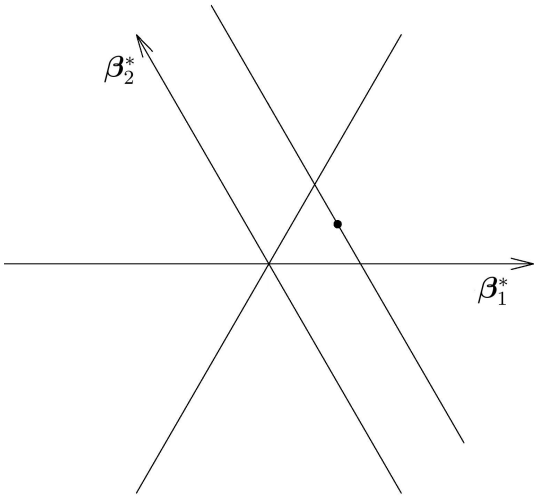

Figure 3.12: Deformation of the subleading term. Starting from the shaded point we deform parallel to $\boldsymbol{\beta}_2^*$.

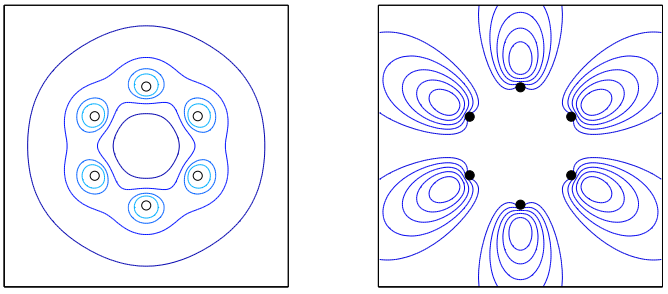

Figure 3.13: D_6-symmetric $\boldsymbol{k} = (2,1)$ periodic monopole with spectral curve $w^3 - \zeta^2 w^2 - 1 = 0$. On the left is plotted the energy density and on the right the discriminant of $\hat{\Phi}$.

$\underline{\mathfrak{v}_2 \neq \mathfrak{v}_3}$

Following [War82] we deform by adding to $\boldsymbol{\mathfrak{v}}$ a constant diagonal term $\delta\boldsymbol{\beta}_2^*$ for some complex δ (we can rearrange the entries such that $\mathrm{Re}(\delta) \geq 0$), figure 3.12. The total energy (2.8) is unchanged, but there is a different pattern of symmetry breaking. Explicitly, $a_{1,2}$ and $a_{1,1}$ are unaltered, while

$$a_{2,1} \;=\; 2\mathrm{e}^{\mathfrak{v}}\cosh(\delta) \qquad\qquad a_{2,0} \;=\; \mathrm{e}^{\mathfrak{v}}\left(\mu_1\mathrm{e}^{\delta} + 2\mu_2\sinh(\delta)\right).$$

Such deformations have the effect of moving the three remaining spectral points in from infinity. A particularly symmetric example, with $\delta = \mathrm{i}\pi/2$, is shown in figure 3.13.

The $\boldsymbol{k} = (2,1)$ Nahm data is of rank 2, smooth, and has three zeros. For the spectral curve $w^3 - \zeta^2 w^2 + 2a\zeta w - 1 = 0$ relevant to both the cases considered above (figures 3.11 and 3.13), the Hitchin Higgs fields have

$$\operatorname{tr}(\Phi) \;=\; 2aw^{-1} \qquad \text{and} \qquad -\det(\Phi) \;=\; w - w^{-2}.$$

The determinant has zeros at $\beta s = 0, \pm 2\mathrm{i}\pi/3$. This is reminiscent of the fact that the most symmetric $\boldsymbol{k} = (2)$ configurations were found to have zeros located symmetrically on the Hitchin cylinder (figure 3.7).

3.4.3 Speculative Geodesic

In section 4.1.2 it is shown that of the four real relative moduli of the SU(2) monopole of charge $\boldsymbol{k} = (2)$, there is a two dimensional geodesic submanifold corresponding to varying the two moduli present in the spectral curve. This justifies the identification of one dimensional submanifolds in section 3.2.3. The SU(3) monopole of charge $\boldsymbol{k} = (1,1)$ also has four real relative moduli, and we will assume that the two which appear in the spectral curve again provide a geodesic submanifold.

The reduced moduli are constrained by looking for configurations invariant under a reflection in the x-axis, which we perform by mapping $\zeta \mapsto \bar{\zeta}$ and $w \mapsto \bar{w}$. This requires all the coefficients $a_{i,j}$ in (3.30) to be real. A symmetric choice of boundary conditions is provided by requiring the two fundamental monopoles to be of the same size, which we do by further imposing invariance of the spectral curve under $\zeta \mapsto -\zeta$ and $w \mapsto w^{-1}$. These conditions result in $\mathrm{e}^{\mathfrak{v}_2} = -1$ and

$$a_{1,1} \;=\; -\mathrm{e}^{\mathfrak{v}_1} \qquad a_{1,0} \;=\; 1 - \mu_1 \mathrm{e}^{\mathfrak{v}_1} \qquad a_{2,1} \;=\; -\mathrm{e}^{\mathfrak{v}_1} \qquad a_{2,0} \;=\; \mu_1 \mathrm{e}^{\mathfrak{v}_1} - 1,$$

where $\mu_1 \in \mathbb{R}$ provides a one parameter family once we fix the remaining boundary data $\mathfrak{v}_1 = 0$ (note that this is a different situation to the trivial embedding of section 3.4.1, where $\mathfrak{v}_2 = 0$). Figure 3.14 illustrates the resulting scattering process. As mentioned in [MS04], the monopoles scatter back off each other in a head-on collision, although with a deformed shape. By allowing different boundary conditions, one can in fact find one parameter families describing the less symmetric cases in which the monopoles are of different sizes, or when one of the incoming monopoles is rotated by an angle of $\pi/2$. As was noted for the SU(2) periodic monopole in sections 3.1.2 and 3.2.3, we find

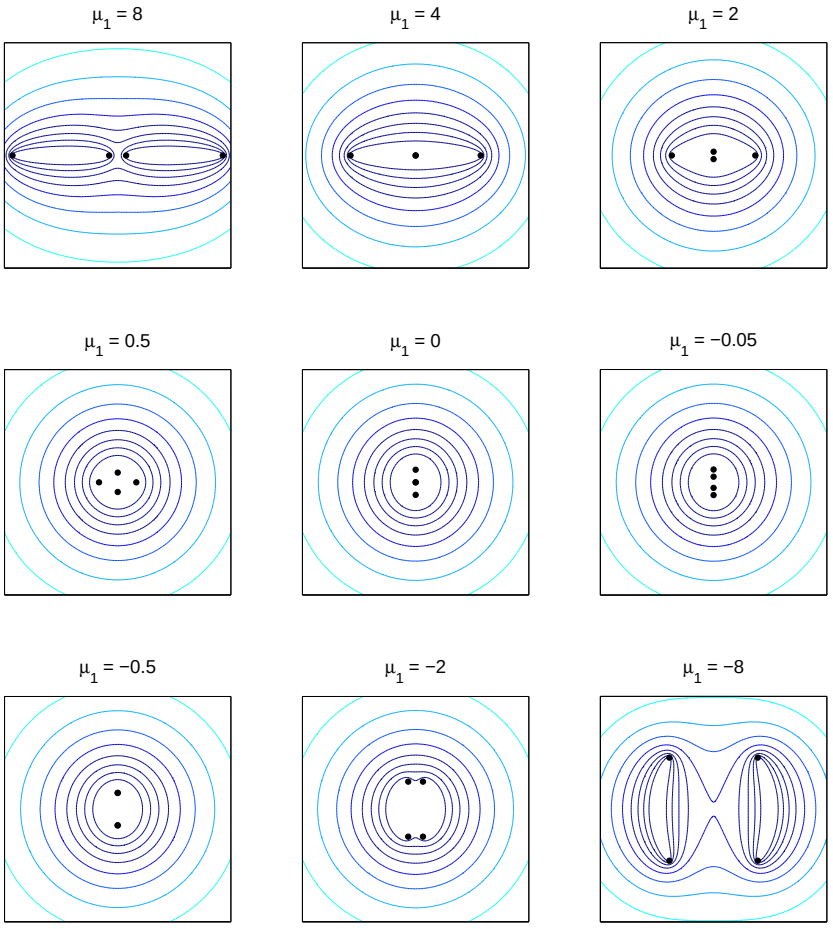

Figure 3.14: Sequence arising by varying the real parameter μ_1 with $\mathfrak{v}_1 = 0$ and $\mathfrak{v}_2 = \mathrm{i}\pi$. Plots show the discriminant of $\hat{\Phi}$. In the Nahm transformed picture, motion of the zeros of $\det(\Phi)$ follows a similar pattern to that shown in figure 3.7, although now with the third zero fixed at $s = 0$ and the singularity at $s = \mathrm{i}\pi/\beta$. The zeros are coincident when $\mu_1 = 4$ and two of them reach the singularity when $\mu_1 = 0$. The energy density is peaked at all the spectral points except the central point for $\mu_1 = 0$ (see the discussion of section 3.2.1).

that when the spectral points are well separated, those of each fundamental monopole are joined by lines of vanishing discriminant.

3.5 Singularities and the Doubly Periodic Instanton

In the region where z dependence can be ignored, the fields of a configuration of positive and negative Dirac monopoles at $\zeta = \zeta_i^{\pm}$ are

$$\mathrm{i}\beta\hat{\Phi} \;=\; \frac{1}{2}\sum_{i=1}^{n_+}\log\left(|\zeta-\zeta_i^+|^2\right) - \frac{1}{2}\sum_{i=1}^{n_-}\log\left(|\zeta-\zeta_i^-|^2\right)$$

$$\mathrm{i}\beta\hat{A}_z \;=\; \frac{\mathrm{i}}{2}\sum_{i=1}^{n_+}\log\left(\frac{\bar{\zeta}-\bar{\zeta}_i^+}{\zeta-\zeta_i^+}\right) - \frac{\mathrm{i}}{2}\sum_{i=1}^{n_-}\log\left(\frac{\bar{\zeta}-\bar{\zeta}_i^-}{\zeta-\zeta_i^-}\right)$$

allowing us to compute the holonomy and hence write down the spectral curve,

$$\left(\prod_{i=1}^{n_-}(\zeta-\zeta_i^-)\right)w - \left(\prod_{i=1}^{n_+}(\zeta-\zeta_i^+)\right) \;=\; 0, \tag{3.32}$$

and there are thus no moduli. Cherkis & Kapustin [ChK03] argue that singularities can be introduced to the SU(N) periodic monopole by modifying the spectral curve (2.16) to

$$P_{0,n_-}(\zeta)w^N + P_{1,k_1}(\zeta)w^{N-1} + \ldots + P_{N-1,k_{N-1}}(\zeta)w + (-1)^N P_{N,n_+}(\zeta) \;=\; 0$$

where $P_{0,n_-}(\zeta)$ and $P_{N,n_+}(\zeta)$ are the monic polynomials appearing in (3.32).

The principal use of Dirac singularities is in changing the boundary conditions on the Nahm/Hitchin data. In particular, adding K positive and K negative singularities to the monopole with $\boldsymbol{k} = (K, K, \ldots, K)$ renders $\det(\Phi)$ bounded at $|r| \to \infty$ (which will allow us to identify the ends of the cylinder to form a torus), albeit with singularities at finite $|r|$ due to K appearing more than once in $\boldsymbol{k}$. We illustrate this by means of the SU(2) charge $\boldsymbol{k} = (1)$ monopole with two singularities, where we require the spectral curve to be invariant under $w \mapsto w^{-1}$ in order that the monopole fields are valued in $\mathfrak{su}(2)$. The relevant spectral curve is

$$(\zeta-\zeta_0)w^2 - 2(a\zeta+b)w + (\zeta-\zeta_0) \;=\; 0 \tag{3.33}$$

such that the boundary conditions (2.10) translate to

$$a = \cosh(\mathfrak{v}) \qquad b = \mu \sinh(\mathfrak{v}) - \zeta_0 \cosh(\mathfrak{v})$$

and the spectral curve (3.33) can be rearranged to give the Hitchin Higgs field

$$\Phi = \zeta = \zeta_0 + \frac{\mu \sinh(\mathfrak{v})}{\cosh(\beta s) - \cosh(\mathfrak{v})}. \tag{3.34}$$

Applying the method of section 3.1, the spectral points are located at

$$\zeta = \frac{\zeta_0 + b}{1 - a} \qquad \text{and} \qquad \zeta = \frac{\zeta_0 - b}{1 + a},$$

which are centered if $ab + \zeta_0 = 0$, and are coincident if $a\zeta_0 + b = 0$. The monopole Higgs field is

$$\hat{\Phi} = \frac{\mathrm{i}}{\beta} \operatorname{Re} \cosh^{-1} \left(\cosh(\mathfrak{v}) + \frac{\mu \sinh(\mathfrak{v})}{\zeta - \zeta_0} \right) \sigma_3.$$

In the case where $a = 0$ and $\mathrm{i}b = C$, this simplifies to

$$\hat{\Phi} = \frac{\mathrm{i}}{\beta} \operatorname{Re} \cosh^{-1}(C/\zeta) \sigma_3$$

which is related to the fields of sections 3.1.1 and 3.1.2 by a simple inversion transformation $\zeta \mapsto C^2/\bar{\zeta}$, with a corresponding change of boundary conditions.

In analogy with monopoles appearing as constituents of periodic instantons (see, for example, [KvB98*a*, KvB98*b*, LL98]), it is expected that the doubly periodic instanton will be related to the periodic monopole [ChK03, FP04]. The Nahm data for the doubly periodic instanton are Hitchin equations on a 2-torus T^2. The charge 1 case is considered in [FP04], where the Hitchin system is Abelian. This allows the Hitchin gauge potentials to be expressed as derivatives of a harmonic potential, and the Higgs field is chosen to be proportional to A_s in order to share its singularities,

$$A_s = \partial_s \varphi \qquad A_{\bar{s}} = -\partial_{\bar{s}} \varphi \qquad \Phi = \zeta_0 + \alpha \partial_s \varphi$$

where, in our notation, the fundamental solution to Laplace's equation on the torus is

$$\varphi \;=\; \frac{1}{2}\,\log\frac{\left|\vartheta_3\left(\frac{\mathrm{i}}{2\pi}(\bar{s}\beta_1+\bar{\mathfrak{v}})+\frac{1}{2}+\frac{\mathrm{i}\beta_1}{2\beta_2},\frac{\mathrm{i}\beta_1}{\beta_2}\right)\right|^2}{\left|\vartheta_3\left(\frac{\mathrm{i}}{2\pi}(\bar{s}\beta_1-\bar{\mathfrak{v}})+\frac{1}{2}+\frac{\mathrm{i}\beta_1}{2\beta_2},\frac{\mathrm{i}\beta_1}{\beta_2}\right)\right|^2}$$

with β_1 and β_2 the periods of the instanton, and ϑ_3 is the doubly periodic Jacobi theta-function, which can be conveniently expressed as

$$\vartheta_3(w,\tau) \;=\; \sum_{n=-\infty}^{\infty} \mathrm{e}^{\mathrm{i}\pi n^2\tau+2\mathrm{i}\pi n w}. \tag{3.35}$$

The result (3.34) is recovered in the limit $\beta_1=\beta$, $\beta_2\to 0$, such that only the $n=0$ and $n=-1$ terms contribute to (3.35),

$$\varphi \;=\; \frac{1}{2}\,\log\frac{\left|1-\mathrm{e}^{\beta\bar{s}+\bar{\mathfrak{v}}}\right|^2}{\left|1-\mathrm{e}^{\beta\bar{s}-\bar{\mathfrak{v}}}\right|^2} \qquad\Rightarrow\qquad \Phi \;=\; \zeta_0-\frac{\alpha\beta}{2}\frac{\sinh(\mathfrak{v})}{\cosh(\beta s)-\cosh(\mathfrak{v})},$$

which is precisely of the form (3.34). In [FP04], α is interpreted as a size, which when set to zero provides axially symmetric fields. In the monopole picture this corresponds to setting $\mu=0$, in which case $a\zeta_0+b=0$ and the spectral points coincide, again leading to axial symmetry.

The need for singularities when making the comparison with the doubly periodic instanton is reminiscent of the intepretation of periodic instantons as monopoles whose gauge group is a loop group [GM88]. In practice, this amounts to adding a root to the gauge group such that all of the ℓ_i vanish and we are at the origin of the root diagram, see figure 2.1 and section 2.4. From the discussion of sections 2.1 and 3.1, the additional fundamental monopole expected from the extra root fits in with the observation in [FP04] that the doubly periodic instanton consists of two periodic monopole constituents, separated in one of the periodic directions.

3.6 Concluding Remarks

This chapter developed a technique, motivated by [ChK01, ChK03, War05, HW09], to study the singly periodic BPS monopole. This was checked against numerical studies of the SU(2) cases of charge 1 and 2. Geodesic motion on an effective two dimensional moduli space compared favourably with analytic results for charge 2. In particular, it was found that motion transverse to the periodic direction provides a geodesic submanifold. Some simple SU(3) configurations and singular periodic monopoles were also considered in this context. The Nahm transform relates the periodic monopole to a Hitchin system on the cylinder, giving rise to lumps whose motion is described, at large separations, by the motion of zeros of the spectral curve polynomial.

4

Nahm Transform

The aim of this chapter is to study the moduli which are not encoded within the spectral approximation of chapter 3. The approach will be to use the Nahm transform to study symmetries of the monopole chain for two distinct solutions of the Nahm/Hitchin data. This is done in section 4.1, and is followed in section 4.2 by a discussion of numerical solutions to the Hitchin equations. Finally, in section 4.3 we construct the metric on the moduli space by means of suitable approximations to the Nahm/Hitchin data at large K. By considering the symmetries of the system, two geodesic submanifolds are identified, and these are compared with the Atiyah-Hitchin cone and trumpet. The work in this section is based on the joint publication *Geometry of periodic monopoles* [MW13], and care has been made to indicate my supervisor's contribution.

4.1 Charge 2

The centered SU(2) charge $\boldsymbol{k} = (2)$ periodic monopole has four real moduli, two of which, as was seen in sections 2.3 and 3.2.1, are encoded in the spectral curve and describe the relative xy positions of the fundamental monopoles in $\mathbb{R}^2$. The remaining two moduli are expected to describe the relative phase and z separation. By considering the action of gauge transformations on the inverse Nahm operator (as defined in section 2.2) we will see that the two reduced moduli appearing in the spectral curve provide a geodesic submanifold of the full moduli space. The one parameter families $K \in \mathbb{R}$ and $K \in \mathrm{i}\mathbb{R}$ are studied, and we will find that the details of z behaviour depend on our choice of solution of the Hitchin equations on the Hitchin cylinder. The work in this

section is motivated by [HW09, Har*a*], and it should be noted that the results are independent of the spectral approximation of chapter 3.

4.1.1 Hitchin Equations on the Cylinder

The Nahm data of interest are $\mathfrak{u}(2)$-valued (or $\mathfrak{su}(2)$-valued if the monopole is centered) Hitchin fields (Φ, A) (2.11) on the dual cylinder,

$$F_{s\bar{s}} \;=\; -\frac{1}{4}\,[\Phi, \Phi^\dagger] \qquad\qquad D_{\bar{s}}\Phi \;=\; \partial_{\bar{s}}\Phi + [A_{\bar{s}}, \Phi] \;=\; 0 \tag{4.1}$$

with $\det(\Phi)$ determined by the spectral curve as described in section 3.3.5. It is straightforward to show [HW09] that the Hitchin equations can be solved (up to U(1) gauge transformations) by

$$\Phi \;=\; \begin{pmatrix} 0 & \mu_+ \mathrm{e}^{\psi/2} \\ \mu_- \mathrm{e}^{-\psi/2} & 0 \end{pmatrix} \qquad\qquad A_{\bar{s}} \;=\; a\sigma_3 + \alpha\Phi \qquad\qquad A_s \;=\; -\bar{a}\sigma_3 - \bar{\alpha}\Phi^\dagger \tag{4.2}$$

where

$$-\det(\Phi) \;=\; \mu_+\mu_- \;=\; C\cosh(\beta s) + K/2$$

and a, α and ψ are functions of $(s, \bar{s})$ satisfying $4a = -\partial_{\bar{s}}\psi$,

$$\nabla^2 \mathrm{Re}(\psi) \;=\; 2(1 + 4|\alpha|^2)\left(|\mu_+|^2 \mathrm{e}^{\mathrm{Re}(\psi)} - |\mu_-|^2 \mathrm{e}^{-\mathrm{Re}(\psi)}\right) \tag{4.3}$$

and

$$\mathrm{e}^{-\mathrm{Re}(\psi)/2}\,\partial_s\left(\alpha\mu_+ \mathrm{e}^{\mathrm{Re}(\psi)}\right) + \mathrm{e}^{\mathrm{Re}(\psi)/2}\,\partial_{\bar{s}}\left(\bar{\alpha}\bar{\mu}_- \mathrm{e}^{-\mathrm{Re}(\psi)}\right) \;=\; 0, \tag{4.4}$$

with the imaginary part of ψ chosen in such a way that Φ has the correct t-period of $2\pi/\beta$. We remark on the similarity of (4.3) and (4.4) to the Toda and Ernst equations, respectively [MW96]. However, the standard methods used to tackle these systems have not so far been successful in providing analytical solutions to the present generalisation. Instead, we will resort to studying the symmetries of the equations and look for numerical solutions.

It is clear that $\alpha = 0$ allows (4.4) to hold trivially, and in the next subsection it will be seen that it in fact provides a two dimensional geodesic submanifold of the relative moduli space. When this is the case, there are two fundamentally different solutions for Φ according to the allocation of the zeros of $\det(\Phi)$ between its two non-vanishing components:

- Harland's solution [Har*a*] places both zeros in the same component,

$$\mu_+ \;=\; C\cosh(\beta s) + K/2 \qquad\qquad \mu_- \;=\; 1 \tag{4.5}$$

  with $\mathrm{Im}(\psi) = 0$. We call this the 'zeros together' solution.

- On the other hand, Harland & Ward [HW09] place one zero in each component of Φ,

$$\mu_\pm \;=\; \sqrt{\frac{C}{2}}\left(\mathrm{e}^{\beta s/2} + W^{\pm 1}\mathrm{e}^{-\beta s/2}\right) \qquad \text{where} \qquad \frac{K}{C} \;=\; W + \frac{1}{W} \tag{4.6}$$

  this time with $\mathrm{Im}(\psi) = -\beta t$. This is the 'zeros apart' solution.

For $\alpha = 0$ the Hitchin Higgs fields with 'zeros together' and 'zeros apart' are thus of different matrix rank (in particular, for $K/C = -2$ at $s = 0$, the 'zeros apart' Higgs field is of rank 0, which can never be the case in the 'zeros together' configuration) and there is no smooth gauge transformation between them. As such, the 'zeros together' and 'zeros apart' solutions are disconnected two dimensional submanifolds of the moduli space. It is expected that in the full four dimensional moduli space one can interpolate between the two cases.

4.1.2 Symmetries

In this section we impose symmetries on the Hitchin equations and use the Nahm operator (2.12) to determine the resulting symmetry groups of the monopole fields. This will allow us to identify one parameter families of monopoles, which are plotted in chapter 5.

Once the Hitchin equations of section 4.1.1 have been solved, one should apply the procedure of section 2.2 to extract the monopole fields. This has been done numerically for the 'zeros apart' case [HW09]. Here, we consider symmetries of the Nahm transform by means of gauge transformations (2.15). This is achieved by first looking for transformations of the Nahm data $(s; K) \mapsto (s'; K')$ motivated by the symmetries of the spectral curve presented in section 3.2.3. The equations 4.3 and 4.4 are required to hold in the new coordinates, with the transformed fields

$$\begin{aligned} (\Phi, A)(s; K) &\mapsto (\Phi', A')(s'; K') \\ (\Delta, \Psi)(s; \zeta', z'; K) \mapsto (\Delta, \Psi)(s'; \zeta', z'; K') \;&=\; (\Delta', \Psi')(s; \zeta', z'; K). \end{aligned}$$

We then search for a gauge transformation U and a transformation $(\zeta, z) \mapsto (\zeta', z')$ of the monopole coordinates which express Δ' in terms of Δ, in such a way that the resulting monopole fields are gauge equivalent to the original monopole fields, but evaluated at the new coordinates, (ζ', z'). We recall from equation 2.15 in section 2.2 that U acts as

$$\begin{aligned}\Delta'(s;\zeta',z';K) &= U^{-1}(s)\Delta(s;\zeta',z';K)U(s)\\ \Psi'(s;\zeta',z';K) &= U^{-1}(s)\Psi(s;\zeta',z';K),\end{aligned}$$

and we assume it can be written in block form as $U = h \otimes g$, where h is a constant 2×2 matrix which permutes the entries of Δ. The matrix $g \in \mathrm{U}(2)$ acts as a gauge transformation on the Hitchin fields and is required to be strictly periodic in t, such that Φ and the t-holonomy of A are well defined.[10] If $\det(g) = 1$ (or can be made so by multiplication by a constant phase), then the monopole centering is unchanged. On the other hand, if $\det(g) \propto \mathrm{e}^{\mathrm{i}\beta t}$ then the transformed fields are shifted by $\beta/2$ in z, as will be relevant for the $W \mapsto \overline{W}^{-1}$ symmetry discussed below. In all cases, symmetries are up to gauge equivalence (so they describe symmetries of the energy density isosurfaces).

For completeness, we recall the Nahm operator (2.12) in the $\boldsymbol{k} = (2)$ case,

$$\Delta = \begin{pmatrix} \mathbf{1}_2(2\partial_{\bar{s}} - z) + 2A_{\bar{s}} & \mathbf{1}_2\zeta - \Phi \\ \mathbf{1}_2\bar{\zeta} - \Phi^\dagger & \mathbf{1}_2(2\partial_s + z) + 2A_s \end{pmatrix}. \tag{4.7}$$

A study of the geodesic with $\alpha = 0$, $K \in \mathbb{R}$ and the symmetry $K \mapsto -K$ was carried out in [HW09]. Here we summarise the results and give evidence of new geodesics.

Symmetries can be classified by the dihedral group in three dimensions (see, for example, [Ham62, Mil72]): $D_{n\mathrm{h}}$ describes n-fold rotational symmetry and reflection in a plane whose normal is parallel to the axis of symmetry, while $D_{n\mathrm{d}}$ has an axis with n-fold rotational symmetry and $2n$-fold rotoreflectional symmetry (in which rotation is combined with reflection in a plane orthogonal to the axis). In both cases there are $2n$ axes[11] of 2-fold rotational symmetry orthogonal to the principal symmetry axis. Both of these groups contain the two dimensional D_n group as a subgroup, and $D_{n\mathrm{d}}$ is a subgroup of $D_{(2n)\mathrm{h}}$. The reader may find it useful to visualise these symmetries with reference to

[10] It may be possible, as part of future research, to investigate new symmetries by weakening the periodicity condition on g in such a way that certain key quantities such as $\det(\Phi)$ remain periodic.

[11] In $\mathbb{R}^3$ one has n such axes; the periodicity doubles this number.

the energy density plots of chapter 5 and the generalisations to higher charges in chapter 6.

$\underline{z \mapsto z + \beta}$

To illustrate the process, we note that the Hitchin fields are unchanged under the joint action of $U = \mathrm{e}^{-\mathrm{i}\beta t}\mathbf{1}_4$ and $(\zeta, z) \mapsto (\zeta, z + \beta)$, indicating that the monopole fields are unchanged by a period shift, as hoped.

$\underline{\alpha = 0}$

Again keeping s and K unchanged, we take $U = \sigma_3 \otimes \mathbf{1}_2$ and $(\zeta, z) \mapsto (-\zeta, z)$. As long as $\alpha = 0$ the Hitchin fields become $(\Phi, A) \mapsto (-\Phi, A)$, so that $\Psi_\pm \mapsto \pm\Psi_\pm$ and the monopole fields are thus invariant under a rotation by π about the z-axis. This justifies our assumption throughout section 3.2 that $\alpha = 0$ is a geodesic submanifold in which the two moduli which do not appear in the spectral curve are kept fixed.

Symmetries with $\alpha \neq 0$ are considered in section 4.1.3, where it is also shown that $(\zeta, z) \sim (-\zeta, -z)$ is a symmetry for all α. This implies that configurations other than the symemtric ones considered below have symmetry group $C_{2\mathrm{h}}$ consisting of a 180° rotation and a reflection $z \mapsto -z$.

'Zeros Together'

The geodesic submanifolds $K \in \mathbb{R}$ and $K \in \mathrm{i}\mathbb{R}$ are fixed by the $D_{2\mathrm{h}}$ symmetries (the symmetry group of a cuboid)

- $(s; K) \mapsto (\bar{s}; \bar{K}) \Rightarrow (\zeta, z) \sim (\bar{\zeta}, -z)$ for $K \in \mathbb{R}$,
- $(s; K) \mapsto (\bar{s} + \mathrm{i}\pi/\beta; -\bar{K}) \Rightarrow (\zeta, z) \sim (\mathrm{i}\bar{\zeta}, -z)$ for $K \in \mathrm{i}\mathbb{R}$.

The calculation for the case $K \in \mathbb{R}$ is given in more detail in appendix A, which serves to illustrate the procedure for the remaining cases.

Incoming and outgoing points on these geodesics are related by the symmetry

- $(s; K) \mapsto (s; -K) \Rightarrow (\zeta, z) \mapsto (\mathrm{i}\zeta, z)$,

and hence both geodesics describe 90° scattering in the xy plane. The intermediate point of the scattering process, with $K = 0$, enjoys an enhanced $D_{4\mathrm{h}}$ symmetry.

'Zeros Apart'

In this case we use the coordinate W defined in (4.6) and find symmetries fixing the geodesic submanifolds $W \in \mathbb{R}$ and $W \in \mathrm{i}\mathbb{R}$,

- $(s; W) \mapsto (\bar{s}; \overline{W}) \Rightarrow (\zeta, z) \sim (-\bar{\zeta}, -z)$ for $W \in \mathbb{R}$,
- $(s; W) \mapsto (\bar{s} + \mathrm{i}\pi/\beta; -\overline{W}) \Rightarrow (\zeta, z) \sim (\mathrm{i}\bar{\zeta}, -z)$ for $W \in \mathrm{i}\mathbb{R}$.

These families again have $D_{2\mathrm{h}}$ symmetry. Opposite points on each of these geodesics are related by the symmetry

- $(s; W) \mapsto (\bar{s}; \overline{W}^{-1}) \Rightarrow (\zeta, z) \mapsto (\bar{\zeta}, \beta/2 - z)$.

Overall then, the geodesic with $W \in \mathbb{R}$ has incoming and outgoing monopoles aligned with the x-axis but shifted by half a period in the z direction. The $W \in \mathrm{i}\mathbb{R}$ geodesic, on the other hand, additionally involves a 90° rotation in the xy plane. Note that in the 'zeros together' case a geodesic is allowed to cross the points $K/C = \pm 2$, although this is not possible in the 'zeros apart' configuration (see also section 3.3.3). The symmetry $(s; W) \mapsto (\bar{s}; \overline{W}^{-1})$ fixes an additional geodesic submanifold with $|W| = 1$, for which the monopoles remain centered at $(\zeta, z) = (0, \pm\beta/4)$ and oscillate in shape. This geodesic surface will be discussed in more detail in sections 4.3.6 and 5.3, after the remaining moduli have been identified.

There are particular values of the modulus W for which solutions have an enhanced symmetry:

- $W = 1$ has $(\zeta, z) \sim (\zeta, \beta/2 - z) \sim (\zeta, z + \beta/2)$, denoted by $D_{2\mathrm{h}} \times \mathbb{Z}_2$, and
- $W = \mathrm{i}$ has $(\zeta, z) \sim (\mathrm{i}\zeta, \beta/2 - z) \sim (\mathrm{i}\zeta, z + \beta/2)$, denoted by $D_{2\mathrm{d}} \times \mathbb{Z}_2$,

where the factors of $\mathbb{Z}_2$ indicate that these configurations have eight axes of 2-fold rotational symmetry in each period, instead of the usual four. The fixed points of these symmetries, at $z = \pm\beta/4$, turn out to be the z positions of the monopoles in these cases, and plots of these configurations are given in chapter 5. The symmetries of the $W = \pm 1$ configurations reflect the fact that this is a charge 1 chain of rescaled period, and consequently $F_{s\bar{s}} = 0$. This observation is studied in further detail in section 6.2.

It should be noted that the branching behaviour presented in this section agrees with [MW13, Mal*a*], and supersedes the interpretation found in earlier work [HW09, Mal13].

4.1.3 Symmetries with α

In this section we use the method of section 4.1.2 to study the effect of the moduli encoded by α in equations 4.2, 4.3 and 4.4. We will see that particular spatial symmetries impose constraints on α such as its phase, or its parity under a transformation of the coordinate s. In the special case of $\alpha = 0$ the symmetries are enhanced, and we recover those of the preceding section.

Reflection - 'zeros together'

First of all we consider the transformation $s \mapsto -s$. It is easy to check that the ψ and α equations still hold for all α, such that, in particular, the function ψ remains unchanged and $a \mapsto -a$. The transformed Hitchin fields can be expressed as $(\Phi', A'_{\bar{s}}) = (\Phi, -a\sigma_3 + \alpha'\Phi) = (\Phi, -A_{\bar{s}})$ if $\alpha \mapsto \alpha' = -\alpha$ (with fixed point set $\alpha = 0$). We can also write the transformed fields in a slightly different way, by a different choice of gauge, as $(\Phi', A'_{\bar{s}}) = (-\sigma_3\Phi\sigma_3, -\sigma_3 A_{\bar{s}}\sigma_3)$, with $\alpha' = \alpha$. The two ways of writing the transformed Hitchin fields correspond to the monopole fields being invariant under $(\zeta, z) \mapsto (\zeta, -z)$ (only for $\alpha = 0$) and $(\zeta, z) \mapsto (-\zeta, -z)$ (true for all α and K), together with $\hat{\Phi} \mapsto -\hat{\Phi}$, arising from (2.14) due to $r \mapsto -r$. This transformation of $\hat{\Phi}$ ensures the Bogomolny equations are preserved. Note, however, that it does not force $\hat{\Phi} = 0$ on $z = 0$, due to the gauge equivalence between $\hat{\Phi}$ and $-\hat{\Phi}$.

Reflection - 'zeros apart'

In this case the details of $s \mapsto -s$ work out slightly differently: ($\mu_\pm \mapsto W^{\pm 1}\mu_\mp$, $\psi \mapsto -\psi - 2\log|W|$, $a \mapsto a$), but we still find two ways of expressing the transformed fields: $\sigma_1(\Phi, -A_{\bar{s}})\sigma_1$ for $\alpha = 0$ or $\sigma_2(-\Phi, -A_{\bar{s}})\sigma_2$ for all α.

The above results show that a reversal of all monopole coordinates is always a symmetry. A special case is provided by $\alpha = 0$. If the charge 2 periodic monopole is considered as two parallel chains of small monopoles, then this suggests that $\alpha = 0$ describes the situation with zero z offset. It is then evident that there is an enhanced symmetry in this case. Varying the z offset, the symmetry $(\zeta, z) \mapsto (-\zeta, -z)$ still holds. Continuing with this picture of chains of small monopoles, one might expect an enhanced symmetry in the opposite limiting case, namely when the z separation of each of the chains is half a period, i.e. $(\zeta, z) \sim (-\zeta, z + \beta/2)$, but it is not clear how to implement this symmetry at the level of the Nahm/Hitchin data.

Next, we look at the symmetries with fixed set $K \in \mathbb{R}$ and $K \in \mathrm{i}\mathbb{R}$.

$\underline{K \in \mathbb{R}}$

For 'zeros together' we take $(s;K) \mapsto (\bar{s};\bar{K})$, and for 'zeros apart' $(s;W) \mapsto (\bar{s};\overline{W})$. There are then two possibilities for the transformed Hitchin fields: $(\Phi', A'_{\bar{s}}) = \sigma_1(\Phi^\dagger, A_s)\sigma_1 = \sigma_2(-\Phi^\dagger, A_s)\sigma_2$. In the first case, $\alpha \mapsto -\bar{\alpha}$, so we take $\alpha \in \mathrm{i}\mathbb{R}$, while in the second $\alpha \in \mathbb{R}$. They correspond, respectively, to the symmetries $(\zeta, z) \sim (\bar{\zeta}, -z)$ and $(\zeta, z) \sim (-\bar{\zeta}, -z)$ (again, it is useful to visualise these in the 'chain of small monopoles' picture). It should be noted that this transformation is compatible with the reflection symmetry which was shown above to hold for all α. Furthermore, the enhanced symmetry $(\zeta, z) \mapsto (\zeta, -z)$ is still seen to hold only when $\alpha = 0$.

$\underline{K \in \mathrm{i}\,\mathbb{R}}$

This time we take $(s;K) \mapsto (\bar{s} + \mathrm{i}\pi/\beta; -\bar{K})$ for 'zeros together' and $(s;W) \mapsto (\bar{s}+\mathrm{i}\pi/\beta; -\overline{W})$ for 'zeros apart'. We again find two possibilities for α: $\mathrm{Re}(\alpha) = \mp\mathrm{Im}(\alpha)$, with symmetries $(\zeta, z) \sim (\pm\mathrm{i}\bar{\zeta}, -z)$. The corresponding gauge transformations are $g_\pm = \mathrm{i}(\sigma_1 \pm \sigma_2)/\sqrt{2}$ with $(\Phi', A'_{\bar{s}}) = g_\pm^{-1}(\mp\mathrm{i}\Phi^\dagger, A_s)g_\pm$.

The above considerations suggest a link between the spatial symmetries of the monopole and the complex behaviour of the function α, as well as the direction of the gauge transformations in the σ_1/σ_2 plane of SU(2). In all the cases considered above, the symmetry group is $D_{1\mathrm{d}}$ (note that $D_{1\mathrm{d}} = C_{2\mathrm{h}} \subset D_{2\mathrm{h}}$, so is contained in the symmetries of section 4.1.2), and the axis of rotational symmetry in the ζ plane is parallel to $\mathrm{i}\alpha$. It may be possible to make use of these observations to identify a one parameter family of 'maximally offset' chains, with the $D_{1\mathrm{d}}$ symmetry $(\zeta, z) \sim (-\zeta, z + \beta/2) \sim (-\zeta, -z)$.

4.1.4 Numerical Solutions

Numerical solutions to (4.3) with $\alpha = 0$ were obtained by Harland & Ward [HW09]. They employed a gradient descent method to minimise the functional

$$E[\mathrm{Re}(\psi)] = \int \left(\frac{1}{2}(\partial_j \mathrm{Re}(\psi))^2 + 2|\mu_+|^2 \mathrm{e}^{\mathrm{Re}(\psi)} + 2|\mu_-|^2 \mathrm{e}^{-\mathrm{Re}(\psi)} - \mathrm{Re}(\psi_0) \right) dr\, dt \tag{4.8}$$

with respect to ψ where the boundary condition satisfies

$$\mathrm{Re}(\psi_0) \to \log \frac{|\mu_-|}{|\mu_+|} \qquad \text{as} \qquad r \to \infty. \tag{4.9}$$

This boundary condition comes from the observation that at large $|r|$, $F \approx 0$ and (4.3) is solved by setting both sides to zero (this solution has a singularity at finite r, so is not globally valid, although it will be considered further in sections 4.3.2, 5.1.2 and 6.2). This consideration also allows us to place a cutoff at large $|r|$.

Minimising (4.8) by use of the Euler-Lagrange equations returns the Hitchin equation (4.3). For numerical minimisation, ψ is considered as an n dimensional vector, where n is the number of grid points on the cylinder. The gradient ∇E of (4.8) is again an n dimensional vector given by the bracketed term in

$$\delta E \;=\; \int \left(-\partial_j^2 \mathrm{Re}(\psi) + 2|\mu_+|^2 \mathrm{e}^{\mathrm{Re}(\psi)} - 2|\mu_-|^2 \mathrm{e}^{-\mathrm{Re}(\psi)}\right) \delta\psi \, dr \, dt$$

and acts on $\delta\psi$ (note that this vanishes when (4.3) is satisfied). Deforming a trial function ψ satisfying the boundary condition (4.9) to $\psi + \lambda \nabla E$ for some real parameter λ we search for the value of λ which minimises the error in (4.3). This process is repeated until such an error reaches a predefined tolerance value.

This procedure was used for section 4.2 and in chapter 5. A generalisation to higher charges will be used in chapter 6 (see section 6.2). A modification of this method was also used in [HW09] to perform the inverse Nahm transform numerically. This uses the numerical solutions of ψ to construct Φ and A, and then minimises the quantity

$$E \;=\; \int (\Delta\Psi)^\dagger \Delta\Psi \, dr \, dt,$$

to determine Ψ, where Δ and Ψ are defined in equation 2.12. This numerical Nahm transform is used in chapters 5 and 6.

4.2 Lumps on the Cylinder

In this section, we fix the gauge (4.2) and consider the quantity B defined through

$$F_{s\bar{s}} \;=\; B\sigma_3 \;=\; -\frac{1}{8}\nabla^2 \mathrm{Re}(\psi)\sigma_3$$

with $\alpha = 0$. Equation 4.3 is solved numerically using the relaxation method of section 4.1.4 for different values of the parameters and moduli.

Following the geodesics described in section 4.1.2 results in the motion of two peaks in F which (for large C) closely track the zeros of $\det(\Phi)$, as displayed in figures 3.7 and 3.8. This dual dynamics on the Nahm/Hitchin cylinder suggests a physical interpretation of the moduli, which will be used in section 4.3 to study the moduli space metric. It also provides an interesting example of dual dynamics in the Nahm transformed space. This is in contrast to the Nahm transform for monopoles on $\mathbb{R}^3$, where the Nahm data boundary conditions fix the peaks to the endpoints of the Nahm line segment. It should also be contrasted with the doubly periodic monopole, in which the Nahm transform is self-reciprocal and again describes the motion of doubly periodic monopoles [War05, MW14].

4.2.1 Peaks in the Nahm/Hitchin Gauge Field

Snapshots of $|B|$ through different scattering processes are given in figure 4.1. We note in particular that in the 'zeros apart' case the lumps annihilate at $K/C = \pm 2$, when $\mu_+ = \mu_-$. On the other hand, in the 'zeros together' solution the lumps do not vanish, but reach a minimum size at $K = 0$.

Numerically, a dependence on C is also observed, with two limiting cases. For small monopole size C the lumps widen and lose t-dependence to become Nahm data on a line segment. However, at large C, which is the case of interest in chapter 3, the lumps become sharply peaked and (4.3) is solved by setting both sides to zero (note how the size of the lumps scales inversely to the size of the monopoles as C is varied). It is in the latter case that the spectral approximation improves in accuracy, and that the positions of the lumps are found to most closely track the zeros of $\det(\Phi)$ shown in figures 3.7 and 3.8. This behaviour is illustrated in figure 4.2, and further details of these limiting cases will be given in sections 5.1.1 and 5.2.1.

4.2.2 Holonomies

The quantity B is also relevant to the computation of holonomies of A_t around the cylinder. To see this we integrate B over the cylinder,

$$\mathcal{H} = \int_{\mathbb{R}\times S^1} B\, dr\, dt = -\frac{1}{8}\int_{\mathbb{R}\times S^1} \nabla^2 \mathrm{Re}(\psi)\, dr\, dt.$$

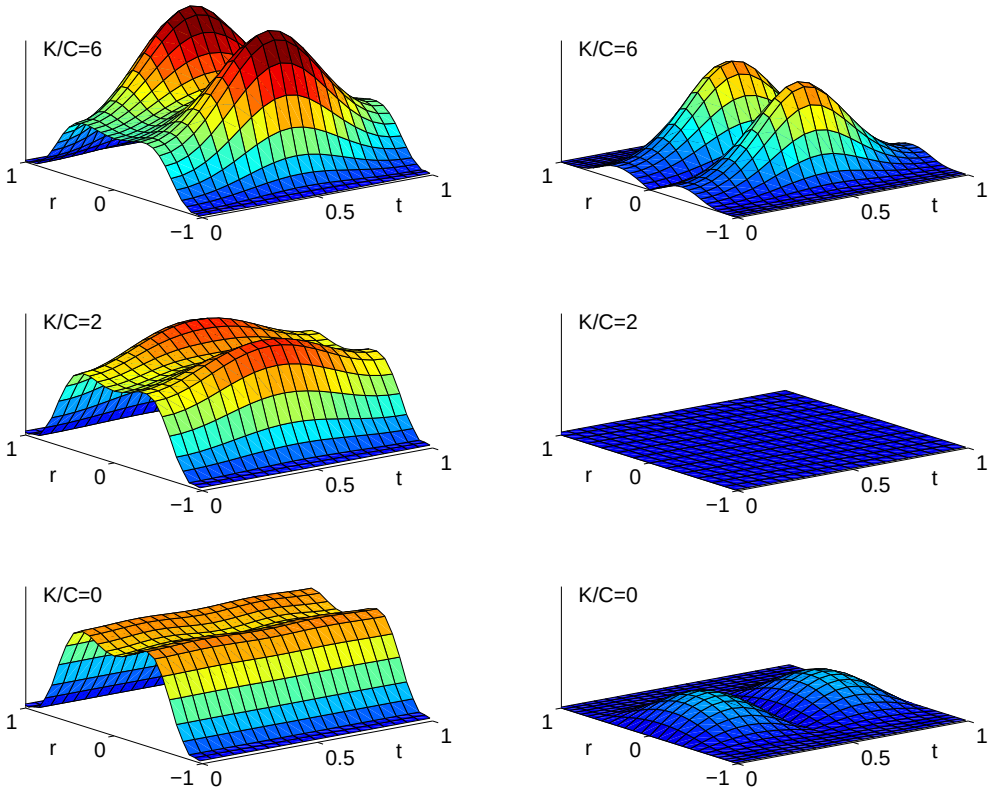

Figure 4.1: Lumps in $|B|$ for various values of K in the 'zeros together' solution (left) and the 'zeros apart' solution (right) for $C = 1$ and $\beta = 2\pi$, using the same vertical scale throughout. The positions of the lumps should be compared with the positions of the zeros of $\det(\Phi)$, as indicated in figures 3.7 and 3.8. It should also be noted that the lumps are of different sign in each case.

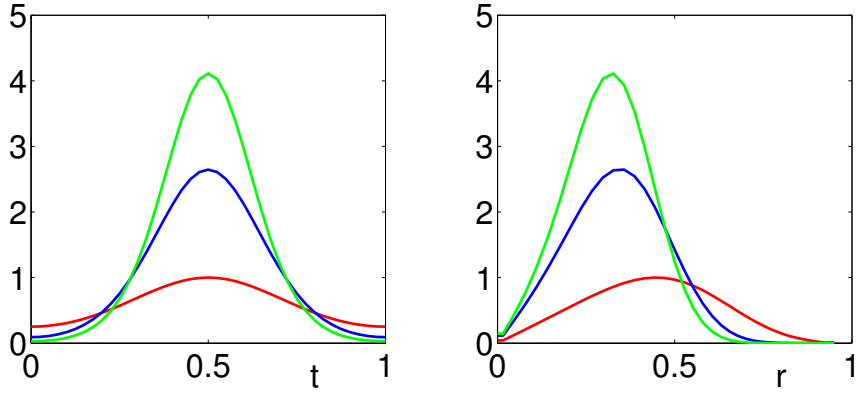

Figure 4.2: Profiles through the maxima of $|B|$ in the t and r directions for various values of C, with $K/C = 6$ and $\beta = 2\pi$ in the 'zeros apart' configuration. The height of the $C = 1$ peak (red) is used to normalise those for $C = 5$ (blue) and $C = 10$ (green). Notice how the peaks get narrower as C is increased. The r positions of the maxima (approximately 0.42, 0.33 and 0.30, respectively) approach the position of the zero of $\det(\Phi)$, at $r = \beta^{-1}\cosh^{-1}(K/2C) \approx 0.28$.

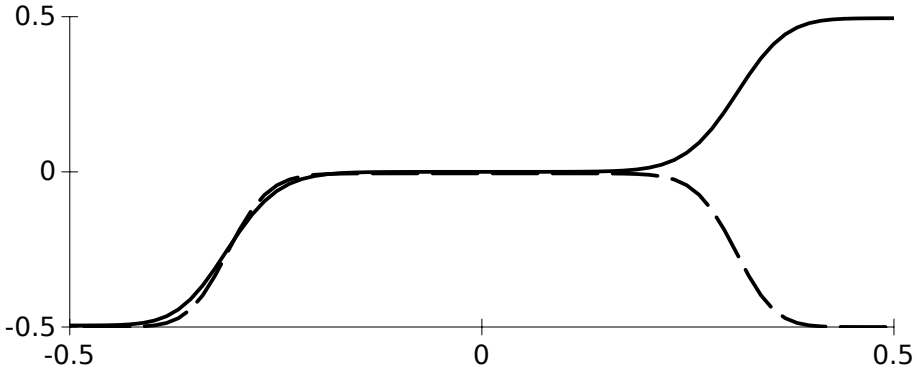

Figure 4.3: $2\gamma/\pi$ as a function of r for the 'zeros together' solution (solid line) and the 'zeros apart' solution (dashed line), in both cases with $K/C = 7$, $C = 200$ and $\beta = 2\pi$.

Applying the divergence theorem and using $A_t = A_s + A_{\bar{s}}$ gives

$$\mathcal{H} \;=\; -\frac{1}{8}\int_{\partial(\mathbb{R}\times S^1)} \partial_r \mathrm{Re}(\psi)\, dt \;=\; \int_{\partial(\mathbb{R}\times S^1)} \left(\mathrm{Re}(a) - \frac{1}{8}\partial_t \mathrm{Im}(\psi)\right) dt. \qquad (4.10)$$

This integral is performed over two circles $S^1_\pm$ bounding the region of interest on the cylinder (the two paths contribute with opposite sign). For both the 'zeros together' and 'zeros apart' solutions (4.5, 4.6), $\mathrm{Im}(\psi)$ is independent of r and linear in t, such that the contribution from the final term in (4.10) cancels between the two integrals, and we are left with

$$\mathcal{H} \;=\; \int_{S^1_+} \mathrm{Re}(a)\, dt - \int_{S^1_-} \mathrm{Re}(a)\, dt \;=\; \gamma_+ - \gamma_-,$$

where the final equality defines $\gamma(r)$ as the integral of $\mathrm{Re}(a(r,t))$ over a t period. Note that for the 'zeros apart' solution (4.6), a change in the sign of $\mathrm{Im}(\beta)$ changes $\gamma \mapsto \gamma + \pi/2$.

We now compute the holonomy $V(r, 2\pi/\beta)$ of A_t around the cylinder, through

$$\partial_t V(r,t) \;=\; -A_t V(r,t)$$

with the condition $V(r,0) = \mathbf{1}_2$. Then we have that $V(r, 2\pi/\beta) = \exp(2\mathrm{i}\gamma\sigma_3)$, which we relate to $\mathcal{H}$ by

$$\frac{1}{2}\,\mathrm{tr}\left(V_+ V_-^{-1}\right) \;=\; \cos\left(2(\gamma_+ - \gamma_-)\right).$$

The volume of the peaks in figure $|B|$ can then be computed from the holonomies of A_t. A plot of γ versus r is given in figure 4.3. It should be noted that

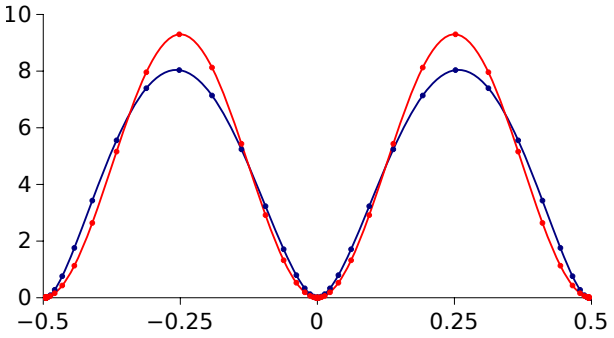

Figure 4.4: Effective potential for the kinks in figure 4.3 (blue) compared with the sine-Gordon potential (4.11) of the same energy (red), which fixes $\lambda \approx 9.3$.

these quantities are not related to the energy of the Hitchin system. Using a similar expression to the Bogomolny energy (3.12) gives the energy density of the lumps as

$$\mathcal{E} \;=\; \frac{1}{8}\,\nabla^2\left(|f|^2+|g|^2\right),$$

which diverges when integrated over the cylinder.

It is interesting to attempt a description of the holonomy in figure 4.3 in terms of one dimensional kinks. This is motivated by the classical work of Atiyah & Manton [AM89], who showed that computing the holonomy of an instanton gauge potential along some fixed direction in $\mathbb{R}^4$ provides an approximate Skyrmion field (in fact, it provides an exact BPS Skyrme field in which the Skyrme field couples to a tower of vector mesons, [Sut10]). A lower dimensional analogue was described in [Sut92], where approximate sine-Gordon solitons are constructed from $\mathbb{CP}^1$ lumps, which are in turn dimensional reductions of the self-duality equations on $\mathbb{R}^{2,2}$, [MW96]. In the present case, if the kinks in $\varphi \equiv 2\gamma/\pi$ (figure 4.3) are considered to be static, then they can be approximated by solutions to the sine-Gordon equation,

$$\frac{d^2}{dr^2}\,\varphi \;=\; \frac{d}{d\varphi}\,U(\varphi) \qquad \text{with} \qquad U(\varphi) \;=\; 2\lambda^2\sin^2(2\pi\varphi), \tag{4.11}$$

where each soliton provides an energy $E = 2\lambda/\pi$. An effective potential is obtained numerically using

$$U(r) \;=\; \frac{1}{2}\left(\frac{d}{dr}\,\varphi(r)\right)^2,$$

and can be approximated with the sine-Gordon potential (4.11) so that the total energy is the same in both cases. The results are displayed in figure 4.4.

4.3 The Moduli Space Metric

In this section we compute the asymptotic moduli space metric from the Nahm transformed fields. Firstly we implement the gauge orthogonality condition for Nahm/Hitchin data, which can be done explicitly when C is large or the lumps of section 4.2 are well separated ($|K|/C \gg 2$). This procedure gives the metric for $\alpha = 0$ in both of these cases. Next, we discuss the remaining moduli by their effect on the Hitchin lumps and compare the resulting asymptotic metric (valid for large separations) with that computed by Cherkis & Kapustin from the monopole side of the Nahm transform [ChK02]. Part of this work was published in collaboration with Ward [MW13].

4.3.1 General Considerations

In order to obtain a well defined metric we impose the condition that perturbations to the fields are orthogonal to the gauge orbits. This is implemeted by a dimensional reduction of the equivalent condition for instantons, $D_\mu(\delta A_\mu) = 0$ (see sections 1.4 and 3.3), with $A_1 = A_s + A_{\bar{s}}$, $A_2 = \mathrm{i}(A_s - A_{\bar{s}})$, $A_3 = \frac{1}{2}(\Phi - \Phi^\dagger)$, $A_4 = -\frac{1}{2}\mathrm{i}(\Phi + \Phi^\dagger)$,

$$4\left(D'_s\delta A'_{\bar{s}} + D'_{\bar{s}}\delta A'_s\right) \;=\; \left[\Phi', \delta(\Phi'^\dagger)\right] + \left[\Phi'^\dagger, \delta\Phi'\right] \tag{4.12}$$

where the primes indicate that this is only true in a particular gauge, and δ is a change in the fields due to an increment in the moduli (here denoted K_i), e.g.

$$K_i \;\mapsto\; K_i + \delta K_i \qquad \Rightarrow \qquad \Phi(K_i) \;\mapsto\; \Phi(K_i) + \sum_j \delta K_j \frac{\partial \Phi(K_i)}{\partial K_j}.$$

Combining the Hitchin equations (4.1) with the gauge fixing condition (4.12), we find that perturbations to the Hitchin fields must obey

$$D'_{\bar{s}}(\delta\Phi') \;=\; [\Phi', \delta A'_{\bar{s}}] \qquad\qquad [\Phi', \delta(\Phi')^\dagger] \;=\; 4D'_{\bar{s}}(\delta A'_s) \tag{4.13}$$

together with boundary conditions $\delta\Phi \to 0$, $\delta A \to 0$ as $r \to \pm\infty$ and the constraint $\delta(\det(\Phi)) = \text{constant}(r, t)$.

Once this gauge has been found (either analytically or numerically), the metric on the moduli space is given by a dimensional reduction of the instanton

metric, $g \propto \int \delta A'_\mu \delta A'_\mu$,

$$g \;=\; \frac{1}{2}\int_{\mathbb{R}\times S^1} \mathrm{tr}\left(\delta\Phi'(\delta\Phi')^\dagger + 4\delta A'_{\bar{s}}(\delta A'_{\bar{s}})^\dagger\right)\, dr\, dt. \tag{4.14}$$

4.3.2 Large C

Harland & Ward's [HW09] solution (4.2) allows a residual local gauge transformation with $g = \mathrm{e}^{\mathrm{i}u\sigma_3}$ where u is a real function of r, t and K (see also section 4.2). This has the effect of mapping $\psi \mapsto \psi' = \psi - 4\mathrm{i}u$. We now look for a function u such that the primed fields satisfy the gauge condition (4.12), which becomes (with $\nabla^2 = 4\partial_s\partial_{\bar{s}}$)

$$4\left(\partial_s\delta a - \partial_{\bar{s}}\delta\bar{a}\right) + 2\mathrm{i}\nabla^2\delta u \;=\; f\delta\bar{f} - \bar{f}\delta f + \bar{g}\delta g - g\delta\bar{g} + 4\mathrm{i}(|f|^2+|g|^2)\delta u. \tag{4.15}$$

We now use the definitions $f = \mu_+\mathrm{e}^{\psi/2}$, $g = \mu_-\mathrm{e}^{-\psi/2}$ and $a = -\frac{1}{4}\partial_{\bar{s}}\psi$. Equation 4.15 then becomes

$$2\mathrm{i}\partial\nabla^2 u \;=\; -\left(\bar{\mu}_+\partial\mu_+\mathrm{e}^{\mathrm{Re}(\psi)} - \bar{\mu}_-\partial\mu_-\mathrm{e}^{-\mathrm{Re}(\psi)}\right) + 4\mathrm{i}(|f|^2+|g|^2)\partial u \tag{4.16}$$

which we compare with the K derivative of the ψ equation,

$$\partial\nabla^2\psi \;=\; 2\left(\bar{\mu}_+\partial\mu_+\mathrm{e}^{\mathrm{Re}(\psi)} - \bar{\mu}_-\partial\mu_-\mathrm{e}^{-\mathrm{Re}(\psi)}\right) + 2\left(|\mu_+|^2\mathrm{e}^{\mathrm{Re}(\psi)} + |\mu_-|^2\mathrm{e}^{-\mathrm{Re}(\psi)}\right)\partial\psi \tag{4.17}$$

where we simplify notation by using (for the remainder of this section) the abbreviations $\partial = \partial_K$ and $\bar{\partial} = \partial_{\bar{K}}$, and noting that $\partial\mathrm{Im}(\psi) = 0$. Comparing these equations suggests we take

$$u(K,\bar{K}) \;=\; \frac{1}{4}\mathrm{i}\psi + v(\bar{K}). \tag{4.18}$$

Similarly, imposing the gauge condition for $\bar{K}$ variations gives

$$u(K,\bar{K}) \;=\; -\frac{1}{4}\mathrm{i}\psi + \tilde{v}(K) \tag{4.19}$$

for functions $v(\bar{K})$ and $\tilde{v}(K)$ which can be determined up to a constant by equating (4.18) and (4.19). Together these imply that $\bar{\partial}\psi' = \partial\bar{\psi}' = 0$ and consequently $\bar{\partial}f' = \partial\bar{f}' = \bar{\partial}g' = \partial\bar{g}' = \bar{\partial}a' = \partial\bar{a}' = 0$.

Having fixed the gauge we use the definition of the fields in terms of f', g' and a' to obtain the metric $g_{K\bar{K}} = \Omega(K) dK d\bar{K}$ with

$$\Omega(K) \;=\; \frac{1}{2}\int_{\mathbb{R}\times S^1} \partial\bar{\partial}\left(|f'|^2 + |g'|^2 + \frac{1}{2}|\partial_{\bar{s}}\psi'|^2\right) dr\, dt. \tag{4.20}$$

A similar computation to that above has been implemented numerically by Ward (see figure 4.6 at the end of this discussion). Here we ask whether it is possible to obtain more explicit information in the limit of large C. The fact $|\mu_+\mu_-|$ scales as C suggests solutions to (4.3) are only supported when both sides vanish, as can also be seen numerically by plotting figure 4.1 for larger C. This gives the singular solution[12]

$$\mathrm{Re}(\psi) \;=\; \log\frac{|\mu_-|}{|\mu_+|},$$

from which (4.18) and (4.19) result in

$$u \;=\; \frac{\mathrm{i}}{8}\log\left(\frac{\mu_-\bar{\mu}_+}{\mu_+\bar{\mu}_-}\right) \qquad \Rightarrow \qquad \Phi' \;=\; \sqrt{fg}\begin{pmatrix} 0 & 1 \\ 1 & 0 \end{pmatrix}. \tag{4.21}$$

In this gauge the metric reduces to

$$\Omega(K) \;=\; \frac{1}{2}\int_{\mathbb{R}\times S^1} \mathrm{tr}\left(\partial\Phi'\bar{\partial}(\Phi'^{\dagger})\right) dr\, dt \;=\; \frac{1}{2}\int_{\mathbb{R}\times S^1} \mathrm{tr}\left(\partial\Phi'(\partial\Phi')^{\dagger}\right) dr\, dt$$

$$=\; \frac{1}{4}\int \frac{|\partial\mathrm{det}(\Phi')|^2}{|\mathrm{det}(\Phi')|}\, dr\, dt \;=\; \frac{1}{16}\int \frac{1}{|C\cosh(\beta s) + K/2|}\, dr\, dt \tag{4.22}$$

where the second equality follows from the fact Φ is holomorphic in K and the third is a rewriting of (4.20), where the final term vanishes in this limit. The integral for the conformal factor is straightforward to perform numerically. The result is shown in figure 4.5 and should be compared with figure 3.4, obtained from the monopole fields within the spectral approximation. The equality between the integrals (4.22) and (3.24) can in fact be seen directly by the coordinate transformation $\zeta = \sqrt{C\cosh(\beta s) + K/2}$, such that

$$dr\wedge dt \;=\; \frac{\mathrm{i}}{2}\, ds\wedge d\bar{s} \;=\; \frac{2\mathrm{i}|\zeta|^2}{\beta^2 C^2|\sinh(\beta s)|^2}\, d\zeta\wedge d\bar{\zeta} \;=\; \frac{4|C\cosh(\beta s) + K/2|}{\beta^2\prod_{i=1}^4|\zeta-\zeta_i|}\, dx\wedge dy$$

[12] It should be noted that although this solution only depends on K/C, numerical solutions away from this singular limit (such as those of figure 4.1) depend on both K/C and C. Furthermore, whenever this solution is valid, then ψ, and hence Φ and F, do not depend on the moduli encoded in the function α.

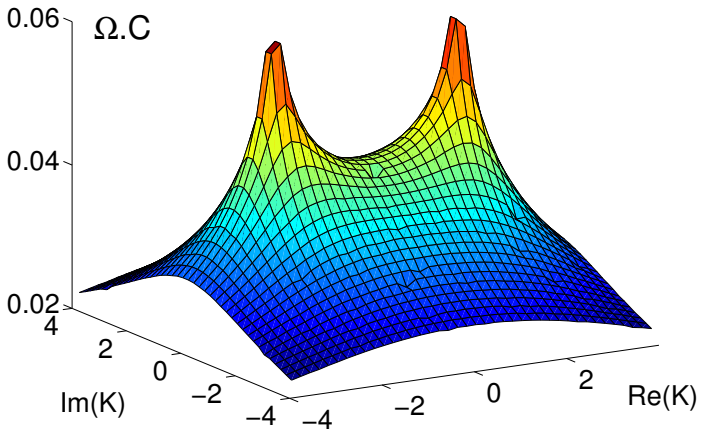

Figure 4.5: Surface plot of the conformal factor. Peaks are at $K = \pm 2C$.

where the product is over the spectral points (3.14). It is possible to evaluate the integral (4.22) explicitly when $K = 0$ in terms of elliptic integrals,

$$\iint \frac{dr\,dt}{|\cosh(\beta s)|} = \int_{r=-\infty}^{\infty} dr \int_{t=0}^{2\pi/\beta} dt\, \frac{1}{\sqrt{\cosh^2(\beta r) - \sin^2(\beta t)}} =$$

$$= \frac{4}{\beta}\int_{r=-\infty}^{\infty} \mathrm{sech}(\beta r)\mathbf{K}(\mathrm{sech}(\beta r))\,dr = \frac{8}{\beta^2}\int_{y=0}^{1} \frac{\mathbf{K}(y)}{\sqrt{1-y^2}}\,dy = \frac{1}{2\pi\beta^2}\left(\Gamma(\tfrac{1}{4})\right)^4, \tag{4.23}$$

in agreement with (3.26). The gauge condition has been implemented numerically by Ward, with conventions

$$2C_W^2 = C \qquad\qquad CK_W = -K. \tag{4.24}$$

The results presented in figure 4.6 overleaf show that the large C limit is valid for $C \gtrsim 50$. In this limit, we see from (4.21) and (4.22) that the metric is insensitive to our choice of 'zeros together' or 'zeros apart' configuration in section 4.1.1, as was suggested by the spectral approximation of chapter 3. The independence of the singular solution to (4.3) from the moduli encoded in α will be explored further in the next section, where we will see that the resulting contributions are suppressed in this limit. Similar expressions to (4.16) and (4.17) can be given when $\alpha \neq 0$, although in this case there do not seem to be any helpful cancellations.

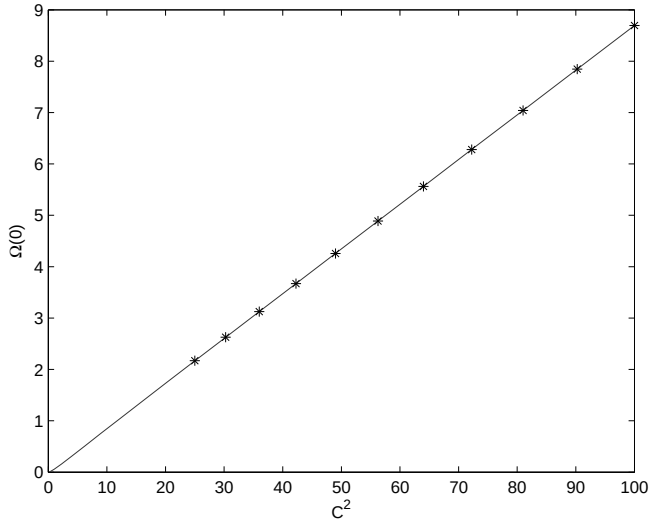

Figure 4.6: $g_{K_W\overline{K_W}}(K=0)$ against $C_W^2 = C/2$ for numerical solutions with $\beta = 2\pi$, with a straight line fit of gradient 0.0870 (the analytical gradient expected from (4.23, 4.24) is $g(0) \approx 0.08708$). The 'large C limit' appears to be a good approximation for $C \gtrsim 50$. (Note the scaling with C arises from combining the conformal factor (4.22) with the rescaled K coordinates.) [Unpublished figure due to Ward.]

A Remark on the SU(3) Metric

The integrand in (4.22) can be obtained from the spectral curve (3.13) using (2.18), which tells us that $\det(\Phi) = -(C\cosh(\beta s) + K/2)$. We apply the same idea to the SU(3) periodic monopole of charge $\boldsymbol{k} = (1,1)$. This monopole was previously discussed in section 3.4.1 and section 3.4.3, where a symmetric one parameter family was described within the spectral approximation. This time, the spectral curve is (equations 3.29 and 3.30; recall that $w = \mathrm{e}^{\beta s} = \mathrm{e}^{\beta(r+\mathrm{i}t)}$)

$$w^3 + (a_{1,1}\zeta + a_{1,0})w^2 + (a_{2,1}\zeta + a_{2,0})w - 1 \;=\; 0$$

together with the centering condition (3.31)

$$a_{1,1}a_{2,1}(a_{1,1}a_{2,0} + a_{1,0}a_{2,1}) + 2(a_{1,1}^3 - a_{2,1}^3) \;=\; 0. \tag{4.25}$$

The coefficients $a_{1,1}$ and $a_{2,1}$ are parameters, and are fixed by the boundary conditions. Using (4.25) to write $a_{2,0}$ in terms of $a_{1,0}$ leaves us with one complex modulus $a_{1,0}$.

The Hitchin spectral curve (2.18) now tells us that $\Phi = \zeta$. For rank 1

Nahm/Hitchin data, the gauge condition (4.12) is automatically satisfied. Considering variations of the modulus $a_{1,0}$, the moduli space metric (4.14) is

$$g_{a_{1,0}\overline{a_{1,0}}} = \int \left|\frac{\partial\zeta}{\partial a_{1,0}}\right|^2 dr\,dt = \frac{1}{|a_{1,1}|^2}\int \left|\frac{a_{1,1}w - a_{2,1}}{a_{1,1}w + a_{2,1}}\right|^2 dr\,dt$$

(note that this formula also works for the charge 2 SU(2) case (4.22)). The integral is now divergent, suggesting that $a_{1,0}$ is not a modulus but must be kept fixed. Thus, although figure 3.14 describes a symmetric one parameter family of SU(3) monopoles, it does not represent their physical scattering. It may, in fact, be necessary to keep not just the overall centre of mass fixed, but also the centre of mass of each species of monopole. If this were the case, the $\boldsymbol{k} = (1,1)$ monopole would have no reduced moduli, while the $\boldsymbol{k} = (2,1)$ monopole would have 2 real reduced moduli describing the relative motion of the monopoles embedded along the root $\boldsymbol{\beta}_1^*$.

$\mathbb{R}^3$ monopoles embedded via different roots of $\mathfrak{su}(3)$ are allowed to interact, in a way described by the Lee-Weinberg-Yi metric [LWY96]. This metric is globally of Taub-NUT type (equation 1.17 with r replaced by $-r$).

4.3.3 Incorporating the Remaining Moduli

The numerical solutions to the Hitchin equations (4.3) studied in section 4.2 show that for $|K|/C \gg 2$ the lumps on the cylinder become sharply peaked at $s = \pm\beta s_0 = \pm\cosh^{-1}(K/2C)$, as shown in figure 4.2. In order to study the effect of the remaining moduli we will work with the approximate fields for $|\mathrm{Re}(s)| < |\mathrm{Re}(s_0)|$

$$\phi = \sqrt{C\cosh(\beta s) + K/2}\;\sigma_3 \qquad a_t = \frac{\beta}{2\pi}\,\mathrm{i}\theta\sigma_3 \qquad a_r = 0. \tag{4.26}$$

In the 'outside' region, where $|\mathrm{Re}(s)| > |\mathrm{Re}(s_0)|$, the Higgs field ϕ is branched along the half-lines $t = t_0$ (for $r > r_0$) and $t = -t_0$ (for $r < -r_0$). The Higgs field changes by a sign across the cut, and is matched by a gauge transformation in the σ_1/σ_2 plane of $\mathfrak{su}(2)$. This allows an additional contribution to the gauge potential a_t, which is independent of r, valued in σ_1/σ_2, and supported only along the cut. The gauge field vanishes everywhere except at $s = \pm s_0$, where a_t is discontinuous, giving rise to delta-function peaks in the field strength f at these points. To each of the peaks we assign a unit vector $f_\pm$ in the σ_1/σ_2 plane of $\mathfrak{su}(2)$.

Motivated by numerical examples by Ward we define one of the two remaining moduli, θ, by the holonomy of a_t in the central region (see also figure 4.3),

$$U_0 \;=\; \mathcal{P}\mathrm{exp}\left(-\int_0^{2\pi/\beta} a_t(0,t)\,dt\right) \qquad\qquad 2\cos(\theta) \;=\; \mathrm{tr}(U_0),$$

which we compute through $\partial_t U(t) = -a_t(0,t)U(t)$, with $U(0) = \mathbf{1}_2$ and $U_0 = U(2\pi/\beta)$. This defines θ up to a sign, and in particular if we take $K = k\mathrm{e}^{\mathrm{i}\varphi}$ then the sign of θ changes as φ goes from 0 to 2π (here we simplify the discussion by taking $\mathrm{Re}(K) > 0$). A prescription to fix the sign was given by Ward [MW13]. This is done by defining the sign of θ as the sign of the real or imaginary part of the quantity $\mathrm{i.tr}(U_0\phi)$ evaluated at $r = t = 0$. The details will not affect our discussion of the asymptotic metric, where we take $\mathrm{Re}(K) > 0$ (section 4.3.4), but we will make use of this procedure in section 4.3.6.

The fourth modulus, ω, is the relative phase between the peaks at $s = \pm s_0$. This is computed by parallel propagating f_- along a path γ from $-s_0$ to s_0 using $\partial_\gamma f_- = -[a_\gamma, f_-]$, to obtain $\tilde{f}_-$. Then ω is the angle between f_+ and $\tilde{f}_-$,

$$2\cos(\omega) \;=\; \mathrm{tr}(f_+\tilde{f}_-),$$

and is defined up to a sign, which can again be fixed by comparing with the sign of $\phi(0)$.[13]

4.3.4 The Asymptotic Metric

The moduli space metric for well separated periodic monopoles was deduced by Cherkis & Kapustin [ChK02] from physical considerations by studying the effective Lagrangian of a system of two monopole chains, following Manton's earlier approach for monopoles in $\mathbb{R}^3$, [Man85]. One can obtain a metric of the same ALG form from the Nahm/Hitchin perspective. We do this by identifying four orthogonal perturbations of the fields, which arise from certain perturbations of the moduli, and then changing coordinates to obtain the metric on

[13] This definition of ω rests on the fact that the peaks in $|f|$ become delta functions for large $|K|/C$, so is only well defined in the asymptotic region of the moduli space. Numerical studies by Ward suggest that a globally valid modulus can be obtained from the difference of the asymptotic holonomies (which individually are fixed by the boundary conditions), $2\cos(\tilde{\omega}) = \mathrm{tr}(U_+U_-^\dagger)$, with $\tilde{\omega} - \omega = \pi$. In section 4.3.4 we will work with ω rather than $\tilde{\omega}$ because, as discussed above, (4.26) is only valid in the interior region, $|\mathrm{Re}(s)| < |\mathrm{Re}(s_0)|$. However, when we come to discuss geodesic surfaces through the centre of the moduli space in section 4.3.6, our definition of ω will be in terms of $\tilde{\omega}$.

the moduli space itself. This scheme was proposed by Ward, while its correct form of implementation arose from various discussions.

The first step is to define a set of vectors of perturbations to the approximate fields (4.26) given by $V_i = (\delta_i\phi, \delta_i a_{\bar{s}})$ (we will see below that $i = 1, \ldots, 4$) with inner product

$$\langle V_i, V_j \rangle \;=\; \frac{1}{2}\,\mathrm{Re}\int \mathrm{tr}\left((\delta_i\phi)(\delta_j\phi)^\dagger + 4(\delta_i a_{\bar{s}})(\delta_j a_{\bar{s}})^\dagger\right)\, dr\, dt.$$

We observe that if $V_1 = (\delta_1\phi, \delta_1 a_{\bar{s}})$ is a perturbation satisfying (4.13) then so are

$$\begin{aligned} V_2 &= (\delta_2\phi, \delta_2 a_{\bar{s}}) = (\mathrm{i}\delta_1\phi, \mathrm{i}\delta_1 a_{\bar{s}}) \\ V_3 &= (\delta_3\phi, \delta_3 a_{\bar{s}}) = (2\delta_1 a_s, \tfrac{1}{2}\delta_1\phi^\dagger) \\ V_4 &= (\delta_4\phi, \delta_4 a_{\bar{s}}) = (2\mathrm{i}\delta_1 a_s, \tfrac{1}{2}\mathrm{i}\delta_1\phi^\dagger) \end{aligned} \tag{4.27}$$

for which the inner product is $\langle V_i, V_j \rangle = p^2\delta_{ij}$ for some constant p (which is computed below).

Each of these perturbations V_i gives rise to a change in the moduli $\delta_i K^a = (\delta_i K_\mathrm{r}, \delta_i K_\mathrm{i}, \delta_i\theta, \delta_i\omega)$ with $K = K_\mathrm{r} + \mathrm{i}K_\mathrm{i}$. The most general perturbation can then be expressed as the linear combination $V = a_i V_i$, with a corresponding change in the moduli $\delta K^a = a_i \delta_i K^a$. The coefficients a_i for a given variation of the moduli are given by

$$a_i \;=\; (Q^{-1})_{ia}\delta K^a,$$

where

$$Q_{ai} \;=\; \delta_i K^a \;=\; \begin{pmatrix} \delta_1 K_\mathrm{r} & \delta_2 K_\mathrm{r} & \delta_3 K_\mathrm{r} & \delta_4 K_\mathrm{r} \\ \delta_1 K_\mathrm{i} & \delta_2 K_\mathrm{i} & \delta_3 K_\mathrm{i} & \delta_4 K_\mathrm{i} \\ \delta_1\theta & \delta_2\theta & \delta_3\theta & \delta_4\theta \\ \delta_1\omega & \delta_2\omega & \delta_3\omega & \delta_4\omega \end{pmatrix} \tag{4.28}$$

and the metric is computed as the inner product of the tangent vectors,

$$\begin{aligned} g \;=\; \langle V, V\rangle &= \langle a_i V_i, a_j V_j\rangle \\ &= (Q^{-1})_{ia}(Q^{-1})_{jb}\delta K^a \delta K^b \langle V_i, V_j\rangle \\ &= p^2\left((Q^{-1})^T Q^{-1}\right)_{ab}\delta K^a \delta K^b \\ \Rightarrow \quad g_{ab} &= p^2\left(QQ^T\right)^{-1}_{ab}. \end{aligned}$$

A suitable perturbation to the Hitchin fields (4.26) corresponding to $K_\mathrm{r} \mapsto$

$K_{\rm r}+\epsilon$ is $\delta_1\phi=\frac{1}{4}\epsilon h(r,t)\sigma_3$, $\delta_1 a_{\bar s}=0$, or equivalently $\delta_1 K_{\rm r}=\epsilon$, $\delta_1 K_{\rm i}=\delta_1\theta=\delta_1\omega=0$, where we define

$$h(r,t) \;=\; (-\det\phi)^{-1/2} \;=\; (C\cosh(\beta s)+K/2)^{-1/2}.$$

The norm-squared of V_1 is

$$\langle V_1,V_1\rangle \;=\; p^2 \;=\; \epsilon^2 I \;=\; \frac{1}{16}\,\epsilon^2\int |h(r,t)|^2\,dr\,dt. \tag{4.29}$$

For V_2 we take $\delta_2\phi=\frac{1}{4}{\rm i}\epsilon h(r,t)$, $\delta_2 a_{\bar s}=0$ and $\delta_2 K_{\rm i}=\epsilon$, $\delta_2 K_{\rm r}=\delta_2\theta=\delta_2\omega=0$.

Continuing with the scheme of (4.27) we get $\delta_3\phi=0$ and $\delta_3 a_{\bar s}=\frac{1}{8}\epsilon\overline{h(r,t)}\sigma_3$, and we must compute the effect of this change on the θ and ω moduli. For θ, we use the approximate solution (4.26) and $\delta_3 a_t=-\frac{1}{4}{\rm i}\epsilon{\rm Re}(h)\sigma_3$ to find $\delta_3\theta=-\frac{1}{4}\epsilon{\rm Re}(h_0)$, where

$$h_0 \;=\; \int_0^{2\pi/\beta} h(0,t)\,dt. \tag{4.30}$$

The perturbation V_3 does not affect $f_\pm$ (this has been checked numerically by Ward), so a variation in ω arises only from the change of the gauge potential a along the path γ between $-s_0$ and s_0, i.e. the new $\tilde f_-$ is computed by parallel propagating f_- using $\partial_\gamma f_-=-[a_\gamma+\delta a_\gamma,f_-]$. This results in $\delta_3\omega=-\epsilon({\rm Im}(J)+{\rm Re}(L))$, where (recalling the definition $K=k{\rm e}^{{\rm i}\varphi}$),

$$J \;=\; \int_0^{r_0} h(r,t_0)\,dr \qquad\qquad L \;=\; \int_{\pi/\beta}^{t_0} h(0,t)\,dt \;\approx\; h_0\,\frac{\varphi}{\beta}. \tag{4.31}$$

The variation of ω is only path-independent up to winding round the cylinder, due to the twisted nature of the moduli. The contour used for (4.31) is sketched in figure 4.7.

Similarly to V_3, the perturbation V_4 has $\delta_4\phi=0$, $\delta_4 a_{\bar s}=\frac{1}{8}{\rm i}\epsilon\overline{h(r,t)}\sigma_3$, with $\delta_4 K_{\rm r}=\delta_4 K_{\rm i}=0$, $\delta_4\theta=-\frac{1}{4}\epsilon{\rm Im}(h_0)$ and $\delta_4\omega=\epsilon({\rm Re}(J)-{\rm Im}(L))$.

The components of the metric are

$$\begin{aligned}
g_{K_{\rm r}K_{\rm r}} &= p^2(\delta_1 K_{\rm r})^{-2}\\
g_{K_{\rm i}K_{\rm i}} &= p^2(\delta_2 K_{\rm i})^{-2}\\
g_{\theta\theta} &= p^2((\delta_3\omega)^2+(\delta_4\omega)^2)\mathcal{D}^{-1}\\
g_{\omega\omega} &= p^2((\delta_3\theta)^2+(\delta_4\theta)^2)\mathcal{D}^{-1}\\
g_{\theta\omega} \;=\; g_{\omega\theta} &= -p^2(\delta_3\theta\delta_3\omega+\delta_4\theta\delta_4\omega)\mathcal{D}^{-1}
\end{aligned}$$

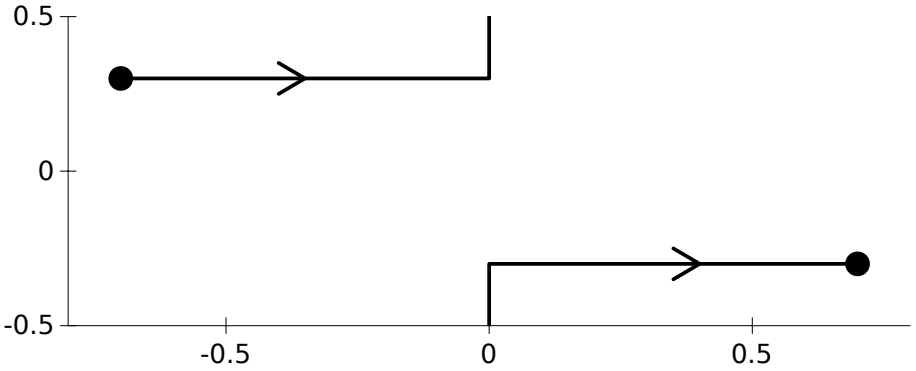

Figure 4.7: Contour on the Hitchin cylinder used to parallel propagate f_- from s_- (the left dot) to s_+ on the right. Circling the cylinder in the opposite direction modifies L to $L \approx h_0(\pi - \varphi)/\beta$.

where $\mathcal{D} = (\delta_3\theta\delta_4\omega - \delta_3\omega\delta_4\theta)^2$ and the integrals I, h_0, J and L can be evaluated by an expansion in $k = |K|$. To first order, we have $h \approx 0$ for $|r| > |r_0|$ and $h \approx (2/K)^{1/2}$ for $|r| < |r_0|$, where $\beta r_0 \approx \log(k/C)$ and $\beta t_0 \approx \varphi + \pi$. Then

$$I \approx \frac{\pi}{2\beta^2 k}\log\left(\frac{4k}{C}\right) \qquad h_0 \approx \frac{2\pi}{\beta}\sqrt{\frac{2}{K}} \qquad J \approx \frac{1}{\beta}\sqrt{\frac{2}{K}}\log\left(\frac{4k}{C}\right), \quad (4.32)$$

where the subleading coefficients (the factors of 4 in I and J) are found by the more careful expansion of appendix B.

Putting everything together and replacing K by the dimensionless quantity $K_W = -K/C$ together with $C = 2C_W^2$ and $dK = -2C_W^2 dK_W$ (equations 4.24) gives the asymptotic metric

$$ds^2 = \frac{\pi\log(4|K_W|)}{\beta^2}\left(C_W^2\frac{|dK_W|^2}{|K_W|} + \frac{\beta^2}{\pi^2}\,d\theta^2\right) + \\ + \frac{\beta^2}{\pi\log(4|K_W|)}\left(\frac{\pi}{2\beta}\,d\omega - \frac{2\pi\varphi}{\beta^2}\,d\theta\right)^2, \quad (4.33)$$

which is of the expected Gibbons-Hawking form [GH78], as was found by Manton [Man85] for the Atiyah-Hitchin metric for monopoles in $\mathbb{R}^3$, (1.17). This metric is therefore Ricci flat and corresponds exactly with the asymptotic metric of Cherkis & Kapustin [ChK02] computed from the long range monopole fields:

$$ds^2_{CK} = \frac{\log(R^2 e^{\pi v_{\rm ren}})}{4\pi}\left(dx^2 + dy^2 + dz^2\right) + \frac{4\pi}{\log(R^2 e^{\pi v_{\rm ren}})}\left(\frac{dt}{2} + \frac{4\pi^2}{\beta}\theta_{\rm rel}\,dz\right)^2.$$

Here the coordinates x, y and z denote the relative positions of the monopole

chains and t is a relative phase. The x and y separations are combined into $x + \mathrm{i}y = R\mathrm{e}^{\mathrm{i}\theta_{\mathrm{rel}}}$. From (3.25) we identify $R = 2C_W\sqrt{|K_W|}$ and $\theta_{\mathrm{rel}} = \varphi/2$. Comparing the remaining moduli and taking into account their respective periodicities, we relate

- the monopole z separation to the holonomy modulus θ via $z = \beta\theta/\pi \in (-\beta, \beta]$, and
- the relative monopole phase t to the Nahm/Hitchin phase ω via $t = -\omega/2 \in [-\pi/2, \pi/2)$.

Our approach also allows us to determine the parameter v_{ren}, which is defined in [ChK02] as a renormalised constant arising from the divergent sum defining the asymptotic Higgs field of an infinite line of Dirac monopoles. In particular, we find $\pi v_{\mathrm{ren}} = \log(2/C)$.

Finally, we note that in the limit of $\beta \to 0$ or $C \to \infty$, the $|dK_W|^2$ term dominates ds^2. Indeed, this is the limit in which the spectral approximation is expected to be valid. In the strict limit, the conformal factor for the $|dK|^2$ part of the metric is given by the integral I (equation 4.29), which is now valid for all values of K/C, including the interior region of the moduli space (see equation 4.22 and figure 4.5).

Sources of Error

It should be noted that in all of the above the knock-on effect of perturbations has been neglected. For example, the perturbation V_2 of the moduli was assumed to affect only ϕ and not $a_{\bar{s}}$. In fact, a change in K affects the positions $s = \pm s_0$ of the delta functions, which in turn alters the path γ between them and hence has an effect on the modulus ω. Including this effect in our computation of the metric gives contributions which decay at large K faster than the leading terms. We note, however, that including such first order corrections fills all the off-diagonal terms in Q.

It should also be noted that the asymptotic metric for two monopoles in $\mathbb{R}^3$ has exponentially small subleading terms [GM86]. In view of the off-diagonal terms in Q, (4.28), this exponential proximity to a Taub-NUT-like metric no longer holds, at least within the crude approximation of the Nahm/Hitchin data as two delta functions.

Another source of error arises in our computation of $\delta\theta$, and whether we use its definition as the t-holonomy at $r = 0$ via (4.30), or attempt to read it off directly from the variations of the fields via (4.26). These approaches agree

to first order, but differ in their subleading terms, at $\mathcal{O}((k/C)^{-3/2})$. However, the factors of 4 appearing in (4.32) and computed in appendix B have been confirmed numerically by Ward for smaller C.

These observations may reduce the relevance of the study of geodesics on the asymptotic metric, which will nevertheless be discussed briefly in the next subsection.

4.3.5 Geodesics on the Asymptotic Metric

Conserved quantities for motion on the asymptotic metric (4.33) can be identified either by solving the Killing equations, or by considering the metric as a Lagrangian and studying the Euler-Lagrange equations of motion, via a similar argument to that of Gibbons & Manton [GM86] for two monopoles in $\mathbb{R}^3$. Writing $\boldsymbol{\rho} = x\hat{\boldsymbol{x}} + y\hat{\boldsymbol{y}}$, the metric is

$$ds^2 \;=\; f(\rho)(dx^2 + dy^2 + dz^2) + f(\rho)^{-1}(dt + h(\theta)dz)^2,$$

and the Killing equations $\partial_a\xi_b + \partial_b\xi_a = 2\xi_c\Gamma^c_{ab}$ can be solved on Maple if we impose the condition $\partial_a\xi^a = 0$. The most general Killing vector under this assumption is then

$$\xi \;=\; c_1(-y\partial_x + x\partial_y - \alpha z\partial_t) + c_2\partial_z + c_3\partial_t \;=\; c_1\xi^{\boldsymbol{J}} + c_2\xi^{p_z} + c_3\xi^q,$$

for constants c_1, c_2, c_3.

The conserved quantities p_z and q also follow directly from the Lagrangian

$$\mathcal{L} \;=\; f(\rho)(\dot{x}^2 + \dot{y}^2 + \dot{z}^2) + f(\rho)^{-1}(\dot{t} + h(\theta)\dot{z})^2,$$

as the canonical momenta $p_{x_i} = \partial\mathcal{L}/\partial\dot{x}_i$ conjugate to translations in z and the phase direction,

$$q \;=\; p_t \;=\; 2f(\rho)^{-1}(\dot{t} + h(\theta)\dot{z}) \qquad\qquad p_z \;=\; 2f(\rho)\dot{z} + qh(\theta),$$

and these are conserved due to the Euler-Lagrange equations, $\dot{p}_{x_i} = \partial\mathcal{L}/\partial x_i$. The conserved quantity $\boldsymbol{J}$ is a modified angular momentum in the xy plane plus a 'Poincaré term' consisting of a z dependent translation in the phase direction t. To see this, we combine the momenta p_x and p_y into

$$\boldsymbol{p} \;=\; 2f(\rho)\dot{\boldsymbol{\rho}},$$

for which the Euler-Lagrange equations give

$$\dot{\boldsymbol{p}} = f'(\rho)\left(\dot{\rho}^2 - \dot{z}^2 - \frac{q^2}{4}\right)\hat{\boldsymbol{\rho}} + \frac{q\dot{z}h'(\theta)}{\rho}\hat{\boldsymbol{z}} \times \hat{\boldsymbol{\rho}}.$$

The planar angular momentum $\boldsymbol{\rho} \times \boldsymbol{p}$ is not conserved (in particular, $\boldsymbol{\rho} \times \dot{\boldsymbol{p}}$ contains a term proportional to $\boldsymbol{\rho} \times (\hat{\boldsymbol{z}} \times \hat{\boldsymbol{\rho}}) = \rho\hat{\boldsymbol{z}}$). We compensate for this by adding a term $-qh'(\theta)\boldsymbol{z}$ and making use of the fact that $\dot{q} = h''(\theta) = 0$ to find

$$\boldsymbol{J} = \boldsymbol{\rho} \times \boldsymbol{p} - qh'(\theta)\boldsymbol{z}.$$

We note that the Poincaré term is parallel to the 'orbital term', in contrast to the case of Gibbons & Manton [GM86], in which the two terms are orthogonal. Despite the similarities with the $\mathbb{R}^3$ monopole case, there does not appear to be a generalisation of a conserved Runge-Lenz vector of the form $\boldsymbol{K} = \boldsymbol{p} \times \boldsymbol{J} + \boldsymbol{v}$ for some suitably chosen vector $\boldsymbol{v}$ (the case of Gibbons & Manton being specific to the case $f = 1 - 1/r$). Furthermore, we note that the vectors $\xi^{\boldsymbol{J}}$ and ξ^{p_z} do not commute.

With the conserved quantities $\boldsymbol{J}$, p_z and q in mind, we can search for geodesics on the asymptotic moduli space. We again simplify the problem by looking for geodesics with $\dot{\rho} = 0$, and in this case it is easy to see that no such geodesics exist.

It is worth reiterating the caveat that unlike the case of the Atiyah-Hitchin metric, the metric currently under consideration is not exponentially close to the complete metric on the moduli space of two monopole chains. There is thus no guarantee that any geodesics on the metric (4.33) provide an accurate description of two such monopole chains, even when well separated.

4.3.6 Geodesic Surfaces

As was outlined in sections 4.1.2 and 4.1.3, the symmetries of the Hitchin equations, spectral curve and Nahm operator fix geodesic submanifolds of the full moduli space, which are valid even in the interior region of the moduli space. In particular, it was shown that setting the modulus α to zero provides two two-dimensional families of solutions (which we referred to as 'zeros together' or 'zeros apart', according to the allocation of the zeros of $\det(\Phi)$ among the entries of the 2×2 matrix Φ). We are now in a position to study these surfaces with reference to the moduli θ and ω. Recall from section 4.1.3 that there is a symmetry $z \mapsto -z$ associated with the transformation $(\Phi, A) \mapsto (-\Phi, A)$,

which sets the modulus α appearing in (4.3, 4.4) to $\alpha = 0$. Furthermore, from the prescription given in section 4.3.3 to fix the signs of θ and ω, this symmetry of the Hitchin fields is associated with the transformations $\theta \mapsto -\theta$ and $\omega \mapsto -\omega$. We then have four geodesic surfaces, with $\theta, \omega \in \{0, \pi\}$ (recall from section 4.3.3 that in the central region of the moduli space, ω is defined via the globally valid $\tilde{\omega} = \omega + \pi$).

From the discussion of holonomies in section 4.2.2, we see that the 'zeros together' solution has $\omega = 0$, and $\theta = 0$ or π according to the choice of $\mathrm{Im}(\psi) = 0$ or $2\beta t$. This gives two disconnected surfaces describing physically equivalent scattering processes. Geodesics on either of these surfaces describe monopole scattering in the xy plane, and particularly symmetric examples are the 90° scattering processes with $K \in \mathbb{R}$ and $K \in \mathrm{i}\mathbb{R}$. Each of the surfaces is analogous to the Atiyah-Hitchin cone, which describes 90° scattering of $\mathbb{R}^3$ monopoles in the plane. Energy density plots illustrating this geodesic are given in chapter 5.

On the other hand, the 'zeros apart' configuration has $\omega = \pi$, and asymptotically we have two separate sheets, with $\theta = 0$ and $\theta = \pi$. Unlike in the previous case, however, the 'zeros apart' case contains configurations which are invariant under a shift by $\beta/2$, namely when $K/C = \pm 2$, which is a charge 1 chain of period $\beta/2$ (see [HW09] and section 6.3). Thus, in this case the central region of the moduli space is branched over the line segment $-2 \leq K/C \leq 2$, and crossing this line segment transfers us from one sheet to the other. This branching structure explains the use of the coordinate W in section 4.1.2, where $K/C = W + 1/W$, ensuring that the correct branch is chosen when crossing $|W| = 1$. This surface is analogous to the Atiyah-Hitchin trumpet, although, unlike in the case of monopoles in $\mathbb{R}^3$, the trumpet has two openings to become a 'double trumpet', with a closed geodesic about its waist (see figure 4.8 overleaf).

Referring to figure 4.5, which gives the conformal factor multiplying the $K\bar{K}$ part of the metric for large C, we note that in the 'zeros together' configuration geodesics are allowed to pass over the peaks at $K/C = \pm 2$. However, for 'zeros apart', geodesics reaching these points bounce back to give two distinct scattering processes: a scattering geodesic for $K/C \geq 2$ (or $K/C \leq -2$) and a closed geodesic with $-2 \leq K/C \leq 2$. For 'zeros together', Ward has implemented the gauge condition (4.12) numerically and plotted the conformal factor for various values of C (see figure 1 of [MW13]). This illustrates the smoothing out of the peaks and the approach to the rotational symmetry of

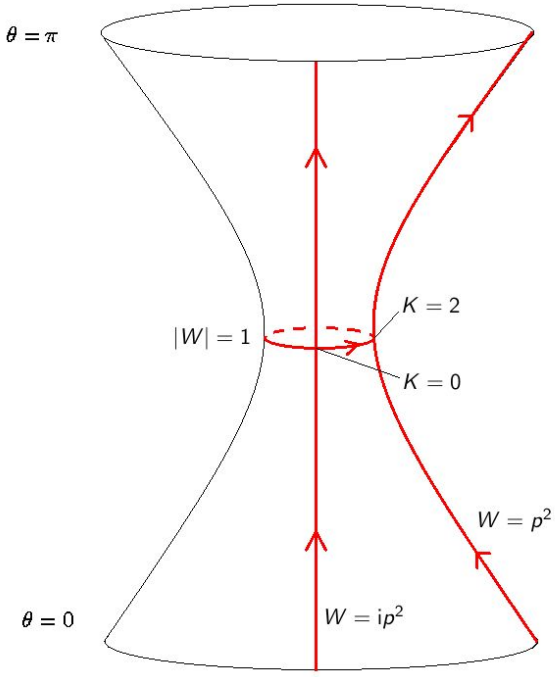

Figure 4.8: Sketch of the 'double trumpet' showing the geodesics with $W \in \mathbb{R}$, $W \in \mathrm{i}\mathbb{R}$ and $|W| = 1$ identified in section 4.1.2.

the $\mathbb{R}^3$ limit as $C \to 0$. In this limit, we expect there to be an approximate symmetry fixing geodesics with $W = p^2 \mathrm{e}^{\mathrm{i}\nu}$ for $p \in \mathbb{R}$ and a given $\nu \in \mathbb{R}$. The resulting trajectories describe two consecutive 90° scattering processes, with an overall scattering angle of ν and a shift by $\beta/2$. This can be seen by applying the method of section 4.1.2. For general C, the asymptotic form of (4.6) for $|W| \ll 1$ is

$$\mu_+ \approx \sqrt{\frac{C}{2}}\, \mathrm{e}^{\beta s/2} \qquad \mu_- \approx \sqrt{\frac{C}{2}}\, W^{-1} \mathrm{e}^{-\beta s/2},$$

then transforming $W \mapsto \mathrm{e}^{2\mathrm{i}\nu} W^{-1}$ and using a similar approximation for $|W| \gg 1$ gives

$$\mu_+ \approx \sqrt{\frac{C}{2}}\, W \mathrm{e}^{-\beta s/2} \qquad \mu_- \approx \sqrt{\frac{C}{2}}\, \mathrm{e}^{\beta s/2},$$

which relates the Higgs fields at large and small $|W|$ by the gauge transformation

$$\Phi \mapsto \mathrm{e}^{\mathrm{i}\nu} g^{-1} \Phi g \qquad \text{with} \qquad g = \begin{pmatrix} 0 & \mathrm{e}^{\mathrm{i}\nu} \\ \mathrm{e}^{\mathrm{i}\beta t} & 0 \end{pmatrix},$$

and the transformation of the gauge potential describes the $\beta/2$ shift.

4.4 Summary

We began this chapter by identifying two solutions of the Hitchin equations required for the Nahm construction of periodic monopoles. This allowed a study of the spatial symmetries of the corresponding monopole chains via the symmetries of the inverse Nahm operator. This also allowed us to get a feel for the effect of the moduli which were missing from the spectral approximation of chapter 3. Numerical investigations illustrating monopole chains with these symmetries will be given in the next chapter. We then turned our attention to the properties of the solutions of the Hitchin equations, and in particular to the holonomy of the Hitchin fields over the periodic direction of the cylinder.

Finally, an approximate solution to the Hitchin equations allowed us to derive the asymptotic moduli space metric from the Nahm transformed fields. This was favourably compared to results obtained from the monopole side of the transform. Symmetry considerations allowed the identification of geodesic submanifolds resembling the Atiyah-Hitchin cone and trumpet for monopoles in $\mathbb{R}^3$, although in this case the periodic nature of the solutions allows for the existence of a closed geodesic describing a chain of rotating monopoles. These submanifolds were described by the same moduli which appeared in the large C 'spectral approximation', and the metrics were found to agree in this limit. It would be interesting to consider an effective electromagnetic description of well separated lumps on the Hitchin cylinder and to use this as physical motivation of the asymptotic metric by constructing the Lagrangian of this system, following [Man85] and [ChK02].

Many of the arguments of this section can be applied to the doubly periodic monopole. In this case one expects the Nahm transform to be self-reciprocal and the metric of two well separated walls is of ALH form [HKM14]

$$ds^2 \;=\; 16\pi^2 M(dM^2 + dp^2 + dq^2) + \frac{1}{16M}\left(d\omega - 8\pi(qdp - pdq)\right)^2 .$$

Studying the symmetries of this system gives rise to scattering geodesics (for which the moduli space is asymptotically four cylinders) and closed geodesics describing scattering in the periodic plane (here the moduli space is topologically a 2-sphere). However, in contrast to the singly periodic monopole, there is the possibility of incoming geodesics getting 'trapped'. More details on doubly periodic monopoles can be found in the references [Lee98, War05, War08, ChW12, MW14].

5

Scaling Limits

This chapter describes the limiting cases of charge 2 monopole chains for small and large values of the size to period ratio. When the monopole size C is small or the period β is large, we expect the monopole chains to behave like monopoles in $\mathbb{R}^3$. In particular, a charge one monopole should be spherically symmetric and two coincident monopoles should have rotational symmetry in place of the discrete symmetry of figure 3.3. Meanwhile, the Nahm data should reduce from Hitchin equations on a cylinder to Nahm equations on a line segment. At the other end of the range, when the monopole size is much larger than the period we expect to recover the results of the spectral approximation (chapter 3). Both of these limits can be implemented by the numerical procedures used in the previous chapters. However, analytical results are delicate due to the expected changes to the boundary conditions. First of all, in section 5.1, we discuss the limit of small monopole size to period ratio, followed by the opposite limit of large size to period in section 5.2. Finally, energy density plots interpolating between these limits are presented in section 5.3. This chapter is based on the preprint [Mal*b*].

Numerical implementation of the inverse Nahm transform to obtain the monopole fields used the gradient descent technique employed by Harland & Ward [HW09] (for details, see section 4.1.4). The energy density was then calculated using equation 1.7.

5.1 Small C

In the limit of small size to period ratio, monopole chains resemble monopoles in $\mathbb{R}^3$, whose energy density peaks roughly at the location of the zeros of the

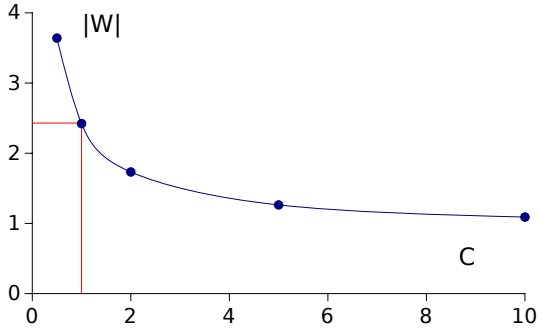

Figure 5.1: $|W|$ against C, showing how the value of $|W|$ at which the monopole Higgs zeros coincide in the 'zeros apart' configuration depends on C, both for $W \in \mathbb{R}$ and $W \in \mathrm{i}\mathbb{R}$. For 'zeros together', the monopole zeros always coincide when $K = 0$.

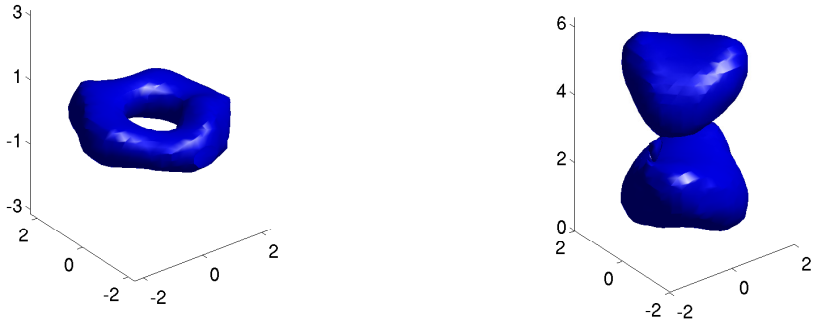

Figure 5.2: Energy density for a charge 2 monopole chain (taken over one period) in the 'zeros together' (left) and 'zeros apart' (right) configurations with $\beta = 2\pi$, $C = 1$ and $W = \mathrm{i}$. In the notation of section 4.1.2 these configurations have symmetry groups $D_{4\mathrm{h}}$ and $D_{2\mathrm{d}} \times \mathbb{Z}_2$.

Higgs field. The two scattering processes identified in section 4.1.2 correspond in this limit to the Atiyah-Hitchin rounded cone ('zeros together') and trumpet ('zeros apart'), as geodesic submanifolds of the full four dimensional moduli space (see sections 1.4.1 and 4.3.6). Although it is straightforward to reach the above conclusions numerically, the limit is nevertheless delicate to provide analytically in the present formulation. In particular, it is not clear how the ALG type metric reduces to the usual ALF of monopoles in $\mathbb{R}^3$ [ChK02]. In this limit we also see that the coordinate W goes bad, in the sense that the value of W at which the monopole Higgs zeros coincide increases as $C \to 0$, as shown in figure 5.1.

The particularly symmetric case with $K = 0$ is shown in figure 5.2 for the 'zeros together' and 'zeros apart' solutions, displaying the expected spatial symmetries (section 4.1.2 and [Mal13]). The 'zeros apart' geodesic for $C = 1$

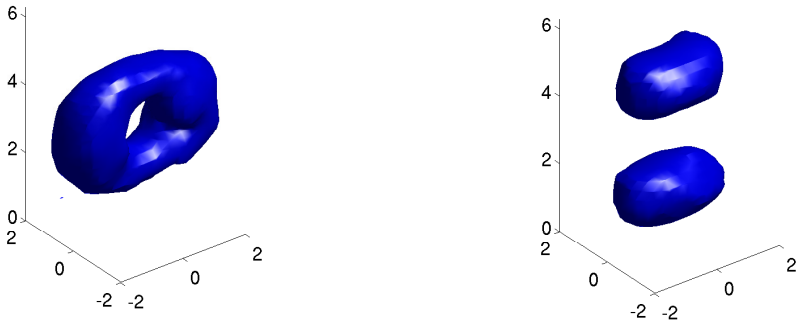

Figure 5.3: Energy density for a charge 2 monopole chain in the 'zeros apart' configuration with $C = 1$ and $W = 2.43$ (left) and $W = 1$ (right). These configurations show the symmetries D_{2h} and $D_{2h} \times \mathbb{Z}_2$.

and $W > 1$ has two monopole chains incoming along the x-axis, whose energy density is peaked at the Higgs zeros. At $W \approx 2.43$ (see figure 5.1) the Higgs zeros coincide to give a toroidal configuration (figure 5.3 left). Reducing W further, the ring breaks up along the z-axis, giving two copies of a charge 1 monopole when $W = 1$ (figure 5.3 right, see also [HW09, Mal*b*]), which move apart parallel to the x-axis for $W < 1$. The geodesic with $W \in \mathrm{i}\mathbb{R}$ again involves a double scattering, although this time the 'doubled' charge 1 chain is not encountered and chains depart at 90° to the incoming chains. This process is illustrated in section 5.3.

5.1.1 Regaining the Nahm Equations

Defining the combinations

$$\Phi = \mathrm{i}(T_1 + \mathrm{i}T_2) \qquad A_r = T_0 \qquad A_t = T_3 \tag{5.1}$$

of the Hitchin fields with $T_i = \frac{1}{2}\mathrm{i}f_i\sigma_i$ (no sum implied), we take the limit $C = 0$, such that $\det(\Phi) = -K/2$ and the Hitchin fields on the cylinder depend only on r. This reproduces the usual Nahm equations in $\mathbb{R}^3$, and although this approach is only valid in the strict limit $C \to 0$, it is interesting to note how the different 'zeros together' and 'zeros apart' solutions can still be seen in this limit.

In the above notation, the Hitchin equations become Nahm equations, such that the functions f_i satisfy

$$\frac{df_i}{dr} = \frac{1}{2}\epsilon_{ijk}f_jf_k \tag{5.2}$$

and the Hitchin fields become

$$\Phi \;=\; -\frac{1}{2}\begin{pmatrix} 0 & f_1+f_2 \\ f_1-f_2 & 0 \end{pmatrix} \qquad\qquad \frac{d\psi}{dr} \;=\; 2f_3$$

where we have chosen a gauge with $A_r = 0$ and we recall from section 4.1.1 that $A_{\bar{s}} = -\frac{1}{4}\partial_{\bar{s}}\psi\sigma_3$. The spectral curve tells us that

$$-\det(\Phi) \;=\; \tfrac{1}{4}(f_1^2 - f_2^2) \;=\; C\cosh(\beta s) + K/2,$$

and (5.2) immediately requires $C = 0$. In this form, with $\alpha = 0$ and $K \in \mathbb{R}$, the Nahm equations can easily be solved in terms of elliptic functions [BPP82, MS04].

For real f_i the Nahm transform provides a clear link between the symmetries of (ζ, z) and those of (Φ, T_3), as described in section 1.3. It is therefore expected that there will be different solutions to the Nahm equations corresponding to the relative magnitudes of f_1^2, f_2^2, f_3^2. We note from [BPP82, MS04] that for large K the monopoles are located on the axis e_i corresponding to the largest of the f_i^2. We will fix $\zeta = e_1 + \mathrm{i}e_2$ and $z = e_3$ (this is a gauge choice on the Nahm data), with monopoles incoming along e_1.

First of all we take $f_1^2 \geq f_2^2 \geq f_3^2$, and define a function $a(K)$ and the elliptic modulus $k \in [0, 1]$ by

$$f_1^2 - f_2^2 \;=\; 2K \qquad\qquad f_1^2 - f_3^2 \;=\; a^2 \qquad\qquad 2K \;=\; a^2k^2$$

which are solved in terms of Jacobi elliptic functions defined for $|ar| < \mathbf{K}(k)$, where $\mathbf{K}(k)$ is the complete elliptic integral (3.20),

$$f_1 \;=\; a\,\mathrm{dc}_k(ar) \qquad\qquad f_2 \;=\; ak'\mathrm{nc}_k(ar) \qquad\qquad f_3 \;=\; ak'\mathrm{sc}_k(ar). \qquad (5.3)$$

In the limit $K \to 0$ the monopole chains approach one another and

$$f_1 \;=\; f_2 \;=\; a\sec(ar) \qquad\qquad f_3 \;=\; a\tan(ar) \qquad\qquad \psi \;=\; 2\log(2ab\sec(ar))$$

for some constant b. The equality $f_1 = f_2$ in this limit describes a monopole configuration which is axially symmetric about the periodic axis, and leads to 90° scattering in the plane when K becomes negative (in other words, when $f_2^2 \geq f_1^2 \geq f_3^2$). Figure 5.4 (left) shows a plot of $f_1 \pm f_2$ for $k = 0.9$, illustrating how both zeros are in the same component of Φ (i.e. the 'zeros together'

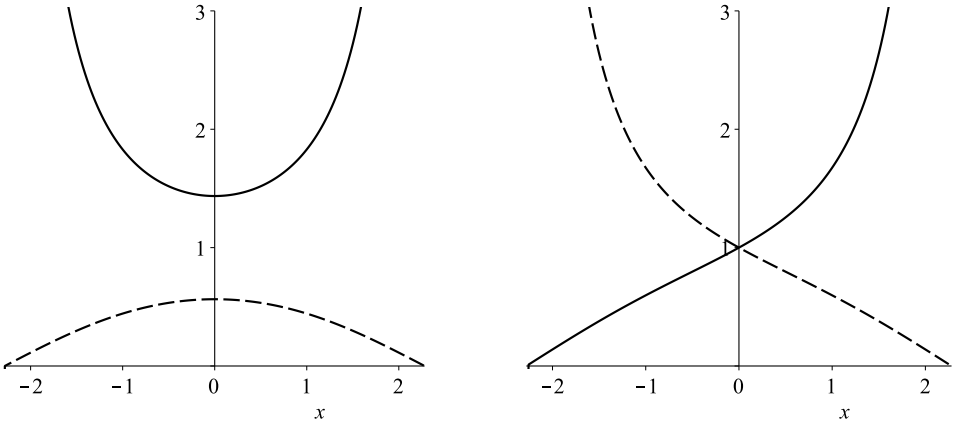

Figure 5.4: Left: $(f_1 + f_2)/a$ (solid) and $(f_1 - f_2)/a$ (dashed) for $k = 0.9$ plotted against $x = ar$, for $f_1^2 > f_2^2 > f_3^2$. Right: $(f_1 + f_2)/\sqrt{2K}$ (solid) and $(f_1 - f_2)/\sqrt{2K}$ (dashed) against $x = \sqrt{2K}r$, for $f_1^2 > f_3^2 > f_2^2$).

solution).

On the other hand, there is the possibility of having $f_1^2 \geq f_3^2 \geq f_2^2$. This time,

$$f_1^2 - f_2^2 = 2K \qquad f_1^2 - f_3^2 = a^2 \qquad 2Kk^2 = a^2$$

and the solution is

$$\begin{cases} f_1 &= \sqrt{2K}\,\mathrm{dc}_k\left(\sqrt{2K}r\right), \\ f_2 &= \sqrt{2K}k'\,\mathrm{sc}_k\left(\sqrt{2K}r\right), \\ f_3 &= \sqrt{2K}k'\,\mathrm{nc}_k\left(\sqrt{2K}r\right). \end{cases}$$

Figure 5.4 (right) shows $f_1 \pm f_2$. The zeros of Φ are now in different components and scattering is consistent with the 'zeros apart' solution. This time, when $K = 0$ we simply have $f_1 = f_2 = f_3 = 0$, which is the Nahm data for a single monopole.

5.1.2 Large Period Limit

A complementary result to that of section 5.1.1 can be obtained via an approximate solution to the Hitchin equations (4.3), showing how the rank 2 Nahm/Hitchin data becomes Nahm data on a line segment for $\beta \to \infty$ or $C \to 0$. The work in this section closely follows unpublished work by Harland, [Har*a*], and no claim is made over its originality.

The idea is to look for non-trivial solutions to

$$\nabla^2\psi \;=\; 2\left(C^2|\cosh(\beta s)|^2\,\mathrm{e}^{\psi} - \mathrm{e}^{-\psi}\right), \tag{5.4}$$

where the 'zeros together' configuration with $K = 0$ is chosen as the easiest to tackle (similar solutions for $K \neq 0$ can be expressed in terms of the Weierstrass $\wp$ function). The idea is to look for t-independent solutions to (5.4) under the assumption that the first term on the right hand side is small. This gives a one dimensional version of the Liouville equation,

$$\nabla^2\psi \;=\; -2\mathrm{e}^{-\psi} \qquad \Rightarrow \qquad \psi \;=\; 2\log\left(h\cos\left(\frac{r}{h}+c\right)\right),$$

where the solution is unique up to real constants c and h. Away from the central region, the Hitchin gauge field vanishes and (5.4) is solved as in section 4.2 by setting both sides to zero. Together, the above considerations provide an approximate solution for ψ,

$$\psi \;=\; \begin{cases} 2\log\left(h\cos(r/h)\right) & |r| \;<\; r_0, \\ -\beta r + \log(2/C) & |r| \;>\; r_0, \end{cases} \tag{5.5}$$

where r_0 is to be determined. Requiring continuity and differentiability at $r = r_0$ gives the conditions

$$\beta r_0 \;=\; \log\left(\frac{2}{Ch^2}\sec^2\left(\frac{r_0}{h}\right)\right) \qquad\qquad \beta \;=\; \frac{2}{h}\tan\left(\frac{r_0}{h}\right),$$

which can be expanded near $r_0/h \approx \pi/2$ (recall that the Nahm data (5.3) is defined in the domain $|ar| < \mathbf{K}(k)$, and that $\mathbf{K}(0) = \pi/2$) to give

$$h \;\approx\; \frac{2}{\pi\beta}\log\left(\frac{\beta^2}{2C}\right),$$

which tends to 0 when $\beta \to \infty$ for fixed C.

The Hitchin fields following from (5.5) using (4.2) are

$$\Phi \;=\; \begin{pmatrix} 0 & C\cosh(\beta s)h\cos(r/h) \\ \sec(r/h)/h & 0 \end{pmatrix} \qquad\qquad A_t \;=\; -\frac{\mathrm{i}}{2h}\tan\left(\frac{r}{h}\right)\sigma_3.$$

Noting the scaling of h with β, then for small C and large β, the 'sec' term is expected to dominate Φ. Making the identifications (5.1), these approximate

fields satisfy Nahm equations with

$$f_1 = -f_2 = -\frac{1}{h}\sec\left(\frac{r}{h}\right) \qquad f_3 = -\frac{1}{h}\tan\left(\frac{r}{h}\right).$$

There are two strengths of this method compared to that of section 5.1.1. In particular, some residual C-scaling is retained (via h). There is also the possibility of seeing explicitly how the linear growth of ψ at large $|r|$ (equation 5.5) increases in gradient, approaching the singular result for $\beta \to \infty$ and illustrating how the Nahm data is defined only on a line segment instead of along the entire length of the cylinder.

5.2 Large C

In the opposite limit, of large monopole size to period ratio, the structure of the chains again simplifies. As C is increased, the fields become increasingly independent of z and the spectral approximation [Mal13] becomes an accurate description of the monopole. The monopole Higgs field is known explicitly in this limit and can be read off directly from the spectral curve as described in chapter 3. For charge 2, we have (3.15),

$$\hat{\Phi} = \frac{\mathrm{i}}{\beta}\,\mathrm{Re}\left(\cosh^{-1}\left(\frac{2\zeta^2 - K}{2C}\right)\right)\sigma_3,$$

and the energy density is calculated through (1.7),

$$\mathcal{E} = \frac{1}{2}\nabla^2\|\hat{\Phi}\|^2. \tag{5.6}$$

Geodesic motion with $K \in \mathbb{R}$ describes the movement of four lumps of energy density located at $\zeta = \pm\sqrt{K/2 \pm C}$ undergoing a double scattering via a cross-shaped configuration at $K = 0$, as shown in figure 3.3.

As was discussed in section 4.3, in the large C limit there is also a simplification in the solutions to the Hitchin system. The C dependence of $\mu_\pm$ in equation 4.3 means a non-trivial solution for $\nabla^2\mathrm{Re}(\psi)$ is only supported at small C and in the vicinity of the two regions $\mu_\pm \approx 0$ (see section 4.2). Thus, in the large C limit, the smooth solution to (4.3) approaches the singular solution obtained by setting both sides to zero. The singular solutions to the Hitchin equations in this limit, referred to above, imply that the metric obtained from this data depends only on $\det(\Phi)$, and is hence the same for the 'zeros together'

and 'zeros apart' solutions (see section 4.3.2). This is identical to the metric found from the spectral approximation to the monopole fields in section 3.3.

5.2.1 Nahm Transform for Large C

The large scale limit allows a demonstration of an example of the Nahm transform for the construction of solutions to the Hitchin equations on $\mathbb{R}^2$. The general theory of Nahm transforms [Jar04] relating solutions of the self-dual Yang-Mills equations on reciprocal 4-tori suggests that the Nahm transform on $\mathbb{R}^2$ is self-reciprocal, thus mapping the large C limit of the periodic monopole to Hitchin equations on $\mathbb{R}^2$, with a different topology and boundary conditions. It is not clear how to 'unwrap' the Hitchin cylinder in this limit, or how one might deal with the singular nature of the solutions. However, as a step towards understanding this instance of the Nahm transform, we show that in this limit the spectral approximation can also be applied to the forward Nahm transform, allowing us to construct the initial Nahm data from the approximate monopole fields. Below we look specifically at the charge 1 periodic monopole, although the argument can equally be applied to higher charges.

The inverse Nahm operator for the charge 1 periodic monopole [War05] is (see chapter 2)

$$\Delta\Psi \;=\; \begin{pmatrix} 2\partial_{\bar{s}} - z & \zeta - \Phi \\ \bar{\zeta} - \Phi^\dagger & 2\partial_s + z \end{pmatrix} \begin{pmatrix} \psi_{11} & \psi_{12} \\ \psi_{21} & \psi_{22} \end{pmatrix} \;=\; 0, \tag{5.7}$$

where $\Phi = C\cosh(\beta s)$. In chapter 3 we studied the large C limit by suppressing z dependence (setting $z = 0$ above) and defining new fields

$$\mathrm{i}\int_{\mathbb{R}^2} s\Psi^\dagger\Psi \, dr\, dt \;=\; \mathrm{i}\hat{\phi} \qquad\qquad \int_{\mathbb{R}^2} \Psi^\dagger\partial_j\Psi \, dr\, dt \;=\; \hat{a}_j$$

where $\mathrm{i}\hat{\phi} = \hat{\Phi} - \mathrm{i}\hat{A}_z$ and $j = x, y$. These fields, (3.8), satisfy Hitchin equations on $\mathbb{R}^2$. As discussed in section 3.1, equation 5.7 has an approximate solution valid at large C, in which the columns of Ψ are Gaussian peaks at $s = \pm s_0$, with $s_0(\zeta)$ defined through $C\cosh(\beta s_0) = \zeta$. In this limit the monopole fields are $\hat{\phi} = s_0\sigma_3$, $\hat{a} = 0$.

The idea is to use these approximate monopole fields to explicitly perform the forward Nahm transform. In other words, starting from $(\hat{\phi}, \hat{a})$ we attempt to obtain Φ and A. The forward Nahm transform requires normalised solutions

to

$$\tilde{\Delta}V \;=\; \begin{pmatrix} 2\partial_{\bar{\zeta}} & 0 & s-s_0 & 0 \\ 0 & 2\partial_{\bar{\zeta}} & 0 & s+s_0 \\ \bar{s}-\bar{s}_0 & 0 & 2\partial_{\zeta} & 0 \\ 0 & \bar{s}+\bar{s}_0 & 0 & 2\partial_{\zeta} \end{pmatrix} \begin{pmatrix} v_1 \\ v_2 \\ v_3 \\ v_4 \end{pmatrix} \;=\; 0, \tag{5.8}$$

which should give the charge 1 Nahm/Hitchin data

$$\Phi \;=\; \int_{\mathbb{R}^2} dx\, dy\, \zeta \sum_{i=1}^{4} |v_i|^2 \;=\; C\cosh(\beta s) \qquad A \;=\; \int_{\mathbb{R}^2} dx\, dy \sum_{i=1}^{4} \bar{v}_i \partial_j v_i \;=\; 0. \tag{5.9}$$

Solutions to the forward Nahm operator (5.8) are found using the same ideas as those for the inverse transform. First of all, we note that the equations for v_1 and v_3 decouple from those for v_2 and v_4. Writing $\zeta_0 = C\cosh(\beta s)$ and $\zeta = \zeta_0 + \epsilon$, we have

$$s - s_0 \;=\; \frac{1}{\beta}\cosh^{-1}\left(\frac{\zeta_0}{C}\right) - \frac{1}{\beta}\cosh^{-1}\left(\frac{\zeta_0+\epsilon}{C}\right) \;=\; -\frac{\zeta-\zeta_0}{\beta}\xi + \mathcal{O}(\epsilon^2)$$

where $\xi^{-1} = C\sinh(\beta s)$. The spinor components v_1 and v_3 are supported away from $s = 0$, and we make the Ansatz $v_1 \sim v_3 \sim \exp(-c|\zeta-\zeta_0|^2)$, resulting in $c = |\xi|/(2\beta)$ and $v_3 = -\xi^{-1/2}\bar{\xi}^{1/2}v_1$.

The important point now is that, if we remain on the correct branch of $\cosh^{-1}$, the quantity $(s + s_0)$ will never be close to zero (as in [War05], we must avoid the points $\zeta_0 = \pm C$). Thus, v_2 and v_4 are small and slowly varying compared to v_1 and v_3. We thus approximate $v_2 \sim v_4 \approx 0$, so that normalising gives

$$|v_1|^2 \;=\; |v_3|^2 \;=\; \frac{|\xi|}{2\pi\beta}\,\mathrm{e}^{-|\xi||\zeta-\zeta_0|^2/\beta}.$$

The consistency relation $v_3 = \pm\bar{v}_1$ arising from (5.8) fixes the phases of v_1 and v_3,

$$v_1 \;=\; -\left(\frac{\xi}{2\pi\beta}\right)^{1/2} \mathrm{e}^{-|\xi||\zeta-\zeta_0|^2/(2\beta)} \qquad v_3 \;=\; \left(\frac{\bar{\xi}}{2\pi\beta}\right)^{1/2} \mathrm{e}^{-|\xi||\zeta-\zeta_0|^2/(2\beta)}, \tag{5.10}$$

and (5.9) yields the expected Hitchin fields, $\Phi = \zeta_0 = C\cosh(\beta s)$, $A = 0$. Note the solution (5.10) is again exponentially localised, and the scaling with β is opposite to that of Ψ (see equations 3.4 and 3.5).

It should be cautioned that although these results appear to suggest a self-dual Nahm transform on $\mathbb{R}^2$, much work remains to be done in studying how

the boundary data is to be adapted in this limit. Although it is possible to construct solutions to the Hitchin equations explicitly (see, for example, the papers [Saç84, GMN13, Kam]), there is the additional caveat that Derrick scaling [MS04] implies that all such solutions have infinite or zero energy. It would be interesting to see whether the Nahm transform in this limit allows the construction of the periodic monopole from the Nahm/Hitchin data of its constituents (this approach has been successfully carried out for the SU(2) periodic instanton by means of its two monopole constituents [LL98]). However, from section 3.1.2 it is not clear whether the constituents can genuinely be considered as particles in their own right.

5.3 Intermediate C

Now that the small and large C limits have been established, our aim is to understand the intermediate régime. Here we focus on the 'zeros apart' case, which displays a rich z behaviour while remaining consistent with the symmetries of section 4.1. The expectation is for solutions to interpolate between the two extremes of sections 5.1 and 5.2, and in fact this occurs non-trivially via a chain-like structure. For $W = \mathrm{i}$, the transition from small to large C involves the resolution of the energy lumps of figure 5.2 into two constituents each. Curiously, however, the constituents are not aligned with the x and y axes but with the lines $x \pm y = 0$, such that the chain has been twisted by different amounts along its length, see figure 5.5 on page 96.

It is instructive to consider these solutions from the point of view of the geodesics identified in sections 4.1.2 and 4.3 and illustrated in figure 3.3. In particular, the $W = \mathrm{i}$ configuration is the midpoint of scattering via the $W \in \mathrm{i}\mathbb{R}$ geodesic. Two points in this geodesic are shown in figure 5.6, which also serve to illustrate the transition between the $W = \mathrm{i}$ configuration with $C = 1$ (figure 5.2) and that with $C = 4$ (figure 5.5).

Similarly, the $W = 1$ configuration (figure 5.7) is the midpoint of scattering via the $W \in \mathbb{R}$ geodesic, for which outgoing chains are simply shifted by $\beta/2$ relative to the ingoing chains. Both these configurations also lie on the closed geodesic with $|W| = 1$, snapshots of which are displayed in figures 5.5 and 5.7. These show how the chains oscillate in shape as we move around the waist of the double Atiyah-Hitchin trumpet of section 4.3.6.

As C is increased, the configuration deforms as shown in figure 5.8. The energy lumps stretch in the xy plane and fuse along z such that when C is

large enough, there are tubes of energy density located in a cross shape aligned with the x and y axes, as expected from the spectral approximation. Although it appears that within the spectral approximation the constituents cannot be described as objects in their own right (section 3.1.2), it is not clear whether this may be possible for intermediate C.

Even for intermediate values of C, one can make a link with the results of the spectral approximation by integrating the energy density over a z-period across the xy plane. The resulting quantity, shown in figure 5.9, is found to resemble the energy density expected from the spectral approximation, insofar as the peaks are located along the coordinate axes and there is an energy minimum at $x = y = 0$.

5.4 Summary

In this chapter we considered the effect of changing the size to period ratio of monopole chains. The limits of large and small size to period ratio were studied by various approximations. For small monopoles, this recovered the Nahm equations on a line segment, while for large monopoles evidence was given for a self-reciprocal Nahm transform mapping between Hitchin equations on $\mathbb{R}^2$. The transition of the spectral curve between these extremes was studied by Cherkis [Che07]. Energy density plots were used to illustrate the symmetries of the one parameter families of solutions and the approach towards the spectral approximation of chapter 3 when the size is much larger than the period.

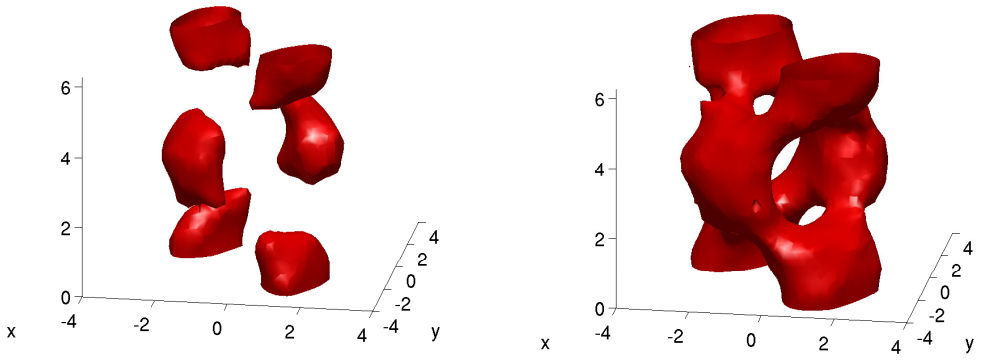

Figure 5.5: Energy density isosurfaces for $C = 4$, $W = \mathrm{i}$. On the left we see the constituent structure, and on the right the twisted chain. The symmetry group can be equivalently described as $D_{2\mathrm{h}} \times \mathbb{Z}_2$ or $D_{2\mathrm{d}} \times \mathbb{Z}_2$. The eight axes of rotational symmetry are $(x = \pm y,\ z = 0)$, $(x = \pm y,\ z = \beta/2)$ for $D_{2\mathrm{h}}$ symmetry, and $(x = 0,\ z = \pm\beta/4)$, $(y = 0,\ z = \pm\beta/4)$ for $D_{2\mathrm{d}}$ symmetry. Note also the similarity to the Skyrmion chain configurations obtained in [HW08].

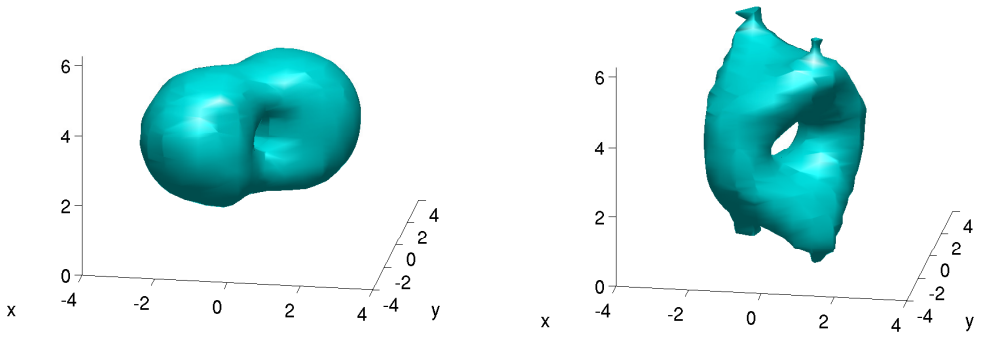

Figure 5.6: Two points on the $W = \mathrm{i}\mathbb{R}$ geodesic with $C = 2$, displaying $D_{2\mathrm{h}}$ symmetry. Left: $W = 2\mathrm{i}$, right: $W = 1.125\mathrm{i}$. As well as illustrating the scattering process, these energy density plots show how there is a transition between the $C = 1$ case, where the energy is peaked in two regions near the z-axis, and the $C = 4$ case, in which the energy is peaked away from the z-axis. The 'four pronged' structures of figure 5.2 can be visualised as splitting the right hand structure above along $z = \pi$.

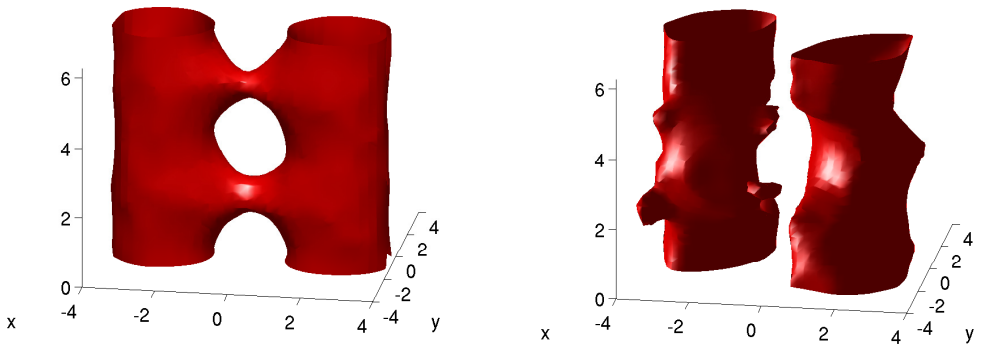

Figure 5.7: Scattering for $C = 4$ on the $|W| = 1$ geodesic. Left: $W = 1$ with symmetry group $D_{2h} \times \mathbb{Z}_2$; right: $W = e^{i\pi/3}$ with symmetry group D_{2h}. The $W = i$ configuration is shown in figure 5.5.

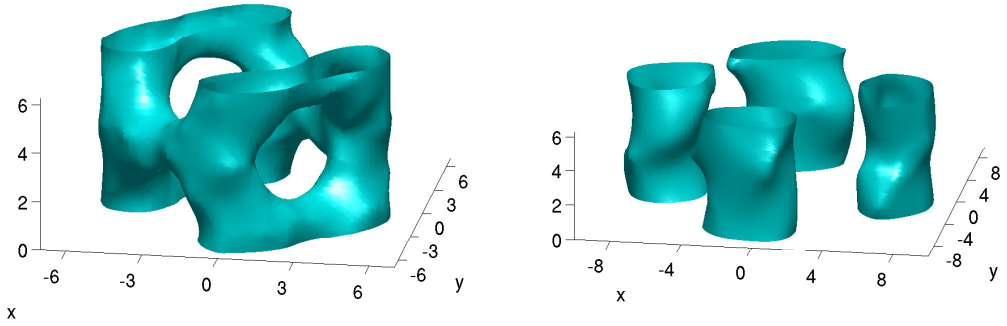

Figure 5.8: Left: $C = 16$, $W = i$, right: $C = 36$, $W = i$. Note how we approach the z-independent result of the spectral approximation (figure 3.3, middle panel).

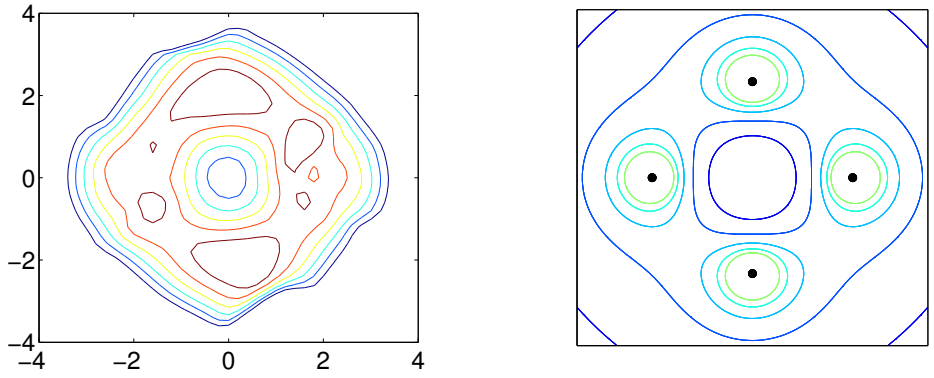

Figure 5.9: Left: energy density integrated over a period for $C = 4$, $W = i$. Unlike in figure 5.5, the energy peaks here are at the locations expected from the spectral approximation (right). Note that this comparison requires a rescaling of the x and y coordinates by a factor of $\sqrt{C}$.

6

Higher Charges

In this chapter we apply the methods of chapters 3 and 4 to periodic monopoles of higher charge, making use of examples of charges $\boldsymbol{k} = (3)$ and $\boldsymbol{k} = (4)$. Firstly, in section 6.1, we consider the symmetries of the spectral curve, then in section 6.2 the Nahm transform is used to construct numerical solutions. Section 6.3 describes ways to construct the Nahm data of higher charge chains from those of lower charges. Most of this work appeared in the preprint [Mal*a*].

6.1 Spectral Approximation

As was done in section 3.2.3 for charge 2 chains, geodesic submanifolds of the $(2k-1)$-real-dimensional reduced relative moduli space can be identified by considering the fixed point sets of symmetries of the spectral curve. We consider two transformations of ζ (corresponding to a rotation by α and a reflection in the line $\theta = \alpha/2$), and find the necessary maps of the coefficients b_i which recover the original spectral curve. The $k = 3$ spectral curve is (2.16)

$$w^2 + w(b_3\zeta^3 + b_2\zeta^2 + b_1\zeta + b_0) + 1 \;=\; 0. \tag{6.1}$$

We take $b_3 = 1$ for the rest of this section, its magnitude setting a scale and its phase an orientation. We also fix the centre of mass of the spectral points at the origin by setting $b_2 = 0$. Then the location of the spectral points is obtained from the discriminant of the w polynomial (6.1),

$$b_3\zeta^3 + b_1\zeta + b_0 \;=\; \pm 2. \tag{6.2}$$

$\underline{\zeta \mapsto \zeta \mathrm{e}^{\mathrm{i}\alpha}}$

To keep the spectral curve invariant we transform $w \mapsto w\mathrm{e}^{-3\mathrm{i}\alpha}$ and look for values of α for which the resulting spectral curve,

$$w^2\mathrm{e}^{-6\mathrm{i}\alpha} + w\left(\zeta^3 + b_1\zeta\mathrm{e}^{-2\mathrm{i}\alpha} + b_0\mathrm{e}^{-3\mathrm{i}\alpha}\right) + 1 \;=\; 0,$$

is the same as the original one, (6.1), for a certain choice of b_1 and b_0. There are three possibilities:

i. $\alpha = \pi/3$, $b_1 \mapsto \mathrm{e}^{2\mathrm{i}\pi/3}b_1$, $b_0 \mapsto -b_0$, with fixed set $b_1 = b_0 = 0$. This corresponds to the hexagonally symmetric configuration of spectral points.

ii. $\alpha = 2\pi/3$, $b_1 \mapsto \mathrm{e}^{4\mathrm{i}\pi/3}b_1$, $b_0 \mapsto b_0$, with fixed set $b_1 = 0$ for all b_0.

iii. $\alpha = \pi$, $b_1 \mapsto b_1$, $b_0 \mapsto -b_0$, with fixed set $b_0 = 0$ for all b_1.

$\underline{\zeta \mapsto \bar{\zeta}\mathrm{e}^{\mathrm{i}\alpha}}$

We also set $w \mapsto \bar{w}\mathrm{e}^{-3\mathrm{i}\alpha}$, such that

$$\begin{aligned} & \bar{w}^2\mathrm{e}^{-6\mathrm{i}\alpha} + \bar{w}\left(\bar{\zeta}^3 + b_1\bar{\zeta}\mathrm{e}^{-2\mathrm{i}\alpha} + b_0\mathrm{e}^{-3\mathrm{i}\alpha}\right) + 1 = 0 \\ \Rightarrow \qquad & w^2\mathrm{e}^{6\mathrm{i}\alpha} + w\left(\zeta^3 + \bar{b}_1\zeta\mathrm{e}^{2\mathrm{i}\alpha} + \bar{b}_0\mathrm{e}^{3\mathrm{i}\alpha}\right) + 1 = 0. \end{aligned}$$

Then

iv. $\alpha = 0$, $b_1 \mapsto \bar{b}_1$, $b_0 \mapsto \bar{b}_0$, with fixed set $b_1 \in \mathbb{R}$ and $b_0 \in \mathbb{R}$.

v. $\alpha = \pi/3$, $b_1 \mapsto \mathrm{e}^{2\mathrm{i}\pi/3}\bar{b}_1$, $b_0 \mapsto -\bar{b}_0$, with fixed set $b_1 = \mathrm{e}^{\mathrm{i}\pi/3}|b_1|$, $b_0 \in \mathrm{i}\mathbb{R}$.

vi. $\alpha = 2\pi/3$, $b_1 \mapsto \mathrm{e}^{-2\mathrm{i}\pi/3}\bar{b}_1$, $b_0 \mapsto \bar{b}_0$, with fixed set $b_1 = \mathrm{e}^{-\mathrm{i}\pi/3}|b_1|$, $b_0 \in \mathbb{R}$.

vii. $\alpha = \pi$, $b_1 \mapsto \bar{b}_1$, $b_0 \mapsto -\bar{b}_0$, with fixed set $b_1 \in \mathbb{R}$ and $b_0 \in \mathrm{i}\mathbb{R}$.

The above symmetries of the spectral curve can be combined to give three distinct scattering processes, described in figures 6.1 and 6.2.

The greater number of moduli in the charge 3 case compared to the charge 2 case allows us to consider 'phase diagrams' showing the values of the moduli for which the monopoles form one, two, or three separate clusters. The number of clusters is defined as the number of groups of spectral points joined by a line of zero discriminant. Numerical checks suggest that the corresponding regions in the moduli space are separated by lines describing configurations for which two spectral points coincide. This occurs when the discriminant of the

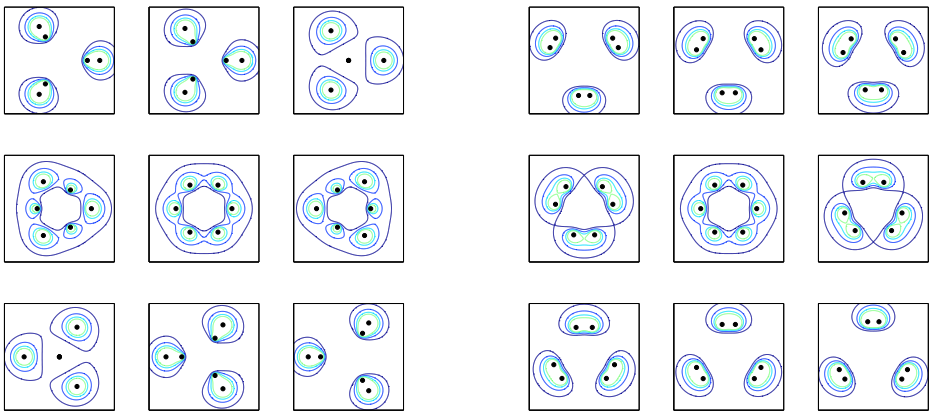

Figure 6.1: Cross section of energy density for two one-parameter families with $b_1 = 0$. Left: $b_0 \in \mathbb{R}$ with $b_0 = -4, -3, \ldots, 4$. The relevant symmetries are i, ii, iv and vi in the list of section 6.1. Right: $b_0 \in \mathrm{i}\mathbb{R}$ with $-\mathrm{i}b_0 = -4, -3, \ldots, 4$, with symmetries i, ii, v and vii. In both cases these define the dihedral symmetry group D_3.

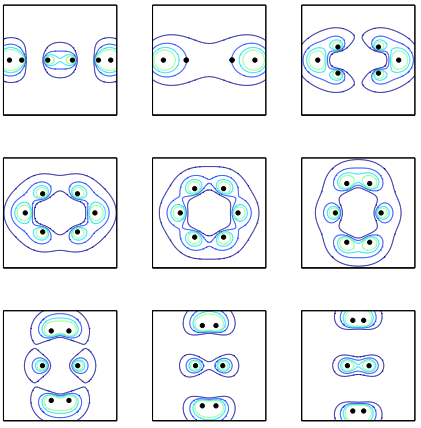

Figure 6.2: Energy density for $b_1 \in \mathbb{R}$, $b_0 = 0$, with $b_1 = -4, -3, \ldots, 4$. Unlike the symmetries in figure 6.1, this family does not have a charge 2 analogue, and in fact the Nahm data is only known for the special case $b_1 = -3$, $b_0 = 0$ (top row, central panel). This configuration is in fact a charge 1 chain with period $\beta/3$ and is described in section 6.3.1. The symmetry group is D_2, described by i, iii, iv and vii in the list above.

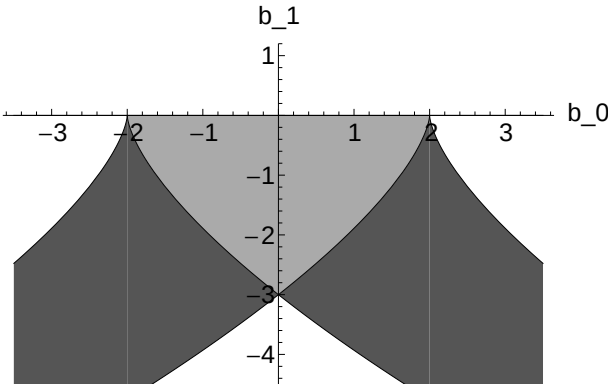

Figure 6.3: Regions of the moduli space for which a charge 3 monopole contains a single cluster (light grey), two clusters (dark grey) and three clusters (white). The lines on which (6.3) holds are shown in black.

polynomial (6.2) vanishes (recall that this in turn was the discriminant of the polynomial in w (6.1)),

$$4b_1^3 \;=\; -27(b_0 \pm 2)^2. \tag{6.3}$$

The 'phases' on the slice of the moduli space with $(b_0, b_1) \in \mathbb{R}^2$ are shown in figure 6.3. It should be noted that even in the asymptotic region of the moduli space there are configurations for which two of the constituent monopoles remain in a single cluster. A similar observation has been made for monopoles in $\mathbb{R}^3$, [AH88]. In the charge 2 case, the region of the moduli space containing a single cluster is the line segment $K/C \in [-2, 2]$.

6.2 Nahm Transform

A straightforward extension of the charge 2 solutions described in section 4.1 is a modification of 'Sutcliffe's ansatz' [Sut96*b*, Bra11]. Solutions generated in this way have $b_i = 0$ for $i \neq 0, k$ in (2.17). We take

$$\Phi \;=\; \begin{pmatrix} 0 & 0 & \cdots & 0 & f_1 \\ f_2 & 0 & \cdots & 0 & 0 \\ 0 & f_3 & \cdots & 0 & 0 \\ \vdots & \vdots & \ddots & \vdots & \vdots \\ 0 & 0 & \cdots & f_k & 0 \end{pmatrix} \qquad A_{\bar{s}} \;=\; \begin{pmatrix} a_1 & 0 & 0 & \dots & 0 \\ 0 & a_2 & 0 & \dots & 0 \\ 0 & 0 & a_3 & \dots & 0 \\ \vdots & \vdots & \vdots & \ddots & \vdots \\ 0 & 0 & 0 & \dots & a_k \end{pmatrix}. \tag{6.4}$$

Mimicking the charge 2 procedure, we define $f_i = \mu_i e^{\psi_i/2}$, with the conditions $\sum_{i=1}^k \psi_i = 0$ and $\prod_{i=1}^k \mu_i = (-1)^{k-1}\det(\Phi) = C\cosh(\beta s) + K/2$. The Hitchin

equations then read

$$2\,(a_{i-1} - a_i) \;=\; \partial_{\bar{s}}\psi_i$$

$$\nabla^2 \log|f_i|^2 \;=\; 2|f_i|^2 - |f_{i-1}|^2 - |f_{i+1}|^2,$$

where the index i is periodic, such that $f_0 = f_k$. As was the case in section 4.1, the determinant of Φ has exactly two zeros, such that smooth solutions must have both zeros in the same or different entries μ_i (then two of the μ_i are given by $\mu_\pm$ (4.5, 4.6) and all the others we choose to set to 1). We are free to fix one of the zeros, so $\mu_1 = \mu_+$, say. Then for a given charge k, the $\ell = 0$ configuration has both zeros in μ_1, and there are $(2k + (-1)^k - 1)/4$ gauge inequivalent configurations with $\ell > 0$, where ℓ is the separation between the positions of $\mu_\pm$ in Φ, and in particular $\mu_{1+\ell} = \mu_-$. This is equivalent (up to changing the sign of z) to placing μ_- in the $(k+1-\ell)^{\text{th}}$ entry.

Given the results of chapter 4, we will assume that the Ansatz (6.4) provides ℓ geodesic submanifolds of the moduli space away from the spectral limit of section 6.1. Each of these submanifolds can be fixed by a symmetry and is parametrised by the complex modulus K or W, as described in chapter 4. Borrowing notation from [HMM95], we denote these surfaces Σ_k^ℓ.

With the above conventions, the Hitchin equations for $k = 3$, $\ell = 1$ are

$$\begin{cases} \nabla^2 \mathrm{Re}(\psi_1) &= 2|\mu_+|^2 \mathrm{e}^{\mathrm{Re}(\psi_1)} - |\mu_-|^2 \mathrm{e}^{\mathrm{Re}(\psi_2)} - \mathrm{e}^{-\mathrm{Re}(\psi_1+\psi_2)} \\ \nabla^2 \mathrm{Re}(\psi_2) &= 2|\mu_-|^2 \mathrm{e}^{\mathrm{Re}(\psi_2)} - |\mu_+|^2 \mathrm{e}^{\mathrm{Re}(\psi_1)} - \mathrm{e}^{-\mathrm{Re}(\psi_1+\psi_2)} \end{cases} \tag{6.5}$$

with $\mu_\pm$ as in (4.5) or (4.6).[14]

Solving the Hitchin equations numerically is now a matter of adapting the charge 2 procedure used by Harland & Ward [HW09] and in chapter 4 of this thesis. First of all we note that the equations (6.5) can be obtained by varying the functional

$$E[\mathrm{Re}(\psi_i)] \;=\; \int dr\, dt \left(\frac{1}{2} \sum_{p=r,t} \left(\partial_p \mathrm{Re}(\psi_i)\right)^2 + 2|\mu_i|^2 \mathrm{e}^{\mathrm{Re}(\psi_i)} \right.$$
$$\left. - \psi_i |\mu_j|^2 \mathrm{e}^{\mathrm{Re}(\psi_j)} + \mathrm{e}^{-\mathrm{Re}(\psi_i+\psi_j)} \right) \tag{6.6}$$

with respect to ψ_i, where $i, j \in \{1, 2 | i \neq j\}$ and no sum is implied. Unfortunately there appears to be no simple way of combining the two functionals

[14] For $k = 3$ we have implicitly redefined $K \mapsto -K$ so as to have an incoming monopole on the x-axis. For general k the effect of this transformation is a rotation by π/k.

generating the separate coupled partial differential equations (6.5) into a single expression. Instead of minimising a single functional, we alternately minimise $E[\mathrm{Re}(\psi_1)]$ and $E[\mathrm{Re}(\psi_2)]$. This approach was found to lead to rapidly convergent solutions as long as the boundary conditions were chosen appropriately. In fact, it is straightforward to write down an asymptotic solution to (6.5) valid away from the zeros of $\mu_\pm$ by making the Ansatz $\psi_i = \log(|\mu_+|^{\nu_i^+}|\mu_-|^{\nu_i^-})$ and solving for the $\nu_i^\pm$ (this solution is singular at the zeros of $\mu_\pm$ and is thus not globally valid). For $k = 3$ and $\ell = 1$ we find

$$\mathrm{Re}(\psi_1) = \frac{2}{3}\log\frac{|\mu_-|}{|\mu_+|^2} \qquad \mathrm{Re}(\psi_2) = \frac{2}{3}\log\frac{|\mu_+|}{|\mu_-|^2} \qquad \mathrm{Re}(\psi_3) = \frac{2}{3}\log\left(|\mu_+||\mu_-|\right).$$

There is some freedom in the choice of imaginary parts of the functions ψ_i, which must be chosen so as to make the Nahm data periodic on the cylinder. We fix $\mathrm{Im}(\psi_1) = -\beta t$, $\mathrm{Im}(\psi_{1+\ell}) = \beta t$ and $\mathrm{Im}(\psi_3) = 0$. A different choice simply corresponds to a global shift in the z direction, and the resulting moduli spaces are isomorphic.

One might also be concerned by the fact that (6.6) is not explicitly positive definite due to the term linear in ψ_i, which does not appear in the charge 2 case. We again resort to the convergence of the numerical solution to justify the validity of this approach.

It is easy to see that for $k > 2$ there are no solutions on the surfaces Σ_k^ℓ with $\mathrm{Re}(\psi_1) = \mathrm{Re}(\psi_2) = 0$ everywhere. This tells us that the charge 1 chain of period $\beta/3$ is not included in this family of solutions, as this requires $F = 0$ (see also section 6.3.1).

6.2.1 SYMMETRIES

Spatial symmetries of the monopole fields can be studied by the procedure outlined in section 4.1. First of all we choose a transformation of K (or W) and s which preserves the spectral curve for a given transformation of ζ. Then we express the transformed Hitchin fields as a gauge transformation of the original fields. This allows us to read off the corresponding change in z from the inverse Nahm operator (2.12), for which the monopole fields are gauge equivalent to those at the original coordinates.

Note that if we restrict to gauge transformations which change the positions and phases of the entries of Φ, then the overall ordering of the f_i is unchanged (or reversed in the case of $\Phi^\dagger$). This property gives the solutions $\ell = 0$ and

$\ell = k/2$ (for k even) an additional $s \mapsto -s$ symmetry (corresponding to $z \mapsto -z$), which is not observed for general ℓ.

Various scattering processes generalising those in section 4.1 are described in the following subsections, and we visualise them with reference to chains of small monopoles ($C \lesssim 1$). In brief, it is found that the geodesics are characterised by the positions of the zeros among the entries of Φ, at μ_1 and $\mu_{1+\ell}$. Then for $|W| > 1$ the monopoles are located on the vertices of a regular k-gon at $z = \beta\ell/k$ (this value of the z position was determined numerically by consideration of examples with large values of $|K|/C$). As $|W|$ is reduced they scatter and split into two clusters of charge ℓ moving along the positive z-axis and $(k-\ell)$ along the negative z-axis. The clusters move at speeds inversely proportional to their charges, such that for $|W| < 1$ the outgoing monopoles emerge at $z = 0$ on a (possibly rotated) k-gon. Following the discussion of [MW13] we expect there to be a closed geodesic with $|W| = 1$, describing stationary monopoles oscillating in shape. A discussion of the motion of Higgs zeros is given in section 6.2.2.

Planar Scattering

The conjectured geodesic surface Σ_k^0 with $K \in \mathbb{R}$ or $K \in \mathrm{i}\mathbb{R}$ describes scattering in the xy plane via a $D_{(2k)\mathrm{h}}$-symmetric toroidal configuration. We see this as follows:

First of all, we have that under the transformation $s \mapsto -s$, $\mu_\pm$ (defined as in equation 4.5) and ψ_i are invariant, and $a_i(s) \mapsto a_i(-s) = -a_i(s)$. The form of the inverse Nahm operator (2.12) now tells us that the monopole fields are invariant if we also replace z by $-z$. Thus, this monopole configuration has the symmetry $(\zeta, z) \sim (\zeta, -z)$, consistent with the k incoming monopoles being located at $z = 0$ (the fixed points of this transformation are $z = 0$ and $z = \beta/2$, the latter occurring if we replace $\psi_1 \mapsto \psi_1 + 2\mathrm{i}\beta t$).

To see the C_{2k} symmetry we perform the transformation $(s; K) \mapsto (s + \mathrm{i}\pi/\beta; -K)$, giving $\mu_\pm \mapsto \mp\mu_\pm$ and $\psi_i \mapsto \psi_i$. Then $\Phi'(s; K) = \Phi(s + \mathrm{i}\pi/\beta; -K)$ is the same as $\Phi(s; K)$ but with the sign of f_1 reversed. Under a suitably chosen diagonal gauge transformation $g = \exp(\pi.\mathrm{diag}(0, 1, \ldots, k-1)/k)$, we then have $\Phi' = \mathrm{e}^{\mathrm{i}\pi/k} g^{-1} \Phi g$, leaving A unchanged. The entry $(\mathbf{1}_k \zeta - \Phi)$ in the inverse Nahm operator (2.12) implies that $\zeta \mapsto \zeta \mathrm{e}^{\mathrm{i}\pi/k}$ when we map K to $-K$. The monopole fields are symmetric under $(\zeta, z; K) \mapsto (\zeta \mathrm{e}^{\mathrm{i}\pi/k}, z; -K)$, and thus $K = 0$ describes a configuration of enhanced symmetry.

SYMMETRIC SPLITTING

For even k, the geodesic submanifold $\Sigma_k^{k/2}$ describes a splitting of k incoming monopoles into two equal clusters. The Σ_2^1 case was given in section 4.1.2. Now we consider the $k = 4$ version, with conventions as in (4.6). Using the method of section 4.1.2, we identify the following symmetries of the Nahm/Hitchin and monopole fields (recall that these symmetries are defined up to gauge transformations, so describe symmetries of gauge invariant quantities such as the energy density):

- $(s; W) \mapsto (-\bar{s}; \overline{W}) \Rightarrow (\zeta, z) \sim (\bar{\zeta}, z)$ for $W \in \mathbb{R}$,
- $(s; W) \mapsto (\mathrm{i}\pi/\beta - \bar{s}; -\overline{W}) \Rightarrow (\zeta, z) \sim (\mathrm{e}^{\mathrm{i}\pi/4}\bar{\zeta}, z)$ for $W \in \mathrm{i}\mathbb{R}$.
- $(s; W) \mapsto (\bar{s}; \overline{W}^{-1}) \Rightarrow (\zeta, z) \mapsto (\bar{\zeta}, \beta/2 - z)$ relates the incoming and outgoing legs of the geodesics $W \in \mathbb{R}$ and $W \in \mathrm{i}\mathbb{R}$. Thus, $W \in \mathbb{R}$ describes monopoles incoming and outgoing parallel to the x and y axes, with a half-period shift along z. On the other hand, $W \in \mathrm{i}\mathbb{R}$ has an additional $\pi/4$ rotation about the z-axis. This symmetry also fixes the closed geodesic $|W| = 1$.
- $(\zeta, z) \sim (\mathrm{i}\zeta, z)$ is a symmetry for all W, as can be seen by the gauge transformation $g = \mathrm{diag}(1, \mathrm{i}, -1, -\mathrm{i})$,
- $s \mapsto -s \Rightarrow (\zeta, z) \sim (\zeta, -z)$ for all W.

There are two particularly symmetric cases which will be considered in more detail in section 6.3:

- $W = 1$ has $(\zeta, z) \sim (\zeta, \beta/2 - z) \sim (\zeta, z + \beta/2)$, with symmetry $D_{4\mathrm{h}} \times \mathbb{Z}_2$
- $W = \mathrm{i}$ has $(\zeta, z) \sim (\mathrm{e}^{\mathrm{i}\pi/4}\zeta, \beta/2 - z) \sim (\mathrm{e}^{\mathrm{i}\pi/4}\zeta, z + \beta/2)$ with symmetry group $D_{4\mathrm{d}} \times \mathbb{Z}_2$.

The clusters are located at $z = \pm\beta/4$.

GENERIC ℓ

Here we consider the example of Σ_3^1. The symmetries are

- $(s; W) \mapsto (-\bar{s}; \overline{W}) \Rightarrow (\zeta, z) \sim (\bar{\zeta}, z)$ for $W \in \mathbb{R}$,
- $(s; W) \mapsto (\mathrm{i}\pi/\beta - \bar{s}; -\overline{W}) \Rightarrow (\zeta, z) \sim (-\bar{\zeta}, z)$ for $W \in \mathrm{i}\mathbb{R}$,
- $(s; W) \mapsto (\bar{s}; \overline{W}^{-1}) \Rightarrow (\zeta, z) \sim (\bar{\zeta}, \beta/3 - z)$ for $|W| = 1$,
- $(\zeta, z) \sim (\mathrm{e}^{2\mathrm{i}\pi/3}\zeta, z)$ is a symmetry for all W.

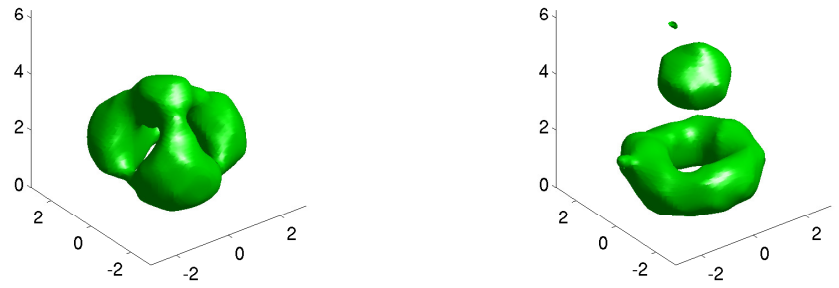

Figure 6.4: Energy density of a charge 3 periodic monopole with $C = 1$ taken over a single period. Left: approximately tetrahedral configuration with $W = 2 + \sqrt{3}$ ($K = 4$). Right: when $W = \mathrm{i}$, clusters of charge 1 and 2 are visible. The symmetry groups are $C_{3\mathrm{v}}$ and $D_{3\mathrm{d}}$, respectively.

In this case, there is no symmetry $z \mapsto -z$ due to the asymmetric splitting. There are still configurations with enhanced symmetry:

- $W = 1$ has $(\zeta, z) \sim (\zeta, \beta/3 - z)$, with symmetry group $D_{3\mathrm{h}}$, and
- $W = \mathrm{i}$ has $(\zeta, z) \sim (-\zeta, \beta/3 - z)$, with symemtry group $D_{3\mathrm{d}}$,

with fixed points at $z = \beta/6$ and $2\beta/3$, which are the positions of the charge 2 and charge 1 clusters, respectively.

These symmetries are consistent with the expected scattering process. Monopoles are incoming on the vertices of an equilateral triangle. They scatter along z via an approximately tetrahedral configuration to form two clusters (figure 6.4). A new tetrahedral configuration forms from clusters in adjacent periods, and outgoing monopoles are shifted by $\beta/3$ and are either rotated by $\pi/3$ about the z-axis (for $W \in \mathrm{i}\mathbb{R}$) or move back along the original directions (for $W \in \mathbb{R}$).

6.2.2 Higgs Zeros

As a further similarity with monopole scattering in $\mathbb{R}^3$, we observe the appearance of an additional zero of $\mathrm{tr}(-\frac{1}{2}\hat{\Phi}^2)$ (termed an 'antizero' in [Sut96*a*, Sut97] and described by a reversal in the local winding number) during the $k = 3$, $\ell = 0$ scattering process with $W \in \mathbb{R}$. The motion of Higgs zeros can thus be described as follows: three zeros move radially inwards on the vertices of an equilateral triangle, falling slightly below the plane $z = \beta/3$ as they approach. At some (C-dependent) value of W, a zero appears on the z-axis, slightly above $\beta/3$ (see figure 6.5 overleaf). Reducing W further, the zero splits into

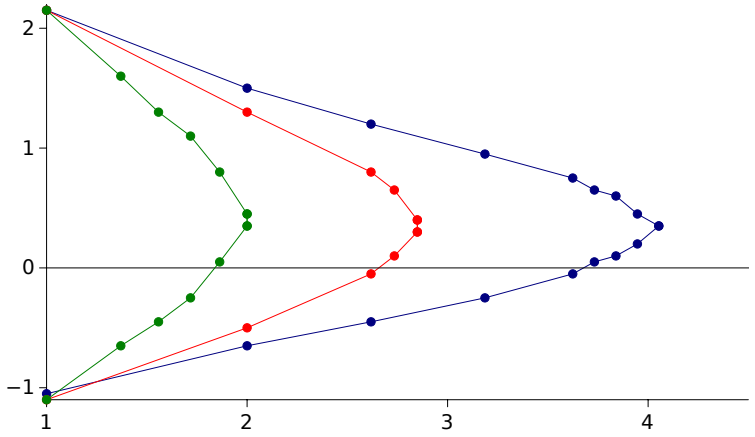

Figure 6.5: Motion of the zero-antizero pair along the z-axis (with 0 corresponding to $z = \beta/3$, and $\beta = 2\pi$) as a function of W for various values of C: $C = 1$ in blue (rightmost curve), $C = 2$ in red (middle) and $C = 5$ in green (left). For small C, the value of W at which the lower zero (the antizero) is centered at $z = \beta/3$ appears to coincide with the monopole configuration closest to tetrahedral symmetry (figure 6.6).

two, moving in the positive and negative z directions, figure 6.6. At some value of W the downward-going zero (the antizero) meets the three original zeros, resulting in the toroidal 2-monopole cluster of figure 6.4. However, the precise value of W at which this occurs is hard to resolve numerically.

6.2.3 Dependence on C

For large C, producing energy density plots such as those of figures 5.5 and 5.7 for the charge 3 case is numerically delicate, with $\hat{\Phi}$ changing rapidly over small distances. It is nonetheless expected that constituent energy peaks will develop. In analogy with the charge 2 case of chapter 5, we expect the charge 3 monopole with $W = \mathrm{i}$ (figure 6.4) to consist of a chain of upturned and rotated tetrahedra. For $z \in [0, \beta)$ and $m \in \mathbb{Z}$, constituents would be located at $(\zeta, z) = (0, 2\beta/3)$ and $(\zeta, z) = (C^{1/3}\mathrm{e}^{m\mathrm{i}\pi/3}, \beta/6)$. The is described by the symmetry group $D_{3\mathrm{d}}$.

6.2.4 Different Symmetries

We remark that the Ansatz (6.4) only encodes a subset of all solutions. In particular, there is evidence [Har*b*] of the existence of monopole chains with the symmetry

$$(\zeta, z) \sim (\zeta \mathrm{e}^{\mathrm{i}\pi/k}, z + m\beta/k) \tag{6.7}$$

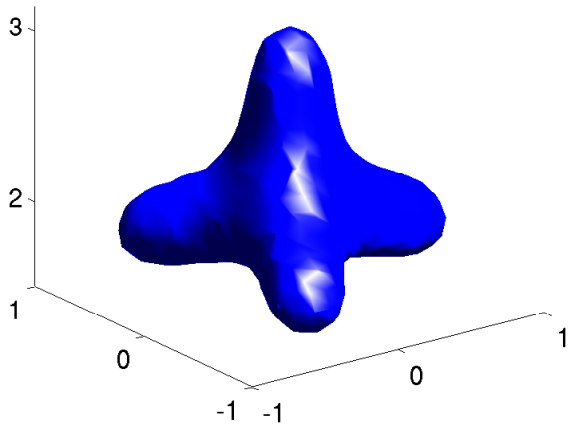

Figure 6.6: A contour of $\mathrm{tr}(\hat{\Phi}^2)$ for the $C = 1$, $W = 2 + \sqrt{3}$ ($K = 4$) charge 3 solution of type $\ell = 1$. This shows the Higgs field is close to zero at the centre of the tetrahedron, although the energy density is not peaked there (see figure 6.4, but note the change of scale).

where k is the monopole charge and $m = 0, \ldots, k-1$. We denote this symmetry by $D_{2\mathrm{h}} \times \mathbb{Z}_k^{(m)}$. Section 6.3 shows that the cases with $m = 0$ and $m = k/2$ can be expressed in the form (6.4). In particular, we suggest the following decompositions:

$$\begin{aligned} D_{2\mathrm{h}} \times \mathbb{Z}_k^{(0)} &= D_{(2k)\mathrm{h}}, \\ D_{2\mathrm{h}} \times \mathbb{Z}_k^{(k/2)} &= D_{k\mathrm{d}} \times \mathbb{Z}_2. \end{aligned}$$

More generally, solutions with the symmetry (6.7) can be given in terms of quasi-periodic Nahm data. For instance, in the charge 2 case we have $\mu_\pm$ as in (4.6), except this time with $\mathrm{Im}(\psi) = 0$. Numerical solutions of the inverse Nahm operator must be performed with the condition $\Psi|_{t=1} = -\Psi|_{t=0}$. However, it has proved difficult to get the scheme outlined in section 4.1.4 to converge with such boundary conditions.

6.3 Multiplying Chains

In this section we investigate how the Nahm data of a monopole chain can be constructed from that of a lower charge chain. This is possible when a chain can be described as a lower charge chain with a rescaled size C and period β.

We will firstly consider a generalisation of the large N limit of the Ercolani-Sinha solution [ES89] given by Harland & Ward [HW09]. Next, we will look at how charge $2k$ Nahm data with $\ell = k/2$ and $W = \pm 1$ can be expressed as charge k Nahm data with $\ell = 0$ and $K = 0$, and suggest an interpretation.

6.3.1 RESCALING A CHARGE 1 CHAIN

Harland & Ward [HW09] considered a rescaling of the Nahm data relevant to a finite chain of N monopoles in the limit $N \to \infty$. In this limit, the Nahm matrices become infinite dimensional and operate on a k dimensional vector of functions. The $k \times k$ matrix corresponding to this action is the Nahm data of a periodic monopole. This procedure allowed the authors to reproduce the Nahm data of monopole chains of charge 1, and for the special charge 2 configuration consisting of a charge 1 chain of halved period. The resulting set of Nahm data is equivalent to that for $W = \mathrm{i}$ on the surface Σ_2^1. For higher charges, this procedure does not give a point on the submanifold Σ_k^ℓ for any ℓ. For instance, the charge 3 version, describing a charge 1 monopole taken in groups of three is

$$\Phi = \begin{pmatrix} 0 & \mathrm{e}^{-\beta r/3} & \mathrm{e}^{\beta(r/3+\mathrm{i}t)} \\ \mathrm{e}^{\beta r/3} & 0 & \mathrm{e}^{-\beta r/3} \\ \mathrm{e}^{-\beta(r/3+\mathrm{i}t)} & \mathrm{e}^{\beta r/3} & 0 \end{pmatrix} \qquad A_{\bar{s}} = \frac{\beta}{6} \begin{pmatrix} 1 & 0 & 0 \\ 0 & 0 & 0 \\ 0 & 0 & -1 \end{pmatrix}. \quad (6.8)$$

This solution is of interest as the only currently known explicit charge 3 Nahm data with spectral curve coefficient $b_1 \neq 0$ (see section 6.1). In fact, the characteristic polynomial of Φ is $\zeta^3 - 3\zeta - (w + w^{-1}) = 0$. This is simply the $k = 3$ version of the spectral curve $\det(\mathbf{1}_2 w - V_1(\zeta)^k) = 0$, where the holonomy of the charge 1 chain, $V_1(\zeta)$, is taken over k periods and satisfies $\mathrm{tr}(V_1(\zeta)) = \zeta$ and $\det(V_1(\zeta)) = 1$. Note that $F = 0$, as expected for a charge 1 monopole chain (for which the Nahm data is of rank 1).

The symmetries of this solution can be studied in the same way as was done in section 6.2.1, to identify the symmetry group as $D_{2\mathrm{h}} \times \mathbb{Z}_3$. We find

$$(\zeta, z) \sim (\zeta, -z) \sim (-\zeta, z) \sim (\bar{\zeta}, z) \sim (\zeta, \beta/3 - z),$$

confirming that the charge 3 chain in question is simply a charge 1 chain with a rescaled period. This should be compared with the result of the spectral approximation, figure 6.2.

6.3.2 Embedding Nahm Data

Another approach to construct higher charge chains is by embedding lower charge Nahm data as blocks along the diagonal of a higher rank matrix, with rescaled periods and a phase shift to ensure the resulting characteristic polynomial of Φ is a valid spectral curve. This construction will in general yield Nahm data of the wrong periodicity, although it can readily be cast into the standard form of section 6.2 by a change of gauge.

Charge k from Charge 1

The charge 1 Nahm data is simply $\Phi^{(1)} = C\cosh(\beta s)$, $A^{(1)} = 0$. We form a traceless rank 2 Hitchin Higgs field by imposing a relative phase of -1, to obtain the charge 2 Hitchin Higgs field $\Phi' = C\cosh(\beta s/2)\sigma_3$. We should not be concerned about the anti-periodicity of Φ' if we notice that it is periodic with period $4\pi/\beta$, while the embedded charge 1 monopole has the dual period, $\beta/2$. Now we perform a non-periodic gauge transformation with

$$g = \frac{1}{\sqrt{2}}\begin{pmatrix} 1 & \mathrm{e}^{\mathrm{i}\beta t/2} \\ \mathrm{e}^{-\mathrm{i}\beta t/2} & -1 \end{pmatrix}$$

resulting in

$$\Phi^{(2)} = g^{-1}\Phi' g = C\cosh(\beta s/2)\begin{pmatrix} 0 & \mathrm{e}^{\mathrm{i}\beta t/2} \\ \mathrm{e}^{-\mathrm{i}\beta t/2} & 0 \end{pmatrix}$$

which is (up to a rescaling of C) the appropriate Hitchin Higgs field of a charge 2 chain, as can be obtained using the method of section 6.3.1. The gauge potential in the usual gauge (4.2) is expected to be $A^{(2)}_{\bar{s}} = \beta\sigma_3/8$. Applying the inverse gauge transformation, we find that $A^{(2)}_{\bar{s}} = g^{-1}A'_{\bar{s}}g + g^{-1}\partial_{\bar{s}}g$ with $A'_{\bar{s}} = A^{(2)}_{\bar{s}}$. The structure of the inverse Nahm operator (2.12) relating the symmetries of ζ and z to those of Φ and A allows us to interpret the embedded charge 1 Nahm data as describing two monopoles of the same orientation (due to the rotational symmetry $(\zeta, z) \sim (-\zeta, z)$) but with z positions shifted by $\pm\beta/4$ from the origin (this is determined from (2.12) as twice the shift in $A^{(1)}_{\bar{s}}$ from $A^{(1)}_{\bar{s}} = 0$ for the single chain centered at $z = 0$).

An analogous procedure can be carried out to construct the charge 3 chain of section 6.3.1 from charge 1 Nahm data. This time we have

$$\Phi' \;=\; 2\,\mathrm{diag}\left(\cosh\left(\frac{\beta s}{3}\right), \cosh\left(\frac{\beta s + 2\mathrm{i}\pi}{3}\right), \cosh\left(\frac{\beta s - 2\mathrm{i}\pi}{3}\right)\right)$$

$$A'_{\bar{s}} \;=\; \frac{\beta}{6}\,\mathrm{diag}(1, 0, -1)$$

which is gauge equivalent to (6.8) by conjugation with

$$g \;=\; \frac{1}{\sqrt{3}} \begin{pmatrix} 1 & \mathrm{e}^{\mathrm{i}\beta t/3} & \mathrm{e}^{2\mathrm{i}\beta t/3} \\ \mathrm{e}^{-\mathrm{i}\beta t/3 - 2\mathrm{i}\pi/3} & 1 & \mathrm{e}^{\mathrm{i}\beta t/3 + 2\mathrm{i}\pi/3} \\ \mathrm{e}^{-2\mathrm{i}\beta t/3 - 2\mathrm{i}\pi/3} & \mathrm{e}^{-\mathrm{i}\beta t/3 + 2\mathrm{i}\pi/3} & 1 \end{pmatrix}.$$

CHARGE 4 FROM CHARGE 2

The same idea can be applied to higher charges. This allows us to take, say, a charge 2 monopole in pairs to give charge 4 Nahm data where the Higgs field is block-diagonal,

$$\Phi^{(4)} \;=\; \begin{pmatrix} \Phi^{(2)} & 0 \\ 0 & \Phi'^{(2)} \end{pmatrix}.$$

This has a valid spectral curve as long as both $\Phi^{(2)}$ and $\Phi'^{(2)}$ have the same ℓ, with a relative overall phase of $\mathrm{e}^{\mathrm{i}\pi/2}$ and with K of opposite signs in each block.

A special case is provided by $\Phi^{(2)}$ with $\ell = 0$ and $K = 0$. The gauge transformation

$$g \;=\; \frac{1}{\sqrt{2}} \begin{pmatrix} 1 & 0 & \mathrm{e}^{\mathrm{i}\beta t/2} & 0 \\ 0 & 1 & 0 & \mathrm{e}^{\mathrm{i}\beta t/2} \\ \mathrm{e}^{-\mathrm{i}\beta t/2} & 0 & -1 & 0 \\ 0 & \mathrm{i}\mathrm{e}^{-\mathrm{i}\beta t/2} & 0 & -\mathrm{i} \end{pmatrix}$$

shows that this is equivalent to the charge 4 case with $\ell = 2$ and $W = 1$ (see section 6.2). In other words, there are particular charge 4 configurations which can be understood as charge 2 chains 'in disguise' [HW09], a result which could have been anticipated by comparing the symmetry groups between each case: here we have gone from $D_{4\mathrm{h}}$ to $D_{4\mathrm{h}} \times \mathbb{Z}_2$, while the previous subsection constructed $D_{2\mathrm{h}} \times \mathbb{Z}_k$-symmetric periodic monopoles from chains with $D_{2\mathrm{h}}$ symmetry.

The decoupling of the Nahm data into block-diagonal form suggests the relevant monopoles are 'maximally separated' and non-interacting.[15] This is reminiscent of the decoupling of the asymptotic moduli space metric of a charge 2 monopole into a direct product of two 1-monopole metrics for two well separated monopoles [GM95, Bie08].

6.4 Summary

This chapter concerns the construction of higher charge periodic monopoles. An Ansatz was constructed for the Hitchin fields, containing precisely the moduli appearing in the spectral curve, and this was found to provide highly symmetric configurations. It is hoped that one could work back from these symmetries to give a more thorough justification of this Ansatz, as was done in section 4.1.3 for the charge 2 chain. This was followed by a comparison with higher charge monopoles in $\mathbb{R}^3$ and a prescription for constructing certain higher charge chains from those of lower charge.

[15] A similar limiting case emerges for the Nahm data of well separated monopoles in $\mathbb{R}^3$. With conventions as in [MS04], the $k \to 1$ limit of the charge 2 Nahm data becomes diagonal, $(T_1, T_2, T_3) \propto (0, 0, \sigma_3)$, although with poles at the endpoints.

7

Conclusions and Outlook

We began this thesis by introducing non-Abelian magnetic monopoles as soliton solutions to the Yang-Mills-Higgs system in $\mathbb{R}^3$, and discussing how the techniques used in the construction of these solutions are adapted to the periodic case of monopoles on $\mathbb{R}^2 \times S^1$. This was followed by the discussion of an approximation to the resulting monopole fields, which increased in validity as the monopole size to period ratio became large. This allowed a study of the symmetries of the monopole chain and of the moduli space in this limit. The next chapter used the Nahm transform, which allowed a dual description of the monopole chain via Hitchin equations on a cylinder. This dual system was seen to describe the motion of lumps on the cylinder, and a study of their properties allowed us to reproduce the metric on the asymptotic moduli space. Following this, the results of the large size approximation were compared to the fields given by a numerical implementation of the Nahm transform. Finally, we briefly discussed how the preceding observations generalise to higher charge monopole chains.

There are various open questions, which could provide the basis for further research. A selection of these is listed below.

- The strength of the 'spectral approximation' was that it gave the monopole fields (in a certain limit) in a very simple way: by just studying the spectral curve, which is a polynomial satisfying certain rules. It would be interesting to try to apply this method to other soliton systems, thereby bypassing the Nahm transform, which is generally harder to implement.
- A particular case in which the 'spectral approximation' could be useful is the doubly periodic monopole on a square lattice, or monopole on $\mathbb{R} \times T^2$, which is self-reciprocal under Nahm transform. This system is believed

to be relevant in describing the wall of a magnetic bag, and has already been considered in some detail [Lee98, War05, War08]. In particular, spectral curves have been defined [ChW12], and the asymptotic moduli space metric of two such 'monopole walls' has been computed from physical considerations [HKM14]. Recent work [MW14] has allowed the identification of geodesic submanifolds using symmetry principles akin to those found throughout this thesis. Open questions include the applicability of the 'spectral approximation', the behaviour of constituents, and whether the Nahm transform can be used for walls with hexagonal symmetry.

- As mentioned briefly in chapter 6, it should be possible to use the Nahm transform to study monopole chains with different symmetries. Examples of this are chains in which monopoles in adjacent periods are rotated, and 2-monopole geodesics with $\theta = \pi/2$ (i.e. two incoming chains of monopoles 'maximally offset' by half a period in the periodic direction). Monopoles with these symmetries are not encoded by the Ansätze described in this thesis, and in particular one would need to modify the solution (4.2) to have $\alpha \neq 0$.
- Related to the question of finding monopoles of different symmetries is the possibility of perturbing known monopole solutions. The 'zeros apart' geodesic described in chapter 4 can be thought of as a perturbation of the 1-monopole chain. However, for higher charge monopoles there are no known geodesics which contain the 'tripled chain' (6.8). In other words, it is not currently known how to perturb the charge 1 monopole chain by perturbations of period other that 2.
- Following the discussion of section 3.4, it would be interesting to study periodic monopoles with higher gauge groups in more detail. The major stumbling block to applying the Nahm transform numerically is that the spectral curve predicts the Nahm/Hitchin data contains singularities. Nevertheless, if this problem could be successfully tackled it would be extremely interesting to compare the behaviour of SU(3) periodic monopoles with known results for SU(3) monopoles in $\mathbb{R}^3$. Indeed, it was this topic which initiated the research presented in this thesis and hence led to the development of the 'spectral approximation'.

Appendix A

Symmetries from Hitchin Data

In this appendix we explain in detail the procedure followed in section 4.1.2, with reference to the example of the $K \in \mathbb{R}$ geodesic of the 'zeros together' solution.

The map $(s;K) \mapsto (\bar{s};\bar{K})$ transforms $(r,t) \mapsto (r,-t)$,

$$\mu_+(s;K) = C\cosh(\beta s) + K/2 \mapsto C\cosh(\beta\bar{s}) + \bar{K}/2 = \bar{\mu}_+(s;K)$$

and

$$\mu_-(s;K) = 1 \mapsto \bar{\mu}_-(s;K).$$

Equation 4.3 is invariant, so $\mathrm{Re}(\psi)(s;K) \mapsto \mathrm{Re}(\psi)(s;K)$. Recalling that in this case $\mathrm{Im}(\psi) = 0$ tells us that a transforms as

$$a(s;K) = -\frac{1}{8}(\partial_r + \mathrm{i}\partial_t)\psi \mapsto -\frac{1}{8}(\partial_r - \mathrm{i}\partial_t)\psi = \bar{a}(s;K).$$

Combining these results we obtain the transformed Hitchin fields (4.2),

$$\begin{aligned}\Phi(s;K) &= \begin{pmatrix} 0 & \mu_+\mathrm{e}^{\psi/2} \\ \mu_-\mathrm{e}^{-\psi/2} & 0 \end{pmatrix}(s;K) \\ &\mapsto \Phi'(s';K') = \begin{pmatrix} 0 & \bar{\mu}_+\mathrm{e}^{\psi/2} \\ \bar{\mu}_-\mathrm{e}^{-\psi/2} & 0 \end{pmatrix}(s;K),\end{aligned}$$

$$A_{\bar{s}}(s;K) = a(s;K)\sigma_3 \mapsto A'_{\bar{s}}(s';K') = \bar{a}(s;K)\sigma_3 = -A_s(s;K),$$

$$A_s(s;K) = -\bar{a}(s;K)\sigma_3 \mapsto A'_s(s';K') = -a(s;K)\sigma_3 = -A_{\bar{s}}(s;K).$$

The Nahm operator Δ constructed from the new fields is

$$\Delta' = \begin{pmatrix} \mathbf{1}_2(2\partial_s - z) - 2A_s & \mathbf{1}_2\zeta - (\Phi')^\dagger \\ \mathbf{1}_2\bar{\zeta} - \Phi' & \mathbf{1}_2(2\partial_{\bar{s}} + z) - 2A_{\bar{s}} \end{pmatrix}.$$

Noting that Φ' can be written in terms of Φ as $\Phi' = \sigma_1\Phi^\dagger\sigma_1$, the new Nahm operator Δ' can be obtained from the original one (4.7) by the combined transformation

$$\Delta' = U^{-1}\Delta U \qquad\qquad (\zeta, z) \mapsto (\bar{\zeta}, -z)$$

with $U = \sigma_1 \otimes \sigma_1$. Consequently, Ψ transforms as

$$\Psi_\pm \mapsto \sigma_1\Psi_\mp$$

such that the new monopole fields evaluated at $(\bar{\zeta}, -z)$ are the same as the old ones at (ζ, z). A monopole configuration symmetric under $(\zeta, z) \mapsto (\bar{\zeta}, -z)$ is thus invariant under $K \mapsto \bar{K}$, and leaves us with the one parameter family of solutions with $\mathrm{Im}(K) = 0$.

Appendix B

Asymptotic Metric Integrals

In this appendix we perform the integrals of section 4.3.4 to one more order in $k = |K|$, using the example of the integral J in equation 4.31.

For complex $K = k\mathrm{e}^{\mathrm{i}\varphi}$,

$$\beta s_0 \;=\; \cosh^{-1}(-K/2C) \;=\; \log(-K/C + C/K + \mathcal{O}((k/C)^{-3})) \tag{B.1}$$

so

$$\beta r_0 \;=\; \log(k/C) + \mathcal{O}((k/C)^{-2}), \qquad\qquad \beta t_0 \;=\; \varphi + \pi + \mathcal{O}((k/C)^{-2}). \tag{B.2}$$

The integrand can be expanded as

$$h(r,t_0) \;=\; (K/2-C)^{-1/2} \sum_{m=0}^{\infty} \frac{(2m)!}{(m!)^2} (2-K/C)^{-m} \cosh^{2m}\left(\tfrac{1}{2}\beta(r+\mathrm{i}t_0)\right).$$

In order to integrate, we expand $\cosh^{2m}$ as a sum of linear terms [GR94*b*],

$$h(r,t_0) \;=\; (K/2-C)^{-1/2}\left(1+\sum_{m=1}^{\infty} \frac{(2m)!}{4^m(m!)^2}(2-K/C)^{-m}\left(\frac{(2m)!}{(m!)^2}+ \right.\right.$$
$$\left.\left. + \sum_{n=0}^{m-1} \frac{2(2m)!}{(2m-n)!n!} \cosh\left((m-n)\beta(r+\mathrm{i}t_0)\right)\right)\right)$$

where the m^{th} term in the sum has m factors of 'cosh' and, as will be seen below, the series can be truncated, with higher terms contributing smaller

powers of k/C. Integrating from $r = 0$ to $r = r_0$,

$$J = (K/2 - C)^{-1/2}\Bigg(r_0 + \sum_{m=1}^{\infty} \frac{(2m)!}{4^m (m!)^2}(2 - K/C)^{-m}\Bigg(\frac{(2m)!}{(m!)^2} r_0 \tag{B.3}$$
$$+ \frac{1}{\beta}\sum_{n=0}^{m-1} \frac{2(2m)!}{(2m-n)!n!}\frac{1}{(m-n)}\Big(\sinh\big((m-n)\beta s_0\big) - \sinh\big((m-n)\mathrm{i}\beta t_0\big)\Big)\Bigg)\Bigg).$$

We now expand the sinh terms in powers of k/C using (B.1) and (B.2),

$$\sinh(m\beta s_0) = \tfrac{1}{2}(-K/C)^m + \mathcal{O}((k/C)^{m-2})$$
$$\sinh(\mathrm{i}m\beta t_0) = \mathrm{i}\sin(2\pi m(\eta + 1/2)) + \mathcal{O}((k/C)^{-2}).$$

Substituting these into (B.3),

$$J = (K/2 - C)^{-1/2}\Bigg(r_0 + \sum_{m=1}^{\infty} \frac{(2m)!}{4^m (m!)^2}(2 - K/C)^{-m}\Bigg(\frac{(2m)!}{(m!)^2} r_0 +$$
$$+ \frac{1}{\beta}\sum_{n=0}^{m-1} \frac{(2m)!}{(2m-n)!n!}\frac{(-1)^{m-n}}{(m-n)}\Big((K/C)^{m-n} + \mathcal{O}((k/C)^{m-n-2}) +$$
$$-2\mathrm{i}\sin(2\pi\eta(m-n)) + \mathcal{O}((k/C)^{-2})\Big)\Bigg)\Bigg).$$

Expanding $(2 - K/C)^{-m}$ and r_0, the summand becomes

$$\frac{1}{\beta}\frac{(2m)!}{4^m (m!)^2}\big(1 + 2mC/K + \mathcal{O}((k/C)^{-2})\big) \times$$
$$\Bigg(\frac{(2m)!}{(m!)^2}(-K/C)^{-m}\log(k/C) + \mathcal{O}((k/C)^{-m-2}) +$$
$$+ \sum_{n=0}^{m-1} \frac{(2m)!}{(2m-n)!n!}\frac{(-1)^n}{(m-n)}\Big((K/C)^{-n} + \mathcal{O}((k/C)^{-n-2}) +$$
$$-2\mathrm{i}((K/C)^{-m}\sin(2\pi\eta(m-n)) + \mathcal{O}((k/C)^{-m-2})\Big)\Bigg).$$

Now we expand the sum term by term, retaining terms of order $(k/C)^{-1}$. To this order we need only consider $m = 1$, plus the terms highlighted in red above (which do not involve negative powers of m), so the double sum evaluates to

$$\frac{1}{\beta}\Bigg(-(K/C)^{-1}\log(k/C) - \mathrm{i}(K/C)^{-1}\sin(2\pi\eta) + \mathcal{O}((k/C)^{-2}\log(k/C)) +$$
$$+ \sum_{m=1}^{\infty} \frac{(2m)!}{m4^m (m!)^2} - (K/C)^{-1}\Bigg(2\sum_{m=2}^{\infty} \frac{(2m)!}{(m-1)4^m (m!)^2} - 1\Bigg) + \mathcal{O}((k/C)^{-2})\Bigg).$$

These sums can in fact be performed (using Mathematica), so putting everything together,

$$J = \frac{1}{\beta}\sqrt{\frac{2}{K}}\Big(\log(k/C) + \log(4) - \mathrm{i}(C/K)\sin(2\pi\eta) + \\ + \mathcal{O}((k/C)^{-2}\log(k/C))\Big)$$

where there is a nice cancellation killing the $(K/C)^{-1}\log(k/C)$ term, and the $\mathcal{O}((k/C)^{-2}\log(k/C))$ piece contains contributions from the magenta and cyan terms.

A similar expansion also gives a factor of 4 in the I integral (here we must consider the regions $|r| > |r_0|$ and $|r| < |r_0|$ separately, although the dominant contribution is from the former). Similarly, the subleading terms in h_0 and L are at $\mathcal{O}((k/C)^{-3/2})$.

Bibliography

[AH85] M. Atiyah, N. J. Hitchin, *Low-energy scattering of non-Abelian magnetic monopoles*, Phil. Trans. R. Soc. Lond. A **315** (1985) 459

[AH88] ——— , *The Geometry and Dynamics of Magnetic Monopoles*, Princeton (1988)

[AHDM75] M. F. Atiyah, N. J. Hitchin, V. G. Drinfeld, Yu. I. Manin, *Construction of instantons*, Phys. Lett. **A 65** (1978) 185

[AM89] M. F. Atiyah, N. S. Manton, *Skyrmions from Instantons*, Phys. Lett. **B 222** (1989) 438

[BH05] A. Basu, J. A. Harvey, *The M2-M5 Brane System and a Generalized Nahm's Equation*, Nucl. Phys. **B 713** (2005) 136, `arXiv:hep-th/0412310`

[Bie08] R. Bielawski, *Monopoles and Clusters*, Commun. Math. Phys. **284** (2008) 675, `arXiv:hep-th/0702190`

[Bol06] S. Bolognesi, *Multi-monopoles and magnetic bags*, Nucl. Phys. **B 752** (2006) 93, `arXiv:hep-th/0512133`

[BPP82] S. A. Brown, H. Panagopoulos, M. K. Prasad, *Two separated SU(2) Yang-Mills-Higgs monopoles in the Atiyah-Drinfeld-Hitchin-Manin-Nahm construction*, Phys. Rev. **D 26** (1982) 854

[Bra11] H. W. Braden, *Cyclic Monopoles, Affine Toda and Spectral Curves*, Commun. Math. Phys. **308** (2011) 303, `arXiv:1002.1216 [math-ph]`

[BvB89] P. J. Braam, P. van Baal, *Nahm's Transformation for Instantons*, Commun. Math. Phys. **122** (1989) 267

[CG84] E. Corrigan, P. Goddard, *Construction of Instanton and Monopole Solutions and Reciprocity*, Ann. Phys. **154**, 253-279 (1984)

[ChD08] S. A. Cherkis, B. Durcan, *Singular Monopoles via the Nahm Transform*, JHEP04(2008)070, `arXiv:0712.0850 [hep-th]`

[Che07] S. A. Cherkis, *A Journey Between Two Curves*, SIGMA **3** (2007) 043, `arXiv:hep-th/0703108`

[ChK01] S. Cherkis, A. Kapustin, *Nahm Transform for Periodic Monopoles and $\mathcal{N} = 2$ Super Yang-Mills Theory*, Commun. Math. Phys. **218** (2001) 333, arXiv:hep-th/0006050

[ChK02] ——— , *Hyper-Kähler metrics from periodic monopoles*, Phys. Rev. **D 65** (2002) 084015, arXiv:hep-th/0109141

[ChK03] ——— , *Periodic Monopoles With Singularities And $\mathcal{N} = 2$ Super-QCD*, Commun. Math. Phys. **234** (2003) 1, arXiv:hep-th/0011081

[ChW12] S. A. Cherkis, R. S. Ward, *Moduli of monopole walls and amoebas*, JHEP05(2012)090, arXiv:1202.1294 [hep-th]

[Dir31] P. A. M. Dirac, *Quantised Singularities in the Electromagnetic Field*, Proc. R. Soc. Lond. A **133** (1931) 60

[DK05] G. V. Dunne, V. Khemani, *Numerical investigation of monopole chains*, J. Phys. **A 38** (2005) 9359

[ES89] N. Ercolani, A. Sinha, *Monopoles and Baker Functions*, Commun. Math. Phys. **125** (1989) 385

[FHP81] P. Forgács, Z. Horváth, L. Palla, *Exact multimonopole solutions in the Bogomolny-Prasad-Sommerfield limit*, Phys. Lett. **B 99** (1981) 232
——— *Generating monopoles of arbitrary charge by Bäcklund transformations*, Phys. Lett. **B 102** (1981) 131

[FP04] C. Ford, J. M. Pawlowski, *Doubly periodic instantons and their constituents*, Phys. Rev. **D 69** (2004) 065006, arXiv:hep-th/0302117

[GH78] G. W. Gibbons, S. W. Hawking, *Gravitational Multi-Instantons*, Phys. Lett. **B 78** (1978) 430

[GM86] G. W. Gibbons, N. S. Manton, *Classical and Quantum Dynamics of BPS Monopoles*, Nucl. Phys. **B 274** (1986) 183

[GM88] H. Garland, M. K. Murray, *Kac-Moody Monopoles and Periodic Instantons*, Commun. Math. Phys. **120** (1988) 335

[GM95] G. W. Gibbons, N. S. Manton, *The moduli space metric for well-separated BPS monopoles*, Phys. Lett. **B 356** (1995) 32

[GMN13] D. Gaiotto, G. W. Moore, A. Neitzke, *Wall-crossing, Hitchin Systems, and the WKB Approximation*, Adv. Math. 234 (2013) 239, arXiv:0907.3987 [hep-th]

[GPY81] D. J. Gross, R. D. Pisarski, L. G. Yaffe, *QCD and instantons at finite temperature*, Rev. Mod. Phys. **53** (1981) 43

[GR94*a*] I. S. Gradshteyn, I. M. Ryzhik, A. Jeffrey (ed.), *Table of Integrals, Series, and Products*, Academic Press (1994), equations 3.617, 6.141, 6.142, 8.111-8.113, 8.126 and 9.100

[GR94*b*] *Ibid.*, equation 1.320.6

[Ham62] M. Hamermesh, *Group Theory and its Physical Applications*, chapter 2 *Symmetry Groups*, Addison-Wesley (1962)

[Har08] D. Harland, *Chains of Solitons*, PhD thesis, University of Durham (2008), `etheses.dur.ac.uk/2303/`

[Har*a*] ——— , personal communication

[Har*b*] ——— , *Cyclic monopole chains*, to appear

[HIM99] C. J. Houghton, P. W. Irwin, A. J. Mountain, *Two monopoles of one type and one of another*, JHEP04(1999)029, `arXiv:hep-th/9902111`

[Hit82] N. J. Hitchin, *Monopoles and Geodesics*, Commun. Math. Phys. **84** (1982) 579

[Hit87] ——— , *The Self-Duality Equations on a Riemann Surface*, Proc. Lond. Math. Soc. (3) 55 (1987) 59

[HKM14] M. Hamanaka, H. Kanno, D. Muranaka, *Hyperkähler Metrics from Monopole Walls*, `arXiv:1311.7143 [hep-th]`

[HMM95] N. J. Hitchin, N. S. Manton, M. K. Murray, *Symmetric monopoles*, Nonlinearity **8** (1995) 661, `arXiv:dg-ga/9503016`

[HS77] B. J. Harrington, H. K. Shepard, *Euclidean solutions and finite temperature gauge theory*, Nucl. Phys. **B 124** (1977) 409

[HS78] ——— , *Periodic Euclidean solutions and the finite-temperature Yang-Mills gas*, Phys. Rev. **D 17** (1978) 2122

[HS96] C. J. Houghton, P. M. Sutcliffe, *Tetrahedral and Cubic Monopoles*, Commun. Math. Phys. **180** (1996) 343, `arXiv:hep-th/9601146`

[HS97] ——— , *SU(N) monopoles and Platonic symmetry*, J. Math. Phys. **38** (1997) 5576, `arXiv:hep-th/9708006`

[HW97] A. Hanany, E. Witten, *Type IIB superstrings, BPS monopoles, and three-dimensional gauge dynamics*, Nucl. Phys. **B 492** (1997) 152, `arXiv:hep-th/9611230`

[HW08] D. Harland, R. S. Ward, *Chains of skyrmions*, JHEP12(2008)093, `arXiv:0807.3870 [hep-th]`

[HW09] ——— , *Dynamics of periodic monopoles*, Phys. Lett. **B 675** (2009) 262, `arXiv:0901.4428 [hep-th]`

[Jar04] M. Jardim, *A survey on Nahm transform*, J. Geom. Phys. **52** (2004) 313, `arXiv:math/0309305 [math.DG]`

[JNR77] R. Jackiw, C. Nohl, C. Rebbi, *Conformal properties of pseudoparticle configurations*, Phys. Rev. **D 15** (1977) 162

[JT80] A. Jaffe, C. Taubes, *Vortices and Monopoles*, Birkhäuser (1980)

[JZ75] B. Julia, A. Zee, *Poles with both magnetic and electric charges in non-Abelian gauge theory*, Phys. Rev. **D 11** (1975) 2227

[Kam] M. Kamata, *Circular symmetry in the Hitchin system*, `arXiv:1307.3840 [hep-th]`

[Kap98] A. Kapustin, *Solution of $N = 2$ gauge theories via compactification to three dimensions*, Nucl. Phys. **B 534** (1998) 531, `arXiv:hep-th/9804069`

[KvB98*a*] T. C. Kraan, P. van Baal, *Monopole constituents inside SU(n) calorons*, Phys. Lett. **B 435** (1998) 389, `arXiv:hep-th/9806034`

[KvB98*b*] ——— , *Periodic instantons with non-trivial holonomy*, Nucl. Phys. **B 533** (1998) 627, `arXiv:hep-th/9805168`

[Lee98] K. Lee, *Sheets of BPS monopoles and instantons with arbitrary simple gauge group*, Phys. Lett. **B 445** (1999) 387

[LL98] K. Lee, C. Lu, *SU*(2) *calorons and magnetic monopoles*, Phys. Rev. **D 58** (1998) 025011

[LWY96] K. Lee, E. J. Weinberg, P. Yi, *Moduli space of many BPS monopoles for arbitrary gauge groups*, Phys. Rev. **D 54** (1996) 1633

[Mal13] R. Maldonado, *Periodic monopoles from spectral curves*, JHEP02(2013)099, `arXiv:1212.4481 [hep-th]`

[Mal*a*] ——— , *Higher charge periodic monopoles*, `arXiv:1311.6354 [hep-th]`

[Mal*b*] ——— , *Scaling limits of periodic monopoles*, `arXiv:1405.3641 [hep-th]`

[Man77] N. S. Manton, *The force between 't Hooft-Polyakov monopoles*, Nucl. Phys. **B 126** (1977) 525

[Man82] ——— , *A remark on the scattering of BPS monopoles*, Phys. Lett. **B 110** (1982) 54

[Man85] ——— , *Monopole interactions at long range*, Phys. Lett. **B 154** (1985) 397 and Phys. Lett. **B 157** (1985) 475

[Mil72] W. Miller, *Symmetry Groups and Their Applications*, chapter 2 *The Crystallographic Groups*, Academic Press (1972)

[MO77] C. Montonen, D. Olive, *Magnetic monopoles as gauge particles*, Phys. Lett. **B 72** (1977) 117

[MS04] N. Manton, P. Sutcliffe, *Topological Solitons*, Cambridge (2004)

[MT+09] D. J. P. Morris, D. A. Tennant, S. A. Grigera, B. Klemke, C. Castelnovo, R. Moessner, C. Czternasty, M. Meissner, K. C. Rule, J.-U. Hoffmann, K. Kiefer, S. Gerischer, D. Slobinsky, R. S. Perry, *Dirac Strings and Magnetic Monopoles in the Spin Ice $Dy_2Ti_2O_7$*, Science **326** (2009) 411, `arXiv:1011.1174 [cond-mat]`

[MW96] L. J. Mason, N. M. J. Woodhouse, *Integrability, Self-Duality, and Twistor Theory*, Oxford (1996)

[MW13] R. Maldonado, R. S. Ward, *Geometry of periodic monopoles*, Phys. Rev. **D 88** (2013) 125013, `arXiv:1309.7013 [hep-th]`

[MW14] ——— , *Dynamics of monopole walls*, Phys. Lett. **B 734** (2014) 328, `arXiv:1405.4646 [hep-th]`

[Nah80] W. Nahm, *A simple formalism for the BPS monopole*, Phys. Lett. **B 90** (1980) 413

[Nak93] H. Nakajima, T. Mabuchi (ed.), S. Mukai (ed.), *Monopoles and Nahm's equations*, in *Einstein metric and Yang-Mills connections*, Marcel Dekker, New York (1993)

[Pol74] A. M. Polyakov, *Particle spectrum in quantum field theory*, JETP Lett. **20** (1974) 194 (for the English version)

[PS75] M. K. Prasad, C. M. Sommerfield, *Exact classical solution for the 't Hooft monopole and the Julia-Zee dyon*, Phys. Rev. Lett. **35** (1975) 760

[Raj12] A. Rajantie, *Magnetic Monopoles in Field Theory and Cosmology*, Phil. Trans. R. Soc. Lond. A **370** (2012) 5705, `arXiv:1204.3073 [hep-th]`

[Saç84] C. K. Saçlioğlu, *Liouville and Painlevé equations and Yang-Mills strings*, J. Math. Phys. **25** (1984) 3214

[Shn] Ya. Shnir, *$SU(N)$ monopoles with and without SUSY*, `arXiv:hep-th/0508210`

[Stu94] D. Stuart, *The Geodesic Approximation for the Yang-Mills-Higgs Equations*, Commun. Math. Phys. **166** (1994) 149

[Sut92] P. M. Sutcliffe, *Sine-Gordon solitons from CP^1 instantons*, Phys. Lett. **B 283** (1992) 85

[Sut96*a*] ——— , *Monopole zeros*, Phys. Lett. **B 376** (1996) 103, `arXiv:hep-th/9603065`

[Sut96*b*] ——— , *Seiberg-Witten theory, monopole spectral curves and affine Toda solitons*, Phys. Lett. **B 381** (1996) 129, `arXiv:hep-th/9605192`

[Sut97] ——— , *Cyclic monopoles*, Nucl. Phys. **B 505** (1997) 517, `arXiv:hep-th/9610030`

[Sut10] P. M. Sutcliffe, *Skyrmions, instantons and holography*, JHEP08(2010)019, `arXiv:1003.0023 [hep-th]`

['tHo74] G. 't Hooft, *Magnetic monopoles in unified gauge theories*, Nucl. Phys. **B 79** (1974) 276

[VS94] A. Vilenkin, E. P. S. Shellard, *Cosmic Strings and other Topological Defects*, Cambridge (1994)

[War81] R. S. Ward, *A Yang-Mills-Higgs Monopole of Charge 2*, Commun. Math. Phys. **79** (1981) 317

[War82] ——— , *Deformations of the Embedding of the SU(2) Monopole Solution in SU(3)*, Commun. Math. Phys. **86** (1982) 437

[War05] ——— , *Periodic monopoles*, Phys. Lett. **B 619** (2005) 177, `arXiv:hep-th/0505254`

[War08] ——— , *Monopole wall*, Phys. Rev. **D 75** (2007) 021701, `arXiv:hep-th/0612047`

[Wei80] E. J. Weinberg, *Fundamental Monopoles and Multimonopole Solutions for Arbitrary Simple Gauge Groups*, Nucl. Phys. **B 167** (1980) 500

[WG76] E. J. Weinberg, A. H. Guth, *Nonexistence of spherically symmetric monopoles with multiple magnetic charge*, Phys. Rev. **D 14** (1976) 1660

[YM54] C. N. Yang, R. L. Mills, *Conservation of Isotopic Spin and Isotopic Gauge Invariance*, Phys. Rev. **96** (1954) 191